

GEOMORPHOLOGICAL CHANGE OF THE UPPER YOM RIVER IN PHRAE PROVINCE



A Thesis Submitted in Partial Fulfillment of the Requirements

for the Degree of Master of Science in Geology

Department of Geology

FACULTY OF SCIENCE

Chulalongkorn University

Academic Year 2022

Copyright of Chulalongkorn University

การเปลี่ยนแปลงกรณีศึกษาของแม่น้ำยมตอนบนในจังหวัดแพร่



วิทยานิพนธ์นี้เป็นส่วนหนึ่งของการศึกษาตามหลักสูตรปริญญาวิทยาศาสตรมหาบัณฑิต

สาขาวิชาธรณีวิทยา ภาควิชาธรณีวิทยา

คณะวิทยาศาสตร์ จุฬาลงกรณ์มหาวิทยาลัย

ปีการศึกษา 2565

ลิขสิทธิ์ของจุฬาลงกรณ์มหาวิทยาลัย

คัคนางค์ ณาน : การเปลี่ยนแปลงธรณีสัณฐานของแม่น้ำยมตอนบนในจังหวัดแพร่ . (GEOMORPHOLOGICAL CHANGE OF THE UPPER YOM RIVER IN PHRAE PROVINCE) อ.ที่ปรึกษาหลัก : ศ. ดร.มนตรี ชูวงศ์, อ.ที่ปรึกษาร่วม : รศ. ดร.ฐาน ธิติมากร

แม่น้ำยมเป็นแม่น้ำสาขาหลักของแม่น้ำเจ้าพระยา แม่น้ำยมตอนบนไหลผ่านแอ่งระหว่างภูเขาในจังหวัดแพร่ งานวิจัยนี้เลือกศึกษาแม่น้ำยมตอนบนเนื่องจากการแปรรูปเป็นแอ่งน้ำที่มีการเคลื่อนตัวอย่างรวดเร็วและมีการเปลี่ยนแปลงภูมิประเทศ งานวิจัยนี้ศึกษาการเปลี่ยนแปลงทางธรณีสัณฐานของแม่น้ำยมตอนบนของจังหวัดแพร่ ระหว่าง พ.ศ. 2497 ถึง พ.ศ. 2562 โดยการวิเคราะห์การตีความทางธรณีวิทยาจากภาพถ่ายทางอากาศ โดยใช้ Geomorphoc criteria การวิเคราะห์ตะกอน การศึกษาสภาพด้านทานไฟฟ้า (ERT) และการสำรวจด้วย วิธีเรดาร์ (GPR) ผลการศึกษาการเปลี่ยนแปลงทางธรณีสัณฐานใน 65 ปี ในตอนบนและตอนกลางของพื้นที่วิจัยพบร่องรอยและหลักฐานการกัดกร่อนของแม่น้ำปรากฏมากกว่าตอนล่าง เนื่องจากบริเวณทั้งสองมีลักษณะภูมิประเทศเป็นพื้นที่ราบน้ำท่วมถึงที่มีความกว้างกว่าพื้นที่ตอนล่าง นอกจากนี้ได้ใช้ เกณฑ์บ่งชี้ทางธรณีสัณฐาน เพื่อเปรียบเทียบการเปลี่ยนแปลง ได้แก่ ความกว้าง ความยาว ดัชนีการคดโค้ง (SI) รัศมีความโค้ง (Rc) และอัตราการกัดกร่อนทางน้ำ โดยผลการศึกษา พบว่าความกว้างของแม่น้ำ มีการลดลงอย่างมากจากอดีตถึงปัจจุบัน เนื่องจากการทับถมของตลิ่งที่เพิ่มขึ้นซึ่งเป็นผลมาจากกิจกรรมของมนุษย์ พบว่าการเปลี่ยนแปลงการใช้ที่ดินมีผลกระทบต่อปริมาณน้ำท่าและตะกอน ความยาว และ ดัชนีการคดโค้ง(SI) มีแนวโน้มลดลง เนื่องจากแม่น้ำมีการเกิดตัดผ่านบริเวณคอขวดแม่น้ำ และการตัดผ่านบริเวณที่มีการสะสมตัวของตะกอนในช่วงน้ำท่วม ซึ่งเกิดขึ้นบ่อยครั้งตั้งแต่อดีตถึงปัจจุบัน นอกจากนี้อัตราการกัดเซาะบริเวณส่วนโค้งของแม่น้ำลดลงในตอนบนและตอนกลางของแม่น้ำยมเนื่องจากการตัดผ่านบริเวณที่มีการสะสมตัวของตะกอนได้เกิดขึ้นในช่วงอดีตไปแล้ว ขณะที่ตอนล่างบริเวณคดโค้งยังมีการเปลี่ยนแปลงไปมา ซึ่งอาจจะเกิดการตัดผ่านบริเวณที่มีการสะสมตัวของตะกอนของโค้งน้ำขึ้นได้ในอนาคต

จากการสำรวจภาคสนามเก็บตะกอนและการศึกษาธรณีฟิสิกส์ พบว่าพื้นที่ศึกษามีตะกอน ได้แก่ mud, sandy mud, muddy sand, sand, gravelly sand, and sandy gravel พบได้ในบริเวณที่มีการสะสมตัวของตะกอน (point bars) and แม่น้ำโบราณ (paleochannels) และพบตะกอนชนิด mud and sandy mud ในบริเวณ ที่ราบน้ำท่วมถึง และ รอยทางน้ำกัดกร่อน (Meandered scar) ของพื้นที่ที่ปรากฏในปัจจุบัน และการวิเคราะห์ การสำรวจธรณีฟิสิกส์สามารถให้ข้อมูลเกี่ยวกับลักษณะชนิดตะกอนและโครงสร้างตะกอนใต้พื้นดินได้ ซึ่งผลจาก ERT สามารถแสดงการเปลี่ยนแปลงชนิดตะกอนทั้งในแนวตั้งและแนวนอนของแม่น้ำโบราณแสดงความหนาลึกลงไปจากผิวดินประมาณ 5 ถึง 20 เมตร สามารถบ่งชี้ว่าเป็นตะกอนใน แม่น้ำโบราณ ที่ราบน้ำท่วมถึง และ รอยทางน้ำกัดกร่อน ในอดีตได้นอกจากนี้ ชุดลักษณะของตะกอนทางน้ำที่สะสมสามารถแบ่งได้เป็น 5 ชุดลักษณะ ได้แก่ Reflection free facies, Inclined facies, Concaved facies, Chaotic facies and Parallel(planar) Facies.

ผลการวิเคราะห์จากเทคนิคหลากหลายของการศึกษานี้ทำให้เข้าใจถึงการเปลี่ยนแปลงทางธรณีสัณฐานวิทยาที่เกิดขึ้นในแม่น้ำยมตอนบนในช่วงหลายทศวรรษที่ผ่านมา การค้นพบนี้ช่วยให้เราเข้าใจพฤติกรรมของแม่น้ำยม วิวัฒนาการของภูมิประเทศชนิดตะกอน และความหนาของของทางน้ำโบราณได้

สาขาวิชา	ธรณีวิทยา	ลายมือชื่อนิสิต
ปีการศึกษา	2565	ลายมือชื่อ อ.ที่ปรึกษาหลัก
		ลายมือชื่อ อ.ที่ปรึกษาร่วม

6270011323 : MAJOR GEOLOGY

KEYWORD: Geomorphological changes, Sinuosity index, Yom River, Meander, Meander belt.

Kakkhanang Na Nan : GEOMORPHOLOGICAL CHANGE OF THE UPPER YOM RIVER IN PHRAE PROVINCE. Advisor: Prof.

MONTRI CHOOWONG, Ph.D. Co-advisor: Assoc. Prof. Thanop Thitimakorn, Ph.D.

Yom River is the main tributary of the Chao Phraya River; the upper Yom River flows through Phrae Province. This research selected the upper Yom River because of meander processing in an active basin, which rapidly migrates and changes landforms all the time. The object of this research is to study geomorphological change, thickness and behavior of the upper Yom River in Phrae Province.

By assessing aerial photographs and satellite images from 1954 to 2019, the researchers were able to interpret the geological changes that occurred over the past 65 years. The study identified several geomorphological changes from channel migration which can be obvious on maps. The upper and middle sections of the research site, characterized by a flat and wider floodplain area, exhibited more remnants of cut-offs compared to the lower section. To compare the changes, five geomorphic criteria were used: channel width (W), channel length (L), sinuosity index (SI), radius of curvature (Rc), and channel migrations. The width (W) underwent significant alterations due to increased bank deposition resulting from human activities and deforestation. Changes in land use were found to have various impacts on runoff and sediment supply. The channel's length and sinuosity index (SI) showed a decreasing trend, indicating frequent cut-offs at the neck and chute during floods. Erosion rates were observed to be lower in the upper and middle parts of the Yom River due to previous cut-offs, while the lower portion exhibited active bending as evidenced by migration rates versus Rc/W values. Lower Rc/W values corresponded to slower rates of bend migration.

The sedimentology and geophysics field investigation from different landforms. Grain size analysis revealed sediment types including mud, sandy mud, muddy sand, sand, gravelly sand, and sandy gravel in point bars and paleo-channels, and mud and sandy mud in floodplains and meander scars. ERT and GPR analyses provided insights into the lithological characteristics of the study area. The ERT profiles displayed visible vertical and horizontal changes in fluvial deposits, which ranged in thickness from 5 to 20 meters, similar to the floodplain, point bar, and paleo-channel. Additionally, five types of radar facies were observed in river deposits: Continuous (Parallel), Inclined, Concaved-up (Channel fill), Chaotic, and Reflection Free.

This study's comprehensive analysis of various data sources and techniques shed light on the geomorphological changes that have occurred in the upper Yom River over the past decades. The findings also contribute to our understanding of the Yom River behaviors, landform evolution, the sediments and the paleochannels' thickness.

CHULALONGKORN UNIVERSITY

Field of Study: Geology

Student's Signature

Academic Year: 2022

Advisor's Signature

Co-advisor's Signature

ACKNOWLEDGEMENTS

The authors would like to express their sincere gratitude to the following individuals and organizations for their invaluable contributions and support throughout the completion of this study on the geomorphological changes of the upper Yom River in Phrae Province.

First and foremost, this thesis was mainly financial support by the Morphology of Earth Surface and Advanced Geohazards in Southeast Asia Research Unit (MESA RU), the 90th Anniversary of Chulalongkorn University Scholarship and also Research Potential Development Projects at the Graduate Level from the Faculty of Science, Chulalongkorn University for their financial assistance. The Department of Geology for their guidance and collaboration. Their facilities and resources were instrumental in the smooth execution of this study.

Special thanks are extended to Professor Dr. Montri Choowong for his advisory role in this study. His vast knowledge and guidance significantly influenced the research methodology and outcomes. Thank you for not only your hard-working, patients and dedication throughout this work but also your kindness in advising me for all the time we work together.

I would also like to thank you Associate Professor Dr. Thanop Thitimakorn for his expertise in geophysics and his valuable contributions as a geophysics advisor. His guidance and advice greatly enhanced the geophysical analysis of the research.

Furthermore, I would like to express our appreciation to Mr. Narongsak Rachukarn for his assistance in the geophysics fieldwork. His technical support and expertise were crucial in collecting accurate and reliable data.

I would also like to thank you for the support and understanding of my friends and colleagues in the Master's and Doctoral degree room, who provided encouragement and assistance throughout the research process and field works. Their motivation, console and advice were invaluable.

My heartfelt thanks go to my family (Mother, Father and my little sister and brother) for their unwavering support, understanding, and love throughout this research process. Their encouragement and belief were a source of myself motivation.

Lastly, I would like to extend our special thanks to the members of Astro, especially Mr. Moon Bin, for their inspiration, inner strength and positive influence. Your music and artistry provided us with the creative energy to pursue this study.

I acknowledge that this study would not have been possible without the collective efforts of all those mentioned above. Any omissions are unintentional, and I sincerely apologize to anyone whose contribution may have been inadvertently overlooked. Thank you all for your invaluable support and contributions to this study.



จุฬาลงกรณ์มหาวิทยาลัย
CHULALONGKORN UNIVERSITY

TABLE OF CONTENTS

	Page
.....	iii
ABSTRACT (THAI).....	iii
.....	iv
ABSTRACT (ENGLISH)	iv
ACKNOWLEDGEMENTS.....	v
TABLE OF CONTENTS.....	vii
LIST OF TABLES.....	xi
LIST OF FIGURES	xii
CHAPTER 1 INTRODUCTIONS.....	1
1.1 Background.....	1
1.1.1 General background.....	1
1.1.2 Study area background	3
1.2 Research Objective	5
1.3 Scope of the Study.....	5
1.4 Benefits	5
CHAPTER 2 Literature Review	7
2.1 River channel pattern.....	7
2.2 Meandering fluvial landforms	13
2.2.1 Oxbow Lake.....	15
2.2.2 Point bar	16
2.2.3 Scroll bars.....	16

2.3 Planform evolution of meandering rivers	18
2.4 Geomorphic Criteria.....	20
2.4.1 Channel Width (W)	20
2.4.2 Sinuosity Index (SI).....	22
2.4.3 Radius of Curvature (Rc).....	23
2.4.4 Channel length	24
2.4.5 Channel migration	24
2.5 Geophysics	26
2.5.1 Ground Penetrating Radar (GPR)	27
2.5.2 Electrical Resistivity Tomography (ERT)	31
2.5.3 Seismic Data in Study Area.....	33
CHAPTER 3 Methodology	36
3.1 Aerial Photo and Satellite Image Interpretation	36
3.1.1. Aerial Photo and Satellite Image Interpretation materials	36
3.1.2 Delineate the geomorphic characters	37
3.1.2.1 Geomorphic mapping.....	37
3.1.2.2 Geomorphic Criteria Calculation	43
3.1.2.2.1 The Sinuosity index (SI)	44
3.1.2.2.2 The radius of curvature (Rc).....	45
3.1.2.2.3 Channel width (W)	46
3.1.2.2.4 Centerline migration rate	46
3.1.2.2.5 Channel length (L)	48
3.2 Field investigation	49

3.2.1 Study area and sites.....	49
3.2.2 Geophysical survey.....	53
3.2.2.1. Ground penetrating radar (GPR).....	53
3.2.2.2. Electrical Resistivity Tomography (ERT).....	54
CHAPTER 4 Result	56
4.1 Geomorphological map	56
4.2 Geomorphological criteria analysis	62
4.2.1 Sinuosity Index (SI).....	62
4.2.2. The Radius of curvature (Rc)	63
4.2.3 Channel Width (W)	69
4.2.4 Channel length (L).....	70
4.2.5. Channel centerline migration from 1954 to 2019.....	71
4.3 Sedimentological data analysis	72
4.3.1 Grain-size analysis from Boreholes data	72
4.3.2 River Bank profiles	76
4.4 Electrical Resistivity Tomography (ERT) profiles.....	77
4.4.1 Ground Penetrating Radar	87
CHAPTER 5 Discussion.....	90
5.1 Geomorphological Changes from aerial photographs.....	91
5.1.1. Geomorphological map	91
5.1.2. The change in geomorphic criteria.....	93
5.1.2.1. Channel width (W).....	93
5.1.2.2. Changing in length (L) and sinuosity index (SI)	95

5.1.2.3. Relationships between Rc/W and channel migrations.....	96
5.2 GPR radar facies of fluvial deposit	97
5.3 Relationship between fluvial sediment and ERT lithological classes.....	99
CHAPTER 6 Conclusion	101
6.1 Conclusions.....	101
6.2 Recommendation	102
REFERENCES.....	112
VITA	121



LIST OF TABLES

	Page
Table 1 The variety of satellite pictures and aerial photographs	36
Table 2 Percentage of land use in the Yom River basin in 1973, 1982, 1989, 1993, 2001, and 2009. From (Namsai et al., 2020).	94
Table 3 Based on radar reflection patterns in the study area, radar facies were mainly interpreted from locations 1 and 2. Radar facies from fluvial deposits can be divided into 5 facies.	98
Table 4 The sediment from on-site boreholes as well as the apparent resistivity data from ERT surveys in this study area.....	100
Table 5 Shows the values from measure of river width since 1954 to 2019 and paleochannels.	105
Table 6 Shows the values from measure of SI since 1954 to 2019.....	106
Table 7 Shows the values from measure of channel migration since 1954 to 2019.....	107

LIST OF FIGURES

	Page
Figure 1 Geological map of Phrae Basin and Yom River	4
Figure 2 The Yom River initially flowed through Payao, Phrae, Sukhothai, Phitsanulok, Phichit, and Nakhon Sawan Provinces.	6
Figure 3 The river process domains defined by (a) Geomorphic and environmental effects of instream gravel mining (Schumm, 1977) as depicted by (Kondolf, 1994) and (b) Process domains and the river continuum (Montgomery, 1999).....	9
Figure 4 Channel pattern (meandering, straight, braided) as a function of channel slope and bankfull discharge.....	10
Figure 5 Classification of alluvial rivers.....	11
Figure 6 Schumm's (1977, 1981, 1985) classification of channel pattern and response potential.....	12
Figure 7 Scroll bars and oxbow lakes on the floodplains and point bars at the inner side of bends.....	14
Figure 8 River Allier in France. Scroll bars are visible on the point bar	15
Figure 9 Paired and unpaired terraces.....	18
Figure 10 Basic plan-form modes of meander-bend transformation with examples from modern rivers.....	19
Figure 11 River Cecina (Italy): evolution of a river bend	21
Figure 12 Parameters of Muller's sinuosity index (SI).....	22
Figure 13 Temporal measurement of radius of curvature near the Dampal bends from	23
Figure 14 Channel migration of the Geul River in the Netherlands from 1935 to 1995 ..	25

Figure 15 Process flow chart for interpreting radar stratigraphy and its final use	29
Figure 16 Typical GPR sections in fluvial settings	30
Figure 17 A section of an ERGI profile and a lithostratigraphic profile based on vibrocores are compared.....	32
Figure 18 Phrae Basin map and cross-sections lines of Seismic investigation	34
Figure 19 Three seismic cross-section profiles from Phrae Basin	35
Figure 20 A series of aerial photographs (1954, 1970,1989) were interpreted via a mirror stereoscope, scanned, and processed into digital files for comparison with Google Earth satellite imagery (2012, 2019).	37
Figure 21 Aerial photographs of 1954 period and interpretation map.....	38
Figure 22 Aerial photographs of 1970 period and interpretation map.....	39
Figure 23 Aerial photographs of 1989 period and interpretation map.....	40
Figure 24 A satellite image of 2012 and geomorphological changes interpretation via using Google Earth.....	41
Figure 25 A satellite image of 2019 and geomorphological changes interpretation via using Google Earth.....	42
Figure 26 Map shows SI measure in 1954 period.....	44
Figure 27 The map shows the locations of measurements Rc values in 3 locations from the study area.....	45
Figure 28 The map shows the channel width and centerline migration.....	47
Figure 29 This map illustrates the channel length	48
Figure 30 The geomorphic map displays the sites of the shallow geophysical survey (ERT and GPR) and sediment samples.	51
Figure 31 The sediment samples were taken from boreholes (Left). The river bank profile near the Yom River (Right).	52

Figure 32	The GPR investigation lines from 2 locations in fieldwork investigation.	53
Figure 33	Resistivity investigation lines (Red lines) in six locations	55
Figure 34	Classification by sediment class (derived from Folk, 1954).....	55
Figure 35	The interpretation of Geomorphological map of Study area in 1954.	57
Figure 36	The interpretation of Geomorphological map of Study area in 1970.	58
Figure 37	The interpretation of Geomorphological map of Study area in 1989.	59
Figure 38	The interpretation of Geomorphological map of Study area in 2012.	60
Figure 39	The interpretation of Geomorphological map of Study area in 2019.	61
Figure 40	The graph of SI values from 1954 to 2019 shows the decreasing trend.	62
Figure 41	Rc had measurements from 3 locations from 1954-2019.	64
Figure 42	The changes of radius of curvature and bend tightness ratio (Rc/W) at Bend 1 was decreasing from 1954 to 2019.....	65
Figure 43	The changes of radius of curvature and bend tightness ratio (Rc/W) at Bend 2.	66
Figure 44	The changes of radius of curvature was varied and bend tightness ratio (Rc/W) at Bend 3 was decreasing from 1954 to 2019.....	67
Figure 45	Meander Migration Rate versus Bend Curvature (Rc/W), a number that falls between 1 and 2 indicates that the bend will either cut off the neck or the chute. Bends will erode quickly if values are between 2.5 and 4. Bends will have a low erosion rate if values increase by more than 5, According to the graph-bends 1 and 2 have a value rise of more than 4, which indicates low erosion rates, and bend number 3 trend to cut off(active bend).	68
Figure 46	The graph of Yom channel width	69
Figure 47	The graph shows compared to the length of Yom River from 1954 to 2019 ..	70
Figure 48	The graph shows migration rate / year of Yom River since 1954 to 2019.	71

Figure 49 The graph shows all values of migration rate/year in each location from fifty-three cross-sections	72
Figure 50 Five boreholes lithological analyses from 3 locations in study area. The first site was collected two boreholes from location 1 (A). The second site was collected two boreholes from location 5 (B). The third site was collected one borehole from location 6 (C).....	75
Figure 51 The river profile from this study represents to sedimentology and stratigraphy of paleo-fluvial succession that profile has shown perfect profile on one site at Ban Huai Mai.	76
Figure 52 The 235 m-resistivity survey line covers a meandered scar, point bar, and floodplain show inversion model of ERT from interpretation base on boreholes data and resistivity values at location 1.....	81
Figure 53 The 470m-resistivity survey; investigates the floodplain and point bar show inversion model of ERT from interpretation base on boreholes data and resistivity values at location 2.	82
Figure 54 The 235m-resistivity survey line covers the floodplain and previous channel trace show inversion model of ERT from interpretation base on boreholes data and resistivity values at location 3.....	83
Figure 55 The 235m-resistivity survey line covers the floodplain and the previous channel trace show inversion model of ERT from interpretation base on boreholes data and resistivity values at location 4.	84
Figure 56 The 235m-resistivity survey line covers the floodplain, meander scar, and point bar show inversion model of ERT from interpretation base on boreholes data and resistivity values at location 5.....	85
Figure 57 The 235m-resistivity survey line covers the floodplain and point bars show inversion model of ERT from interpretation base on boreholes data and resistivity values at location 6.	86

Figure 58 The result of GPR was used 100 MHz antenna from location 1	88
Figure 59 The result of GPR was used 100 MHz antenna from location 1 surveyed on the floodplain and point bar,	88
Figure 60 The result of GPR was used 100 MHz antenna from location 2.....	89
Figure 61 Maps and cross-sections of the floodplain at the upper (A), middle (B), and lower sections (C) are given for comparison.	92
Figure 62 The lithological data from well near ERT survey line at location 1 (Department of Groundwater Resources)	108
Figure 63 The lithological data from well near ERT survey line at location 2 (Department of Groundwater Resources).....	108
Figure 64 The lithological data from well near ERT survey line at location 3 (Department of Groundwater Resources).....	109
Figure 65 The lithological data from well near ERT survey line at location 5 (Department of Groundwater Resources).....	109
Figure 66 The lithological data from well near ERT survey line at location 6 (Department of Groundwater Resources).....	110

CHAPTER 1

INTRODUCTIONS

1.1 Background

1.1.1 General background

In its broadest definition, geomorphology refers to the area of the geosciences that is interested in the evolution of the Earth's surface characteristics. Geomorphology, in a more specific form, is the study of surface features whose shape is principally affected by endogenic (volcanic, tectonic, and isostatic processes) and exogenic processes (weathering, erosion, transportation, deposition, denudation). (Scheidegger, 1982). In recent decades, the demand to improve utilities, agriculture, and other anthropogenic impacts in recent decades has resulted in a rise in population, which has accelerated the rates of land degradation and transformation (Hooke et al., 2012). Due to this, people are most likely the main geomorphic force now sculpting the surface of the Earth.

Rivers have a significant impact on how the topography of the earth is shaped. They take action in a variety of methods, including removing material from its confines, transferring it, and dumping it in distant locations. Even over relatively short periods of time, river paths cannot be considered of as stable. (Glover & Johnson, 1974) has so provided evidence of the river channels being abandoned in several cases in very short periods of time. There are two ways that material might be removed from the confining channel by flowing water: either the channel is being scoured out, deepening it, or the removal takes place on the lateral.

Typically, meander processing in floodplains creates concave on the erosion side and convex on the oppositional deposition side. Rising rates of erosion and deposition can alter the geometry of the channel balance, increasing migrations and sinuosity (SI). Since geomorphological features can be seen on avulsion plains, meander processes will leave traces of evidence of channel modifications, such as oxbow lakes and meandering scars, on floodplains (Choowong, 2011).

Specifying river meander behavior and the forms they take has definitely benefited in recent years from a variety of important developments. Current studies are revealing certain characteristics in meander behavior, and lengthy ideas about the evolution of equilibrium forms and regular meander morphology are currently being investigated. The diversity of measurement and analysis techniques has also increased. For these reasons, it is helpful to look at the most relevant views and information on meander changes (Yousefi et al., 2016).

Changes in geomorphology, use aerial photographs, satellite images, and historical maps to analyze landforms from various eras. These images can illustrate geomorphic changes from a bird's eye view, however, it is impossible to determine how sediment deposition and processing have changed beneath the surface. Borehole surveys have been used in the past to examine the data from the subsurface, but they are costly and it is challenging to link the accurate data from each borehole. Ground penetrating radar (GPR), a non-invasive geophysical technique that might detect electrical discontinuities in the shallow subsurface (less than 50 m), was first applied for subsurface investigations in 1970. It performs by generating, transmitting, propagating, reflecting, and receiving continuous pulses of high-frequency electromagnetic waves (MHz). (Neal, 2004). Additionally, GPR has a variety of uses, particularly glaciology, sedimentary, and civil engineering can be included. GPR can be used to analyze rocks, stratigraphy, and sedimentary layers that produce high-resolution profile images, as well as their sedimentary structure, geometry, and continuity in geological fields. (Jol & Bristow, 2003). Even though the GPR survey technique can instantly gather data and provide high-resolution profile photographs in shallow sedimentary layers, it can nevertheless function in certain restricted conditions. As a result, the sedimentary subsurface profiles from Electrical Resistivity Tomography (ERT), which can operate in a wider range of settings, were displayed using the Electrical Resistivity Survey. A direct current (DC) generator or low-frequency alternating current released into the ground is used to detect the electric potential difference in order to achieve the function of electrical resistivity, which is to measure the subsurface state.

This value can analyze the physical characteristics of sediments from diverse mineral compositions, pores, and inter-pore fluid based on potential differences (Baines, 2002).

1.1.2 Study area background

The Yom River, which flows mainly from north to south through the Phrae basin, has significant tributaries from the northeast and east that transport sediments there. The Phrae Basin, which covers an area of 1,100 square kilometers and is the largest basin in northern Thailand, is comprised of a layer of Cenozoic sediment with a thickness of nearly 2 kilometers. This basin was a triangle-shaped form that was located in a north-northeast to south-southeast direction. Its longitudes and latitudes are 18° 00' N to 18° 30' N and 100° 05' E to 100° 20'E, respectively. The Triassic Lampang group, which consists of shale, mudstone, and limestone, surrounded the basin in the majority; Carboniferous-Permian rocks can also be found in some places. To the east and west, Permian limestone, shale, and chert are less widespread (Figure 1).

The Phrae basin encountered five tectonic events in total, along with five sedimentary cycles in a stratigraphic sequence, according to (Srisuwan, 2000). This research used co-analyzed boreholes, outcrop, and seismic data in the basin. Each cycle begins with the beginning deposition of braided channels and floodplains, which gradually transitioned to shallow swamp-lake and lake margin deposition, which was followed by the deposition of crevasse splays. Doi Khun Yuam in the Phi Pan Nam Mountain Range where the Yom River has its beginnings. It is located in Amphoe Pong and Amphoe Chiang Muan, Phayao Province. The Yom River initially flowed through a valley with a very steep slope; there are narrow plains along the river in some places; afterward, it flowed into the plains of Phrae Province; after that, it flowed into the western valley; and finally, it flowed in a southern direction into the plains of Sukhothai Province, Phitsanulok, Phichit, and Nakhon Sawan then flowed to converge with the Nan River at Ban Koei Chai, Chum Saeng District, Nakhon Sawan Province. The river runs for around 735 kilometers in total length (Figure 2).

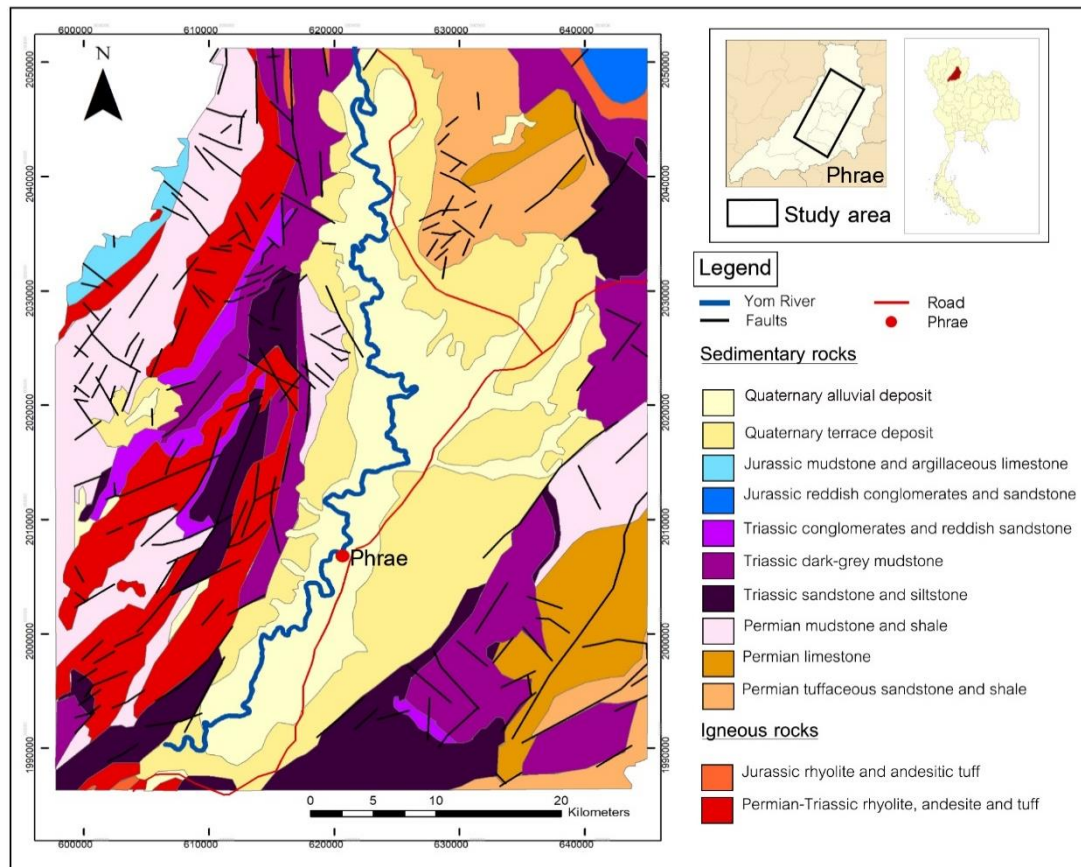


Figure 1 Geological map of Phrae Basin and Yom River (Modified from Department of Mineral Resources, 2007).

The Yom River is the main tributary of the Chao Phraya River, which flows from north to south. In the province of Phrae, the upper Yom River passes through a basin between two mountains. The purpose of the upper Yom River was chosen for this study due to its meandering in an active basin, which has the potential to significantly migrate and modify landforms. Furthermore, since this region periodically experiences both flooding and drought, the Office of the National Water Resources began a Yom-Long project to decrease the risk of both events by managing and reserving water at Oxbow lakes and Meander scars. (National Office of Water Resources, 2020). As a result, this river is a fascinating location to research sediments, paleochannel structure, river mechanics, and river evolution. This study will analyze aerial photos, satellite images, and topographic maps from various time periods to examine the

geomorphological changes in the location. The differences in the geomorphology change over a 65 - year period were assessed using geomorphological criteria. This research will focus on channel sinuosity (SI), bend radius of curvature (Rc), width (W), length (L), and channel migration rates that can assist in comprehending the natural processes of the river (Leopold, 1960); (Williams, 1986). Additionally, electrical resistivity surveys and ground-penetrating radar (GPR) are used to determine the structure and sediment deposits of paleo-channels without damaging the subsurface sediment layer.

1.2 Research Objective

2.1. To study the geomorphological change of the Upper Yom River in Phrae Province.

2.2. To investigate the thickness of the channel deposits for the river behavior and its direction.

1.3 Scope of the Study

This study area covers a total of 1,100 square kilometers (about the Yom River basin in Phrae Basin). Furthermore, this study will interpret the geomorphological changes by aerial photographs, satellite images cover in 65 years from 1954, 1970, 1989, 2012 and 2019.

1.4 Benefits

4.1. Geomorphological changes of the Upper Yom River in Phrae Basin.

4.2. The structure and thickness of channel deposits and paleo-channel that can assess the direction of river flow and river behavior.

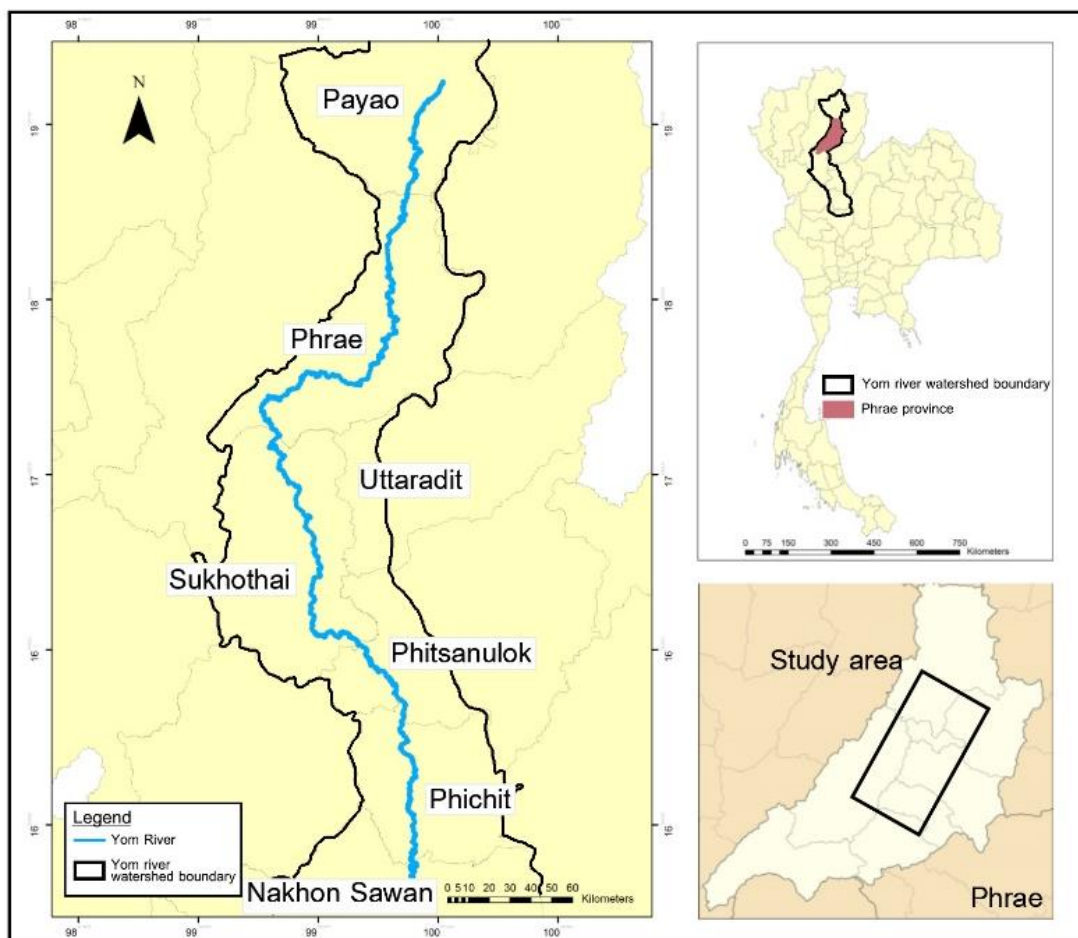


Figure 2 The Yom River initially flowed through Payao, Phrae, Sukhothai, Phitsanulok, Phichit, and Nakhon Sawan Provinces. The river runs for around 735 kilometers in total length.

CHAPTER 2

Literature Review

A morphological continuity is assumed to be formed by river channel patterns. There are three types of plan features (straight, meandering, and branching), and there are three different structural levels of fluvial relief that make up this continuum, which is three (floodplain, flood channel, and low-water channel). These three characteristics are used to define the variety of patterns. Stream power, which is determined by water discharge and river slope, is among the most significant factors in channel development. The higher the branch tendency, the greater the stream power, although the threshold values of stream power vary for each of the three hierarchical levels of channel relief. Effective discharge curves can be used to analyze the pattern type. The channel pattern is defined by the hydrological regime and the critical river power levels together (Alabyan & Chalov, 1998).

2.1 River channel pattern

In order to provide a process-based understanding of sediment flow through river networks over geologic time, (Schumm, 1977) split rivers into sediment production, transfer, and deposition zones (Figure 3a). Process domains are regions of the river network that, on the whole, approximately correspond to the source, transport, and response reach in mountain basins. They are defined by particular suites of related disturbance processes, channel morphology, and aquatic habitats (Figure 3b) (Montgomery, 1999). Although using process domains to categorize rivers is a coarse filter that often groups together different channel types, it does identify the basic geomorphic units within the landscape that shape overall river behavior and the related aquatic habitats. As a result, it is a useful tool for initiatives to manage land and promote conservation (Buffington & Montgomery, 2013).

The majority of river classifications that have been created involve characterizing the morphology of the channel (i.e. the planform geometry, such as straight, meandering, or braided), and these classifications can be approximately categorized as

follows: (1) quantitative relationships (which may be either empirical or theoretical), and (2) conceptual frameworks.

Quantitative relationships: At a given discharge, braided channels occur on steeper slopes than meandering rivers, according to (Lane, 1957) and (Leopold & Wolman, 1957) (Figure 3). Both methods developed a continuum of channel patterns, but (Leopold & Wolman, 1957) proposed a threshold between meandering and braided rivers (Figure 3), giving a way to foresee changes in channel patterns as a result of altered discharge or channel slope. Both studies recognized that other parameters, like grain size, sediment load, riparian vegetation, channel roughness, width, and depth, all impact channel patterns. Later researchers adjusted the framework in Figure 3 to account for grain size (which changes where the boundary between various channel patterns is located) and to distinguish between anastomosing and wandering channels. Wandering rivers lie in the transition zone between meandering and braided morphologies (Desloges & Church, 1989), whereas anastomosed rivers are innovative channels divided by islands cut out of the floodplain (David Knighton & Nanson, 1993), which are distinct from braided channels formed by bar deposition and subsequent in-channel flow splitting ((Leopold & Wolman, 1957)); ((Bridge, 1993)). A wide range of additional variables have also been suggested as ways to distinguish between different channel patterns, including valley slope as compared to stream slope, stream power, width-to-depth ratio, excess shear velocity or excess Shields stress (the ratio of applied shear velocity or excess Shields stress to the critical value for an emerging movement of the streambed), Froude number, bed load supply as compared to transport capacity, and bank strength.

More recently, (Beechie et al., 2006) created a GIS model to forecast channel patterns as a function of slope and discharge, showing that unstable and laterally migrating channels (i.e. braided and meandering patterns) have correspondingly younger and more dynamic floodplain surfaces than stable, straight channels. Because channel and floodplain dynamics impact the diversity and quality of river system

habitats for aquatic, riparian, and hyporheic organisms, this discovery is essential for ecosystem management.

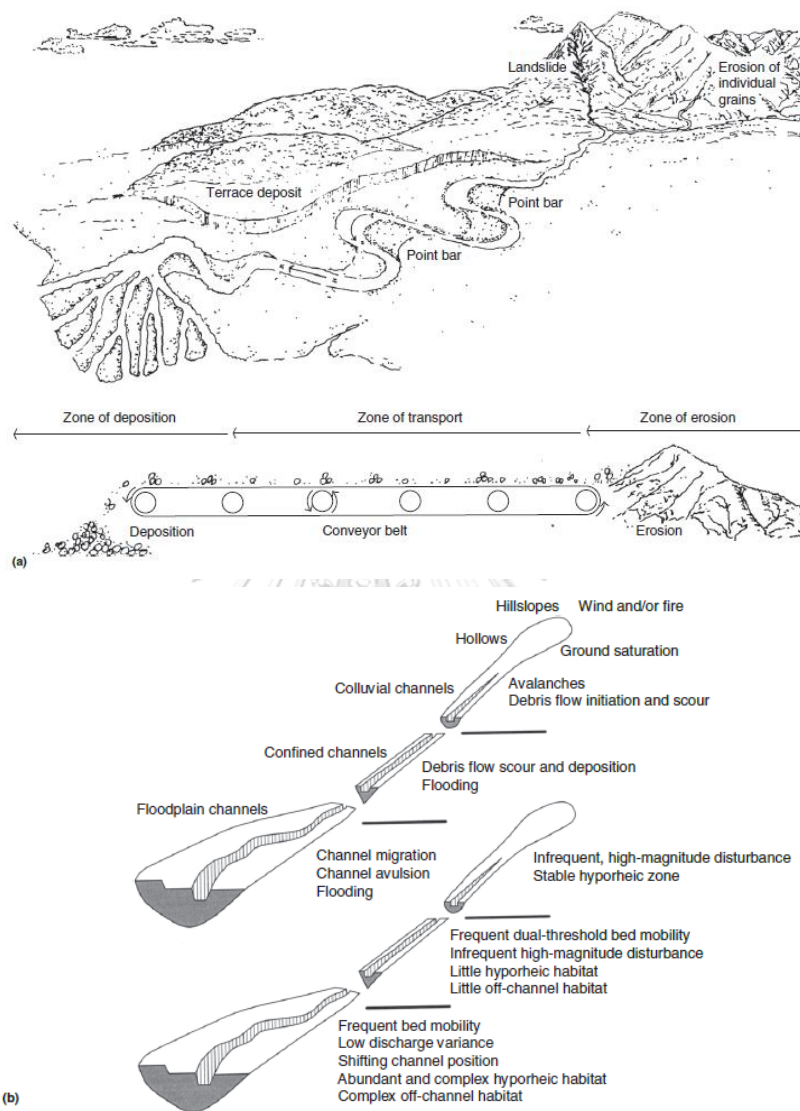


Figure 3 The river process domains defined by (a) Geomorphic and environmental effects of in-stream gravel mining (Schumm, 1977) as depicted by (Kondolf, 1994) and (b) Process domains and the river continuum (Montgomery, 1999).

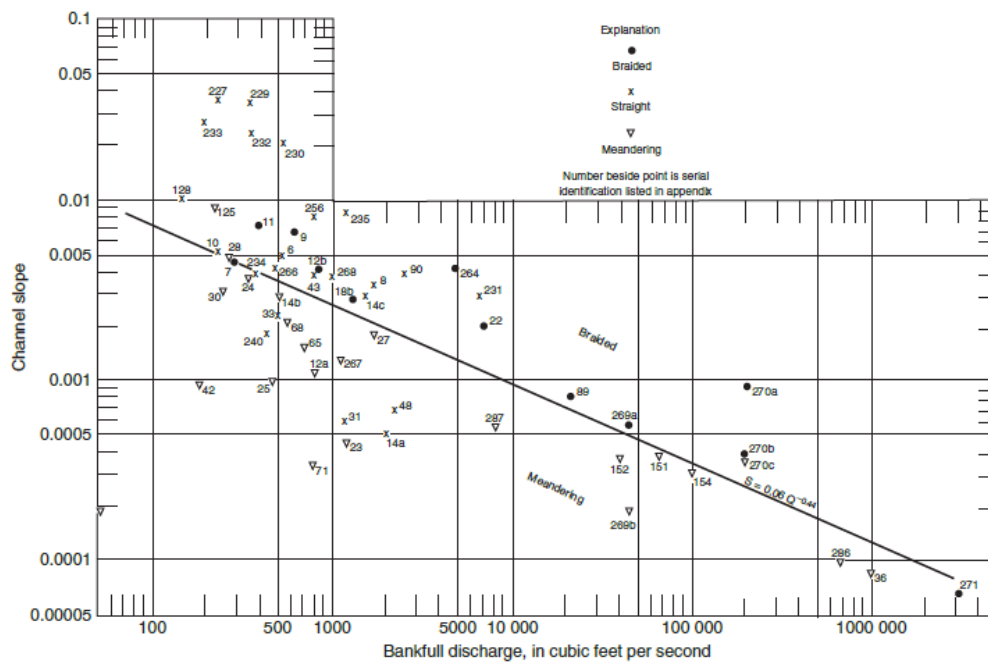


Figure 4 Channel pattern (meandering, straight, braided) as a function of channel slope and bankfull discharge. Reproduced with permission from (Leopold & Wolman, 1957). River channel patterns: braided, meandering, and straight.

Conceptual frameworks; Schumm's (1960, 1963b, 1968, 1971a, b, 1977) studies on sand and gravel-bed rivers in the western United States' Great Plains emphasized that the floodplain's silt-clay concentration and the river's imposed load (size of sediment and mode of delivery) have a significant impact on the channel pattern and stability (providing cohesion necessary for the development of river meandering). Using these observations as a base, (Schumm, 1963, 1977; Schumm, 1981, 1985) proposed a conceptual framework for classifying alluvial rivers that related channel pattern and stability to (1) the silt-clay content of the banks, (2) the mode of sediment transport (suspended load, mixed load, bed load), (3) the ratio of bed load to total load (a function of stream power, sediment size, and supply), and (4) the slope and the width-to-depth ratio of the channel (Figure 4). Since, the categorization proposed by Schumm (1963a, 1977, 1981, 1985) has been improved to incorporate a wider array of channel patterns, including steeper morphology seen in mountain rivers (Figure 5).

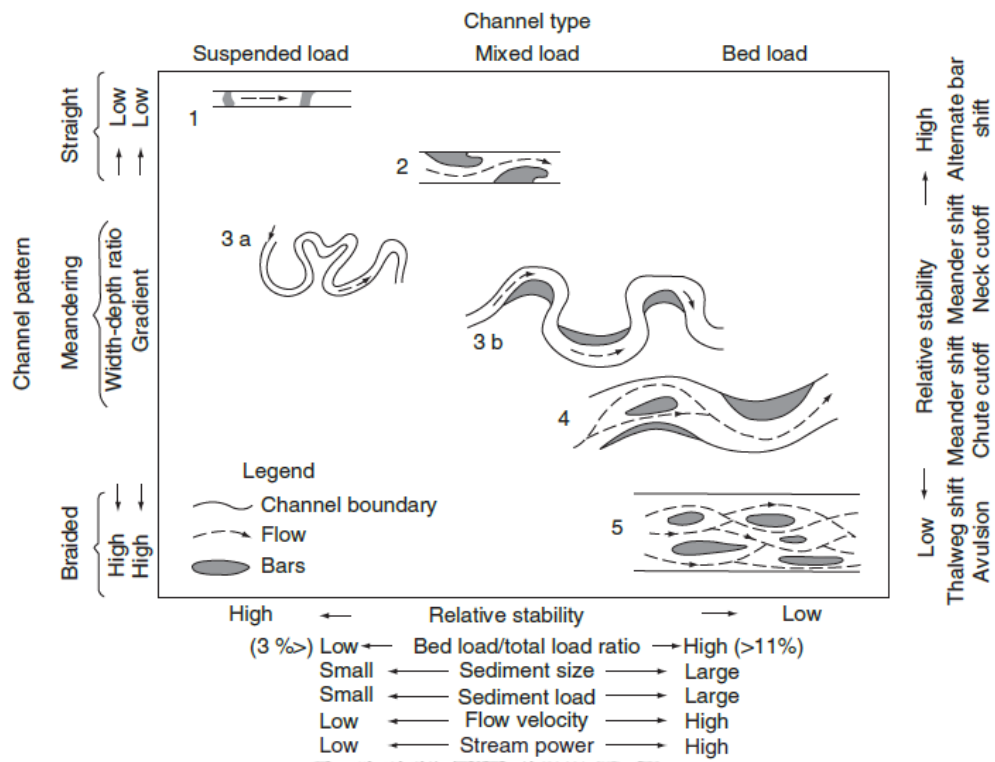


Figure 5 Classification of alluvial rivers. Reproduced from Figure 4 in Schumm, S.A., 1981. Evolution and response of the fluvial system, sedimentological implications (Schumm's (1963a, 1977, 1981, 1985)).

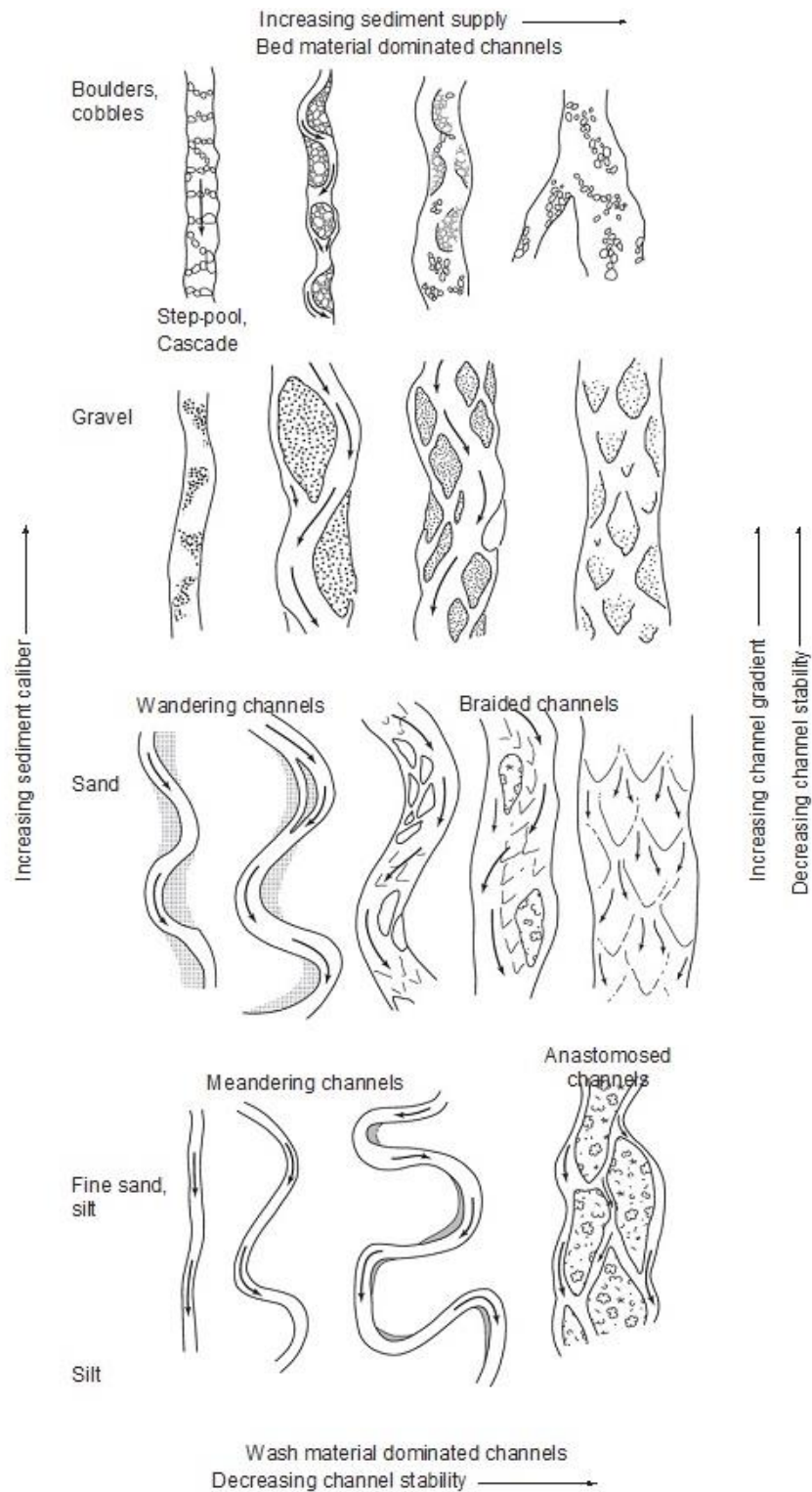


Figure 6 Schumm's (1977, 1981, 1985) classification of channel pattern and response potential as modified by (Church, 2006).

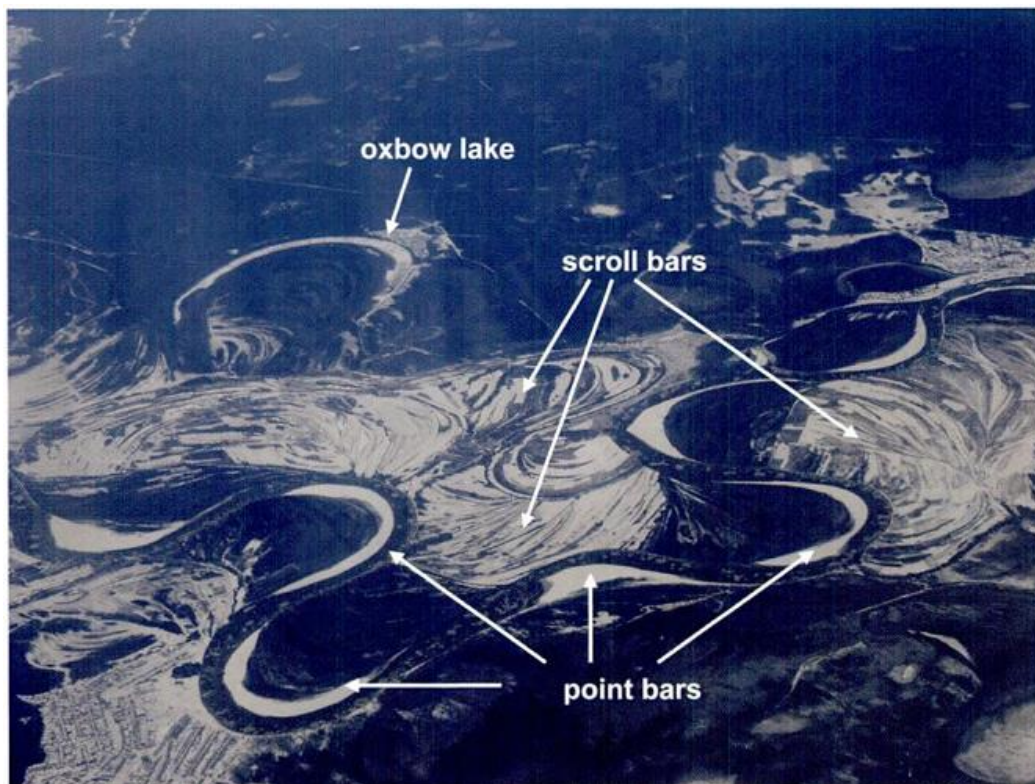
2.2 Meandering fluvial landforms

There are many different types of planforms seen in alluvial rivers. There are rivers generated by a single channel and rivers having many conveying channels, divided by transition sediment deposits or almost permanent islands. As a river's morphology continually changes as it flows from the highlands to the sea, different planform types can even be seen along the same flow path. Rivers often have an irregular planform in their upper parts, which is mostly controlled by the local geology. Gravel, cobbles, and boulders make up the river bed's coarse sediment. Pools and riffles or runs, which alternate between being deep and shallow, are what give the longitudinal bed level profile its distinctive look.

Most usually, meandering rivers could be found in low-land alluvial plains that have cohesive soils and a thick covering of vegetation. They lack significant longitudinal width changes and have a single, very steady sinuous channel. The active form of the point bar is a beach that is created by a sediment deposit at the inner side of the bends (Figure 7). On the side of the channel with the higher flow velocity that is opposite from the channel, there is a pool. As a result of erosion, the outer bank gradually disappears, while sedimentation causes the inner bank to accumulate. Since bank retreat and accretion have essentially the same rate over the long term, the channel width exhibits short-term oscillations but insignificant long-term changes. River bends gradually grow and move as a result of the interaction between bank advance and retreat.

A structure of ridges and swales (scroll bars) is formed by the old placements of the top of the active parts of the point bars which can be observed across floodplains (Figures 7 and 8). The natural levees that are created during floods when the water overflows its confined channel and sediment are dumped close to the channel edge are what provide the scroll bars their distinctive ridges (Pizzuto, 1987). The sediment deposits that occur at lower flow stages are related to the swales. The translation and expansion of the meander continue until the flow wraps up the bend (neck cutoff).

In the beginning, mostly a fraction of the flow passes through the bent neck, but as this fraction gradually rises, the old path is finally abandoned. The former channel now becomes an oxbow lake (Figure 7), which slowly sedimentary up and vanishes. The existence of cutoffs reduces meander growth, which is also known as the meander belt, river corridor, or river stream way, causing the river to seem to migrate in a limited area.



CHULALONGKORN UNIVERSITY

Figure 7 Scroll bars and oxbow lakes on the floodplains and point bars at the inner side of bends (in white, covered with snow) in a meandering affluent of the Ob River, Russia (courtesy of Saskia van Vuren) (Crosato, 2008).



Figure 8 River Allier in France. Scroll bars are visible on the point bar (courtesy of Erik Mosselman) (Crosato, 2008).

2.2.1 Oxbow Lake



The most common kind of fluvial lake is an oxbow lake, which is a crescent-shaped body of water with a distinctively curved form (Hutchinson, 1957). The term "cutoff lakes" also applies to oxbow lakes. (Neuendorf et al., 2011). Such lakes commonly develop as a result of river meandering in unaltered floodplains. A river or stream will develop a sinuous channel when the outside of its bends erode away and sediments build up on the inside, creating a curve that resembles a horseshoe. The fluvial channel eventually forms a cutoff meander by cutting through the limited neck of the meander as a result of its meandering. Because the river is separated from its banks and can flow directly over the neck and erode it with the full power of the flood, the final break-through of the neck, known as a neck cutoff, frequently happens during a severe flood. River water flows into the endpoints of a cutoff meander after it has developed, creating little delta-like features at each end of it during floods. A motionless oxbow lake that is isolated from the flow of the fluvial channel and independent of the river is created when these delta-like landforms block either end of the cutoff meander. Fine-grained silt is deposited into the oxbow lake during floods by the flood flows. As a result, over time, oxbow lakes often fill up with fine-grained, organic-rich sediments (Toonen et al., 2012).

2.2.2 Point bar

A point bar, commonly referred to as a meander bar, is a fluvial bar that develops as a result of the gradual, frequently periodic addition of noncohesive sediment deposition on the inside bank of a meander and the channel's associated migration toward its outer bank (Neuendorf et al., 2011) (Reineck & Singh, 2012). It is known as lateral accretion. When the point bar is covered during high water or floods, lateral accretion normally occurs. Sand, gravel, or a mix of the two are frequently found in sediment. Some point bars underlying material may grade into silty sediments as it progresses downstream. The vertical sequence of sediments that make up a point bar gets fining upward within a single point bar as a result of the decreasing velocity and power of current from the thalweg of the channel to the upper surface of the point bar during the sedimentation process. For instance, it is common for point bars to fining upward from gravel at the base to fine sand at the top. Typically, the source of the sediment is an upstream cut bank from which sand, boulders, and debris have been eroded, dragged, and rolled downstream to the inner bank of a river bend. These silt and debris finally get deposited on the slip-off slope of a point bar on the inner curve (Chant, 2002).

2.2.3 Scroll bars

Scroll bars are formed by the continual lateral migration of a meander loop, which results in an asymmetrical morphology of ridges and swales (Woolfe & Purdon, 1996) on the inside of the bends. The topography runs mainly parallel to the meander and is associated with migrating bar forms and back bar chutes, which, through a process known as lateral accretion, remove material from the outside of the curve and deposit it in the slower-moving water inside the loop. Cross-bedding and an upward-fining pattern define scroll-bar sediments.

If the river keeps occasionally meandering through the plain without reducing its level. The remnants can be seen all over the oxbow lakes, and whenever the river level is lowered, those landform remnants will continue to exist in an oscillating zone known as the avulsion plain, which is the lowest point where rivers or streams cannot continue to erode vertically or lateral, such as lakes or water levels in reservoirs. This level is seen as steady as well. Its base level also changes if its level is altered or destroyed. It has been described as the final probable point at which the river can suddenly erode vertically (temporary base level). This amount of stability is also impacted by the groundwater table. The terraces in many areas, mainly in Thailand, have been explained by the theory of base-level shifting. Terrace provides historical evidence of river oscillation evolution. The terrace's several steps would immediately appear as though the level was constant and dropping and the permanent effect on river vertical erosion before starting to degrade laterally after reaching a new base level. The number of steps on a certain terrace of a large river may be utilized to assess the times of changing erosion levels in that river. If the river hasn't stabilized, it will often oscillate. results in paired terraces since it happens on both sides of the river. But the slope is also influenced by the river's oscillation. Consequently, if the level is stable, several areas found the evolution of meandering in a single river bank. The terrace often referred to as an unpaired terrace, could be located on one side of the river (Choowong, 2011) (Figure 9).

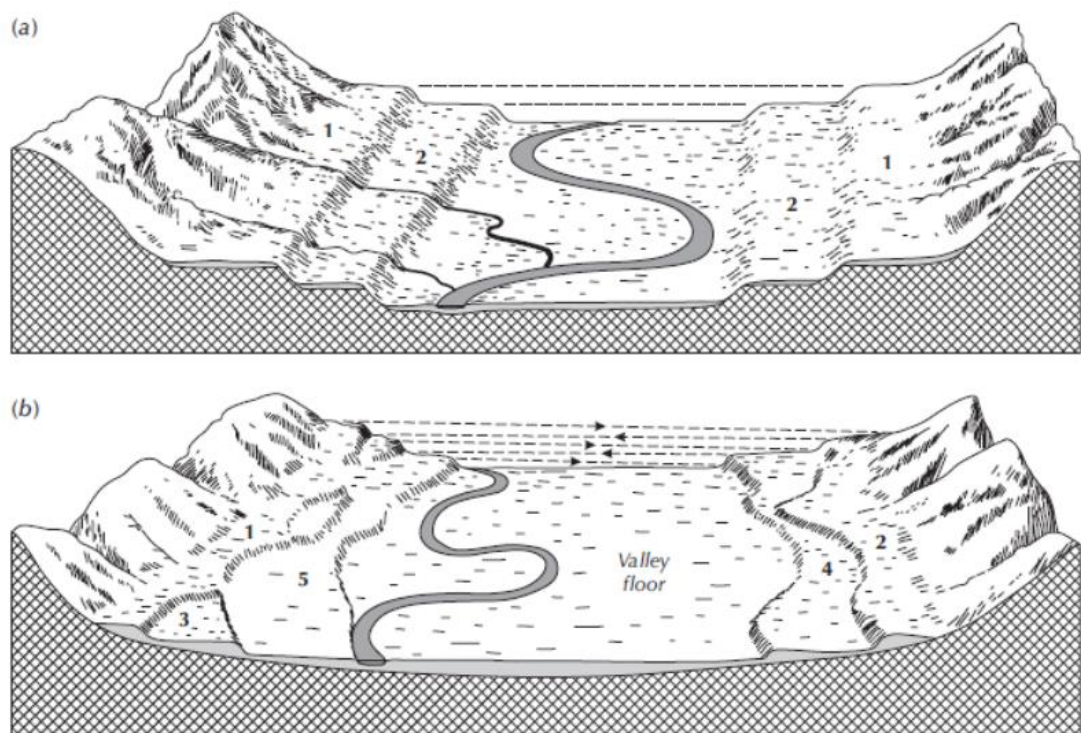


Figure 9 Paired and unpaired terraces. (a) Paired, polycyclic terraces. (b) Unpaired, noncyclic terraces. The terraces are numbered 1, 2, 3, and so on. Sources: Adapted from Sparks (1960, 221–23) and (Thornbury, 1954).

2.3 Planform evolution of meandering rivers

The shape, width, thickness, and variability of the ensuing meander-belt sand body are ultimately determined by the plan-form evolution of a meandering river channel as well as its bankfull depth, aggradation rate, and connectedness of accumulated point-bar features. Idealized geometrical shapes, such as sine curves or circular arcs (Brice, 1974) have been fitted to channel bends in order to explain the pattern of their migration. This has been done in order to analyze the complexity of planform changes in recent meandering rivers. It has been determined that one or more of the following essential types of transformation—expansion, translation, and rotation—can be used to explain how channel bends evolve.

When the bend apex extends transversely away from the channel belt axis, the expansion increases the channel-bend curvature and flow-path length, and hence the channel sinuosity (Figure 10A). The translation preserves the channel's sinuosity, but the bend's peak moves down the valley parallel to the channel-belt axis (Figure 10B). The movement of the bend apex away from (Figure 10C) or in the direction of the channel-belt axis is how rotation creates meander bend asymmetry (Figure 10D). These are comparable with findings made from aerial images of meander scrolls in contemporary rivers and frequently appear in combination (Jackson, 1976) . Other factors, such as the relative rate of channel aggradation, the development of secondary bends or meander lobes within an excessively expanding meander, the formation of intra-channel chute bars, and the abandonment of channel bends by chute or neck cut-off, may also contribute to increased architectural complexity.

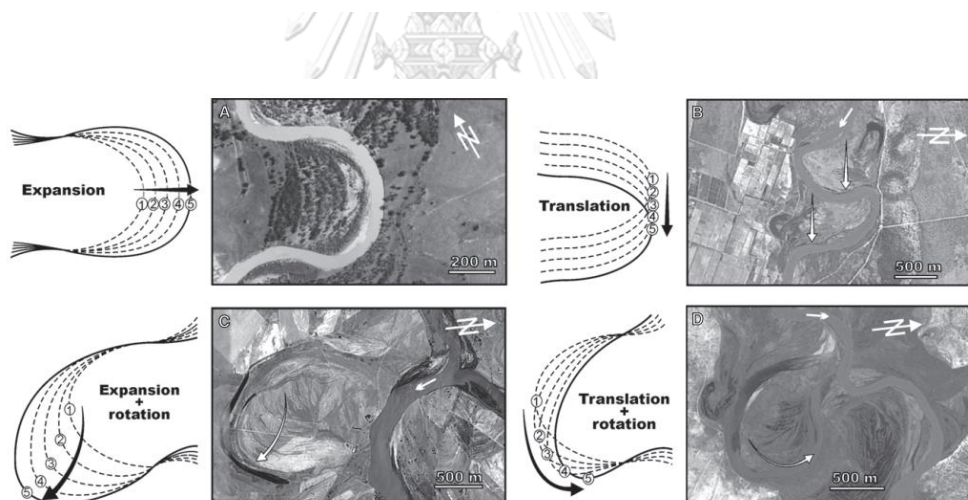


Figure 10 Basic plan-form modes of meander-bend transformation with examples from modern rivers (images with geographical co-ordinates from Google Earth): (A) Murray River, Australia; (B) Rio Colorado, Argentina; (C) Rio Negro; and (D) Rio Colorado, Argentina.

2.4 Geomorphic Criteria

The geomorphic planform parameters include index (SI), the radius of curvature (R_c), channel width (W), channel length, and channel migration.

2.4.1 Channel Width (W)

A relatively uniform river width that may be thought of as constant across time characterizes meandering rivers. The opposing dynamics of bank erosion and accretion, as well as variations in bed level, determine a river's cross-sectional form (Crosato, 2008). The channel width is reduced by bank accretion, but bank erosion has the reverse effect. Hence, the equilibrium river width can only be achieved if opposite bank accretion and bank erosion are balanced out. In this instance, there are no long-term trends (narrowing or widening) in the river's width, while there may still be periodic oscillations. The river changes directions as a result of bank progress and retreat.

In certain meandering rivers, the straight sections between opposite bends are narrower and the river bends themselves are broader. This could be brought on by the fact that opposing bank accretion and bank erosion alternate rather than happening simultaneously (Figure 11). In addition, bank erosion happens during or soon after flood events, whereas bank accretion occurs during high flow stages (deposition) and low flow stages (consolidation and plant cover) and is typically significantly slower.

The main indication for exhibiting a channel's stage and evolution features is the width of the channel at any given time, which corresponds to the channel's cross-sectional distance. (Bag et al., 2019).

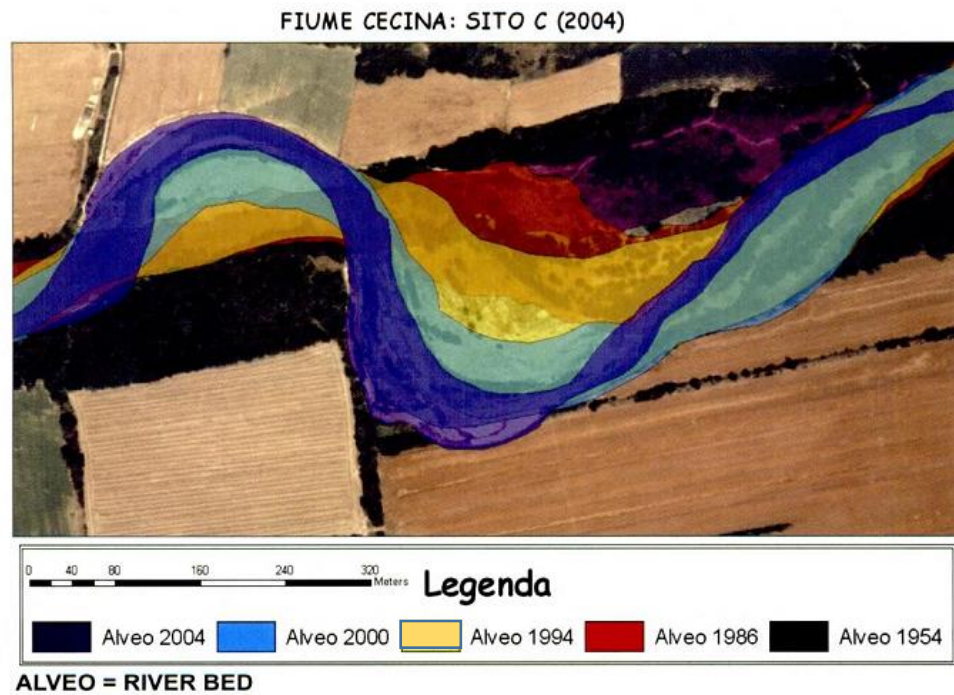


Figure 11 River Cecina (Italy): evolution of a river bend (Figure 7). It is clear to observe that the two phenomena of bank erosion and accretion do not occur simultaneously based on the differences in color (Crosato, 2008).

2.4.2 Sinuosity Index (SI)

The sinuosity of meander rivers is characterized by the ratio between the length of the river measured at its thalweg (line of maximum depth) or along its centerline and the valley length between the upstream and downstream parts. (Rust, 1977). Three periods of the SI coefficient are used to categorize the three types of river shapes. A river is practically straight if the value is less than 1. A river is sinuous when the coefficient is 1.05 but not higher than 1.25. It is evident from 1.25 to 2 that the river meanders. It is quite wandering up to number two.

SI and meandering ratio are frequent indicators of channel activity. Channel length divided by down valley length is used to compute SI (Figure 12).

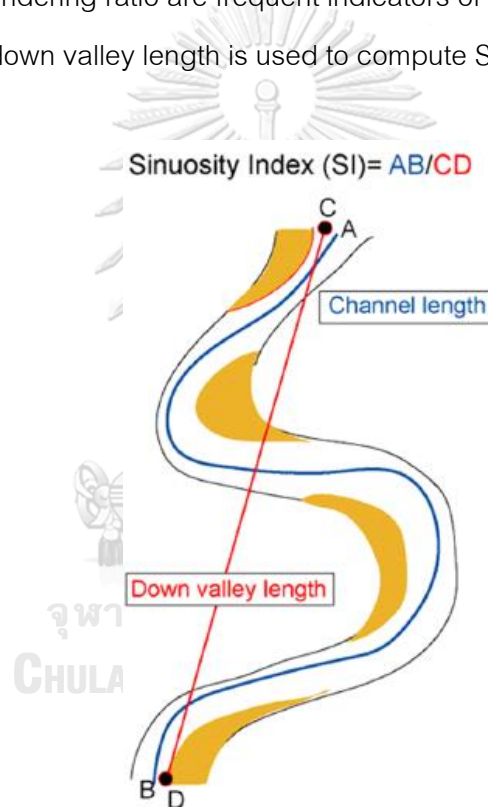


Figure 12 Parameters of Muller's sinuosity index (SI) , (Nimnate, Choowong, et al., 2017)

2.4.3 Radius of Curvature (Rc)

The radius of curvature, or R_c , is one of the metrics used to calculate the curve of a river. The radius of curvature (R_c), which measures how "tight" a single meander bend is, has an inverse relationship to sinuosity. The radius of a circle that fits the meandering arc from the bank-full channel's edge to the intersection of two lines that perpendicularly bisect the tangent lines of each meander departure point is used to calculate the R_c (Figure 13) (Bag et al., 2019).

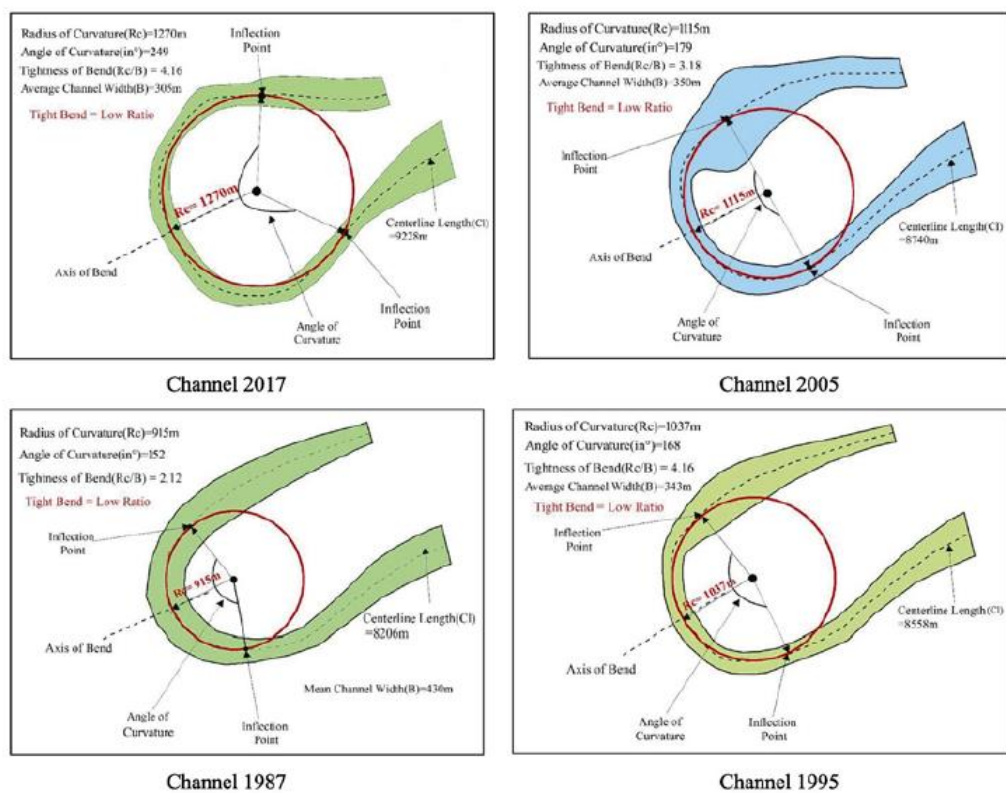


Figure 13 Temporal measurement of radius of curvature near the Dampal bends from (Bag et al., 2019).

2.4.4 Channel length

A stream's length is determined by measuring the length of the stream channel from the beginning to a particular location or to the outlet. This distance can be determined using a map or aerial photos. It is measured along the geometric axis, or the line of greatest depth, on large-scale maps. The source is recognized as the point where a stream originates, which often correlates with the location where the smallest continuous stream manifests. A river channel's map projection is often measured to determine its length. This is notably true for plain areas where rivers have very slight slopes along their longitudinal profiles (Zăvoianu, 1985). By measuring the length of the Bhagirathi River channel midway between the left and right banks of the channel polygon (Bag et al., 2019) have determined its length. The neck cutoff has resulted in a reduction in channel length, highlighting the fact that meander loop cut-off, not lateral river course migration, is what is driving the Bhagirathi river's length to vary at a quicker rate.

2.4.5 Channel migration

Long-term "channel migration" or "meander migration" is a process known as translation and extension that occurs in the supposedly stable meanders (Figure 14) according to (Brice, 1974). The two processes of bank erosion and accretion, which result in bank retreat and advance, respectively, are what contribute to the gradual evolution of river geometry. At river bends, sediment is eroded from the outside banks, producing local bank retreat, and is then further deposited downstream, close to the inner bank (Friedkin, 1945), where it aids in the accretion of the point bar and bank advance.

For rivers to keep their meandering planform, it's necessary that, throughout time, bank retreat be balanced out by bank advance on the other side of the channel. In the absence of this, either the river gradually enlarges and finally develops anabranches or braids, or the river gradually silts up and disappears.

Time sequential bank line diagrams based on historical data (Hooke & REDMOND, 1989) and the presence of scroll bars inside the meander belt, representing the ancient channel placements, both give evidence for meander migration.

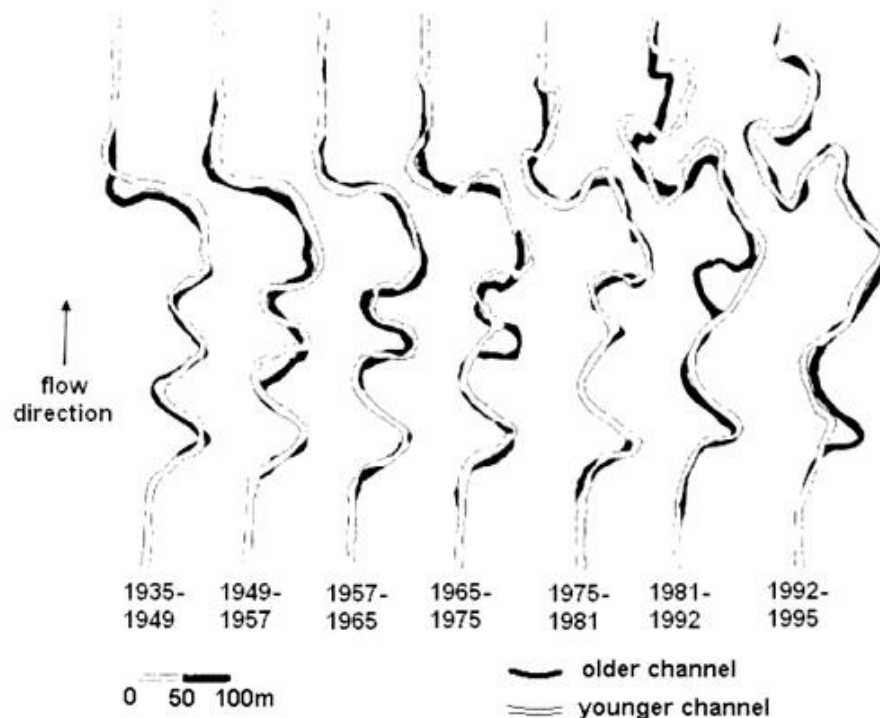


Figure 14 Channel migration of the Geul River in the Netherlands from 1935 to 1995 (Stam, 2002) Picture (Spanjaard, 2004).

Meander migration is an occasional occurrence (Nanson & Hickin, 1983); (Pizzuto, 1994). High, infrequent discharges increase the elevation of the channel margins and cause net bank and bed erosion, which widens the channel. By aggradation and terrace development at the inner side of bends, lower, more frequent flows generate channel narrowing, which moves the thalweg in the direction of the eroding bank. For this event, the type of sediment that makes up the river bed and banks, the patterns of high and low releases, and the existence of riparian vegetation are all essential components.

In general, the position of the pool in relation to the bend apex, the shape of the bend, and the features of the eroding bank all influence the direction—upstream or downstream—of meander migration. The most frequently occurring meanders move in a downstream direction because the largest near-bank flow velocities and water depths are found downstream from the bend apex. According to studies, the ratio of the local

channel curvature radius (R_c) to the bankfull river width (W) affects the local channel migration rates. Reach-averaged channel migration rates reach a maximum depending on the river's sinuosity and change with the evolution of bend and sinuosity expansion (Friedkin, 1945).

2.5 Geophysics

Core drillings, bank exposure sampling, and other invasive methods to measure sediment permeability and the geographic extent of identified low conductivity structures important to groundwater and surface water exchange are costly, time-consuming, and may modify the conditions being studied (Binley, 2015). These earlier, more established techniques offer little spatial information on hydrological characteristics and are frequently inappropriate for assuming the spatial complexity of alluvial sediment systems necessary to allow a thorough hydrogeological characterization (Clifford & Binley, 2010).

To investigate the spatial complexity of alluvial deposits, a variety of geophysical techniques, including electrical techniques, electromagnetic induction (EM), and ground penetrating radar (GPR), have been explored and used (Binley, 2015). Hydrogeological applications have frequently used near-surface geoelectrical techniques such as vertical electrical soundings (VES) and electrical resistivity tomography (ERT) ((Daily & Ramirez, 2000); (Reynolds, 2011)). However, they have not been applied frequently for characterizing complex hydrofacies distributions in riparian zones and streambed environments due to their limitation with accurately resolving lithological boundaries between hydrofacies (Bersezio et al., 2007) and strategic difficulties in setting up larger-scale in-stream surveys in specific.

Aerial photographs, satellite images, and historical maps are used to examine the geomorphology of diverse landforms. From above, these photographs can show geomorphic changes, but it is hard to determine how sediment deposition and processing have altered below the surface. GPR, a non-invasive geophysical method, may be able to find electrical discontinuities in the shallow subsurface. Although the GPR survey method can quickly collect information and deliver high-resolution profile

images in shallow sedimentary layers, it can nevertheless work in some limited circumstances. As a consequence, the Electrical Resistivity Survey was used to illustrate the sedimentary subsurface profiles obtained via Electrical Resistivity Tomography (ERT), which can function in a larger variety of conditions. Based on potential differences, this value may examine the physical properties of sediments from various mineral compositions, pores, and inter-pore fluids.

2.5.1 Ground Penetrating Radar (GPR)

Ground penetrating radar (GPR) is a non-invasive technique mostly used for subsurface research (Cassidy & Jol, 2009; Neal, 2004). High frequency electromagnetic (EM) waves in the range of 10-1000 MHz are used in GPR to detect changes in the shallow subsurface's dielectric characteristics (Neal, 2004). GPR is commonly used to quantify hydrofacies because of its excellent spatial resolution at higher measurement frequencies, ability to determine boundaries, and quick measurement periods. (Theimer et al., 1994; Heteren et al., 1998; Jol & Bristow, 2003) have agreed that poor conductivity layers can severely attenuate GPR signals without limiting the depth of penetration. GPR enables for high resolution, 2D and 3D imaging (vertical resolution up to the order of a decimeter) of deposits in the top 10 meter GPR data may be obtained in real-time, and often very minimum processing is required after that. Radar reflection characteristics and sedimentary stratum characteristics are strongly related.

The main foundation for GPR interpretation is imaging. To accurately interpret the radar images, one requires to be cognizant of the nature and source of reflections as well as the reflection patterns that are unique to particular sedimentary deposits. Radar facies is described as the total of all properties of a reflection method given by a particular rock formation or sedimentary sequence, related to seismic facies. Hence, "radar facies" refers to observable variations in a GPR section's reflection pattern. Both structural and textural subsurface characteristics have an impact on the radar response and result in distinctive outcomes in the radar observations. Radar facies elements are the name given to these processes. The four main ones are the exterior form geometry of the radar facies unit, 1. reflection amplitude, 2. reflection continuity, 3. reflection

configuration, and 4. reflection configuration. The following are examples of secondary radar facies elements: dominating frequency, the number of reflections, the polarity of reflections, the existence of diffractions, and the degree of penetration (Van Overmeeren, 1998).

Seismic facies differ significantly from radar images in that the latter are frequently impacted by both water distribution and sedimentary architecture. As a result, the full picture, including the impacts of the water table, must be considered when defining radar facies. Radar pictures differ from seismic images due to six primary aspects in total:

1. The unsaturated zone and the saturated zone are divided by the water table.
2. Other reasons why signals dispersion at or above the earth.
3. There are much more visible diffractions.
4. There is far less depth to the inquiry.
5. Conductive soils have high signal attenuation.
6. The shorter wavelength.

Recognizing the reflection patterns that are unique to specific sedimentary depositional settings or specific sedimentary rocks might incorporate all radar facies aspects.

Radar stratigraphy is the process of interpreting radar images to ascertain the characteristics and geological histories of sedimentary rocks and their depositional environments. Recognizing radar facies reflection patterns and correlating them with certain sedimentary settings are the goals of radar stratigraphic interpretation methods. A specialized application, such as a hydrogeological description of the subsurface, might then be the last step.

An illustration of this notion is shown in Figure 15. The strata will be sub horizontal and will be distinguished by wide fluctuations in grain size since it was deposited by a braided river system, assuming the horizontal reflection pattern 1 can be attributed to environment A and is understood to represent glacial-fluvial outwash. Vertical groundwater flow will be impeded in this sequence by fine-grained sediments. The characteristics of environment B, which may be thought of as distorted push moraine sediments, are pattern 2 with a lot of diffraction hyperbolas and pattern 3 with

a few coherent reflections of anticlinal shape near diffraction hyperbolas. Push moraines are made up mostly of coarse-grained sedimentary sequences, however, they may occasionally contain thin, almost vertically dipping clay layers that restrict lateral groundwater movement. These reflection patterns display various radar facies that correspond to two distinct, well-defined sedimentary settings, and they have a huge influence on the permeability and preferred flow directions underneath.

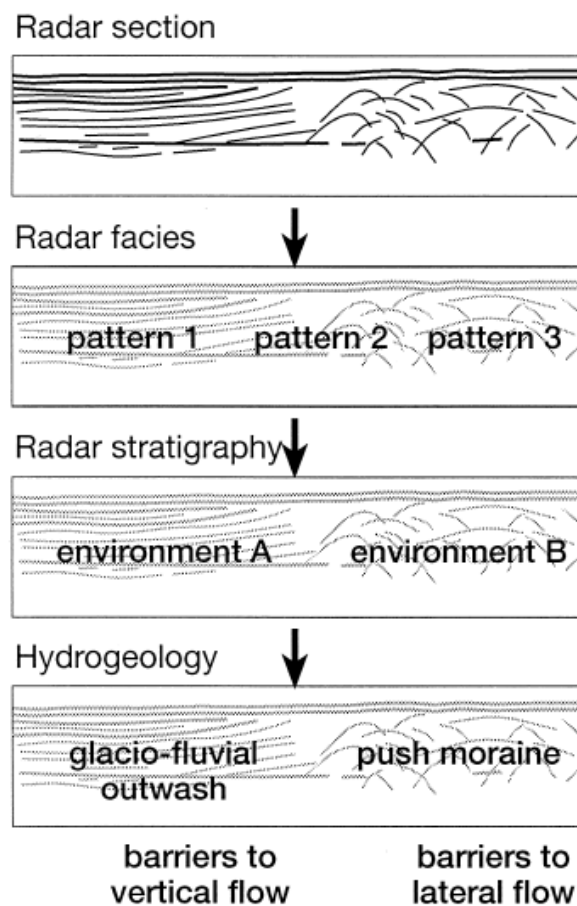


Figure 1 5 Process flow chart for interpreting radar stratigraphy and its final use in characterizing the sub surface's hydrogeology (Van Overmeeren, 1998).

Moreover, radar facies from typical radar surveys in river environments in The Netherlands have been examined by (Van Overmeeren, 1998). In fluvial settings of meandering rivers, material is more neatly organized in point bars, which are created by erosion in the outer bend of the meander and deposition in the inner bend. Point bars possess an interior sigmoidal structure and are characterized by an upward fining sequence. (Makaske & Nap, 1995) In most cases, finer sediments like silts and clays that were also deposited during flooding are found on top of the sandy point-bar deposits. The application of GPR is limited largely in this situation. The 200 GHz segment, which was captured while crossing point bar deposits of a meandering stream, has a typical sigmoidal reflection pattern.

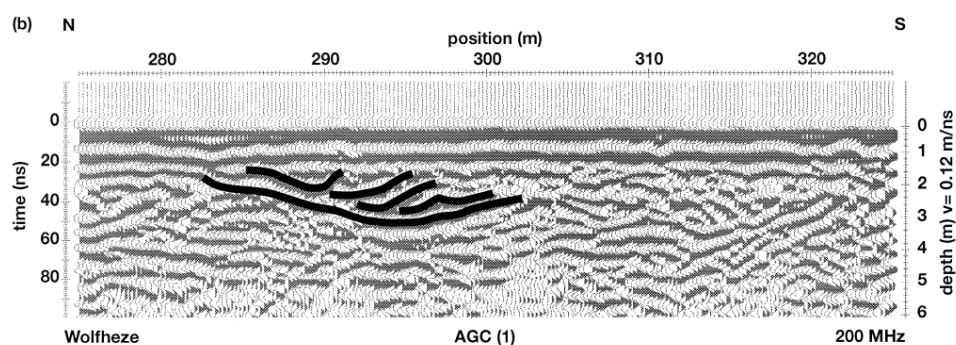


Figure 16 Typical GPR sections in fluvial settings : sigmoidal reflections from point bars from meandering rivers (Van Overmeeren, 1998).

More research on the structure of river sediments using GPR from (Srisunthon & Choowong, 2019). A three-dimensional model of the Mun River in Buriram Province's western region shows the shallow sandbar's structural system. The study's Ground Penetrating Radar (GPR) device, which operates at a frequency of 200 MHz, collects data at a maximum depth of 5 to 6 meters below the site's surface. explore Dragging the instrument along the survey line at the beginning and finishing locations using GPS coordinates allowed for continuous surveying. The surface elevation was also measured using a theodolite. Managed-to-cross tool drag lines are employed in surveys in a particular region to make it possible to build a 3D subsurface structure. The equipment allows for the characterization of the sedimentary structure and the interpretation of

sedimentary deposits. As a group The results of this study suggest that river lateral sandbars and ancient rivers have an oblique sediment structure. Secondary waterways where GPR data and lithofacies demonstrate the development of interlocking streams are exposed via past erosion. It also illustrates the migration of the side sandbars.

2.5.2 Electrical Resistivity Tomography (ERT)

Despite the fact that the radar signal deep survey method may rapidly gather information and offers high-resolution profile photographs in shallow sedimentary strata, it only works effectively under specific circumstances (Baines, 2002) . Hence, the Resistivity Survey was utilized in this work to produce Electrical resistivity ground imaging (ERGI) , which may produce photographs of ancient streams under a wider range of situations; and can be used to create a sedimentary layer profile image. Using a 2D resistivity approach, this kind of instrument's purpose is to evaluate the state of the subsurface. Direct current (DC) generators or low-frequency alternating current generators that are discharged into the earth Measurements are made of the differential voltages and the separations of the current-discharge electrodes. The particular electrical resistivity can then be determined by calculation. What influences the value of change in the physical characteristics of porous, inter-pore fluid-filled sediments with variable mineral compositions include potential difference and the flow of electric current. Gravel-sized sediment often has more resistance than sand-sized sediment. Sand has more electrical resistance than silt, while silt has more electrical resistance than clay sediment.

The effectiveness test findings for ERGI in mapping the appearance and geometry of sediments deposited in the trenches at four sites are as follows: 1. Interlocking sediments in the upper Columbia River, Canada; 2. In the Rhine-Meuse Delta, The Netherlands; 3. Sediment deposits in a valley stream, Yorkton, Canada; and 4. Sediment deposits in the streams of the Yukon River in central Alaska (USA). They were compared with profiles of the rock hierarchy derived from boreholes or GPR data. It was discovered that ERGI could investigate the clay and silt sediment layer and properly determine the depth, width, and lithography of sand and gravel deposits in the channel at depths of 1 to 20 meters (Figure 17).

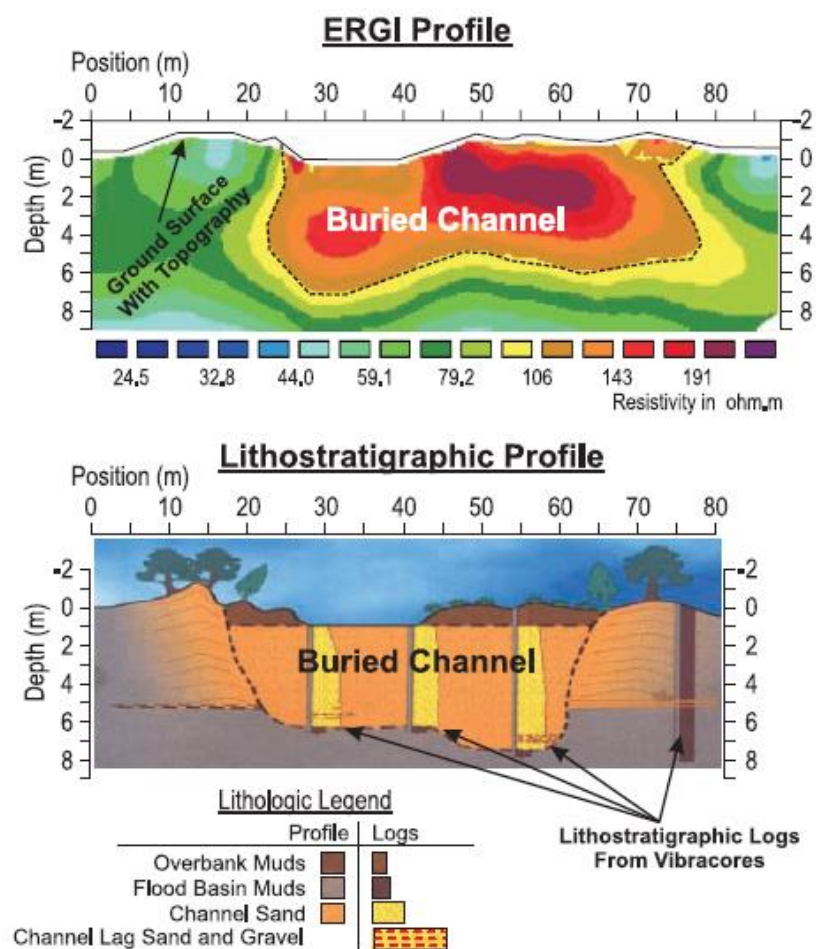


Figure 17 A section of an ERGI profile and a lithostratigraphic profile based on vibrocores are compared. Although the sand-filled Beavertail channel can be seen in both photos, the ERGI survey line is 50 m downstream of the vibrocores survey line.

Both views were taken in the anastomosing stretch of the upper Columbia River, six kilometers northwest of Harrogate, British Columbia, Canada (Baines, 2002).

In the study by (Nimnate, Thitimakorn, et al., 2017), as they both provide high-resolution data, GPR and ERT have been intriguing geophysical methods for the past in 20 years. ERT is frequently used in environmental and engineering geophysical surveys. It offers excellent 2D and 3D subterranean geology imaging, and GPR can find dielectric characteristics in sedimentary strata. Consequently, the collected data demonstrates the inconsistency of the lower sediment layers up to a depth of up to 20 meters, allowing visualization of the structure of the sedimentary layer. The clay layer, which is the sediment that has a special influence on GPR function. The clay sediment profile can be observed overall using the ERT technique. Consequently, in this research, the researchers accordingly decided to use both methodologies to analyze the evolution of the early Mun River flow system. to explain the subsurface morphology of modern and historic rivers with both instruments functioning effectively in locations where sediment modifications occur under various instrument situations. The channel's structure, sediment type, and geometry might also be seen as a result. Interpretations of paleoenvironment depositions can result from those methods.

2.5.3 Seismic Data in Study Area

According to early data, Thailand's Phrae Basin, which is located there, is one of the biggest basins in the region. It has a total size of 1,100 square kilometers and is made up of sedimentary layers from the Cenozoic epoch that are around 2 kilometers thick. The basin is situated in a north-northeasterly direction and has a triangle form. The south-southeast line, which spans latitudes $18^{\circ} 00' N$ to $18^{\circ} 30' N$ and longitudes $100^{\circ} 05' E$ to $100^{\circ} 20' E$, is 15 to 25 kilometers in width and 50 to 60 kilometers in long (Figure 18). Rocks from the Lampang and Triassic eras, including shale, mudstone, limestone, Carboniferous-Permian rocks, and in certain places limestone, shale, and chert from the North Permian, surround the basin in the majority. These formations are less spread to the east and west. The Phrae-Thoen fault, which surrounds the basin on the left and gives it its S form, is what causes the opening of the basin. The primary river in the Phrae basin is the Yom River, which runs from north to south. There are additional

significant streams that deliver silt to the Phrae basin from the northeastern and eastern edges.

Five tectonic processes took place during the basin's formation, according to seismic studies that covered the whole basin. Data on the sediment hierarchy were gathered over a period of five cycles. Each cycle began with sediments from braided rivers and floodplains, continued with shallow wetland-lake sediments, swamp-lake sediments, and finished with a fresh aquatic sediment buildup known as crevasse splay.

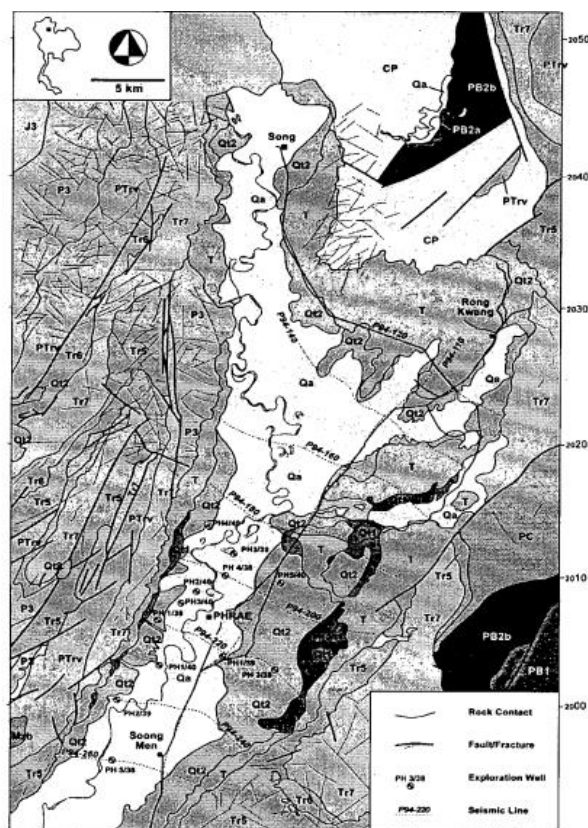


Figure 18 Phrae Basin map and cross-sections lines of Seismic investigation (Srisuwan, 2000).

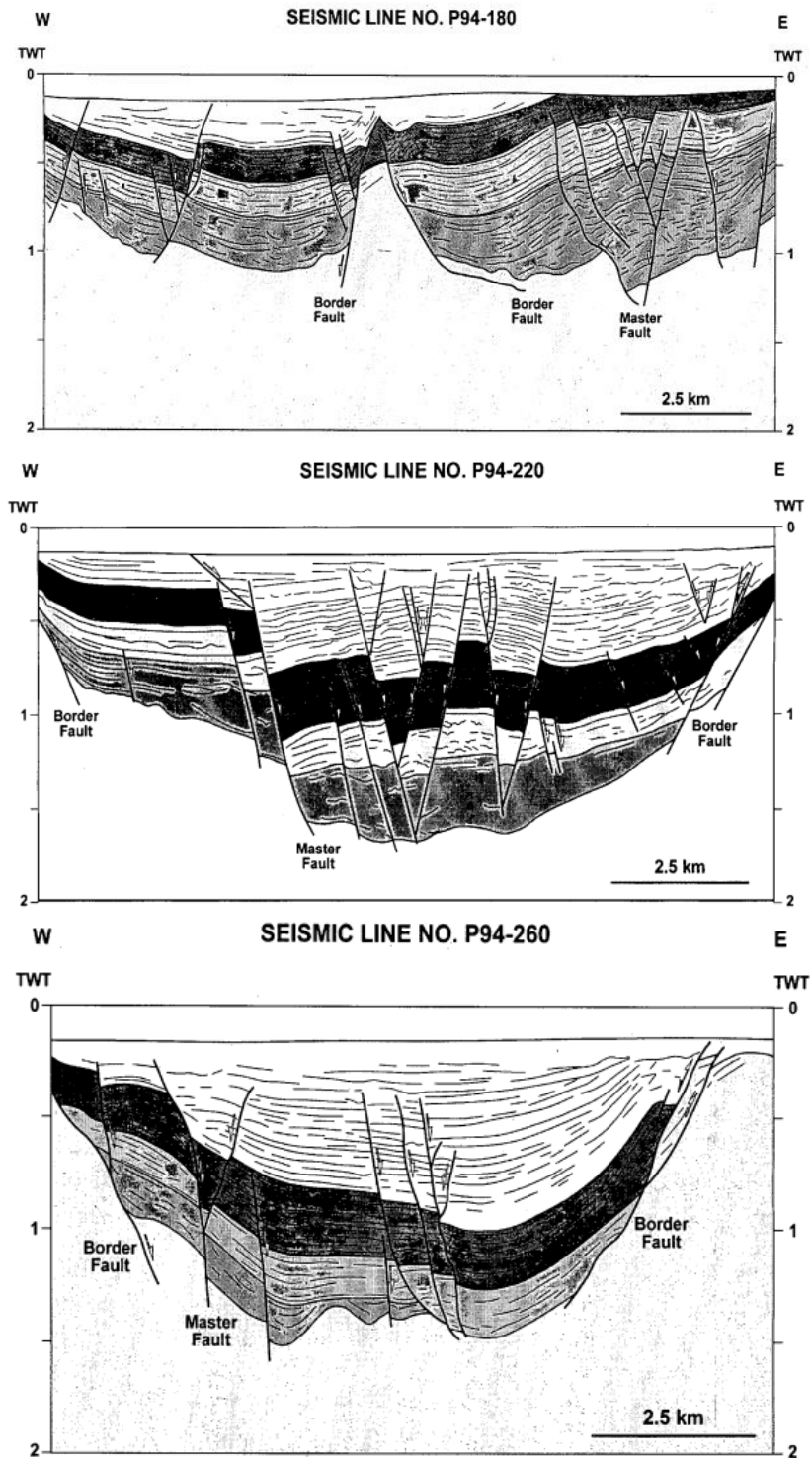


Figure 19 Three seismic cross-section profiles from Phrae Basin in the upper part shown on seismic line no. P94-180, the middle part of basin shown on seismic line no. P94-220 and the lower part of basin shown on seismic line no. P94-260 (Srisuwan, 2000).

CHAPTER 3

Methodology

3.1 Aerial Photo and Satellite Image Interpretation

3.1.1. Aerial Photo and Satellite Image Interpretation materials

For the objective of interpretation, a variety of satellite pictures and aerial photographs encompassing the area illustrated in Table 1 were collected. The entire photographic record spans 65 years, from 1954 to 2019. This study used aerial photographs from the Department of Royal Thai Survey in 1954, 1970, and 1989 to create maps with a scale of 1: 50,000. A mirror stereoscope was used to analyze a collection of grayscale aerial pictures in three dimensions and scan images to create digital files.

Year	Data type	Resolution	Source
February 15, 1954	Arial photo	1: 50000	Royal Thai survey department
January 22, 1970	Arial photo	1: 50000	Royal Thai survey department
December 23, 1989	Arial photo	1: 50000	Royal Thai survey department
October 29, 2012	Satellite image	1 meter	Google Earth
March 10, 2019	Satellite image	1 meter	Google Earth

Table 1 The variety of satellite pictures and aerial photographs were used to interpretation geomorphological changes in the study area.

Each picture was corrected using 5 to 6 ground control points (GCPs) and located throughout the photos in accurate landmarks such as road intersections or man-made construction to obtain the low root mean square error (RMSE). The geomorphic correction was carried out using software from ESRI ArcGIS 10.4.1. For this investigation, an RMSE value of less than or equal to 10 is acceptable. In addition, utilized 1-meter resolution on satellite pictures from Google Earth in 2012 and 2019. Each year's images were characterized as the geometries of channel

landforms in the past and present, and alterations in the ArcGIS software were compared to them.

3.1.2 Delineate the geomorphic characters

3.1.2.1 Geomorphic mapping

A series of aerial photographs were interpreted via a mirror stereoscope, scanned, and processed into digital files for comparison with Google Earth satellite imagery. All images were identified as the geometries of channel landforms in the paleo- and modern ages of each year and contrasted with various alterations using the ArcGIS application. From photos to shifting geomorphological features, the boundaries of geomorphic characters including channels, paleo-channel traces, oxbow lakes, meander scars, scroll bars, and floodplains will be meticulously defined.

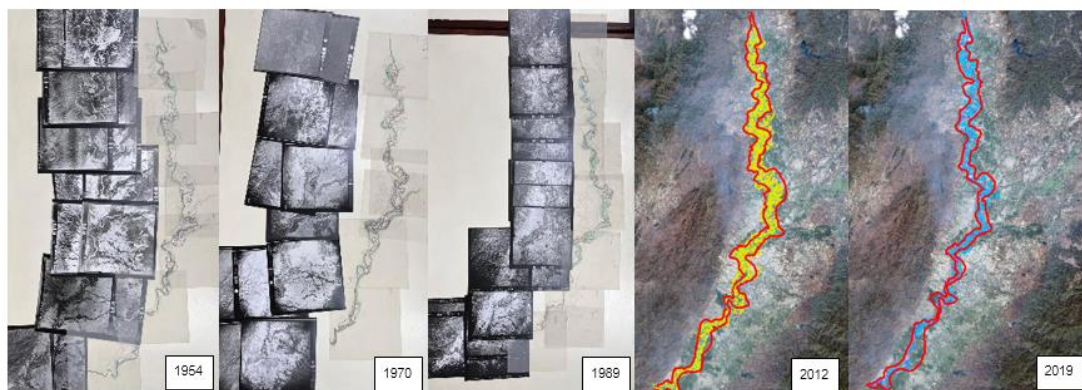


Figure 20 A series of aerial photographs (1954, 1970, 1989) were interpreted via a mirror stereoscope, scanned, and processed into digital files for comparison with Google Earth satellite imagery (2012, 2019).

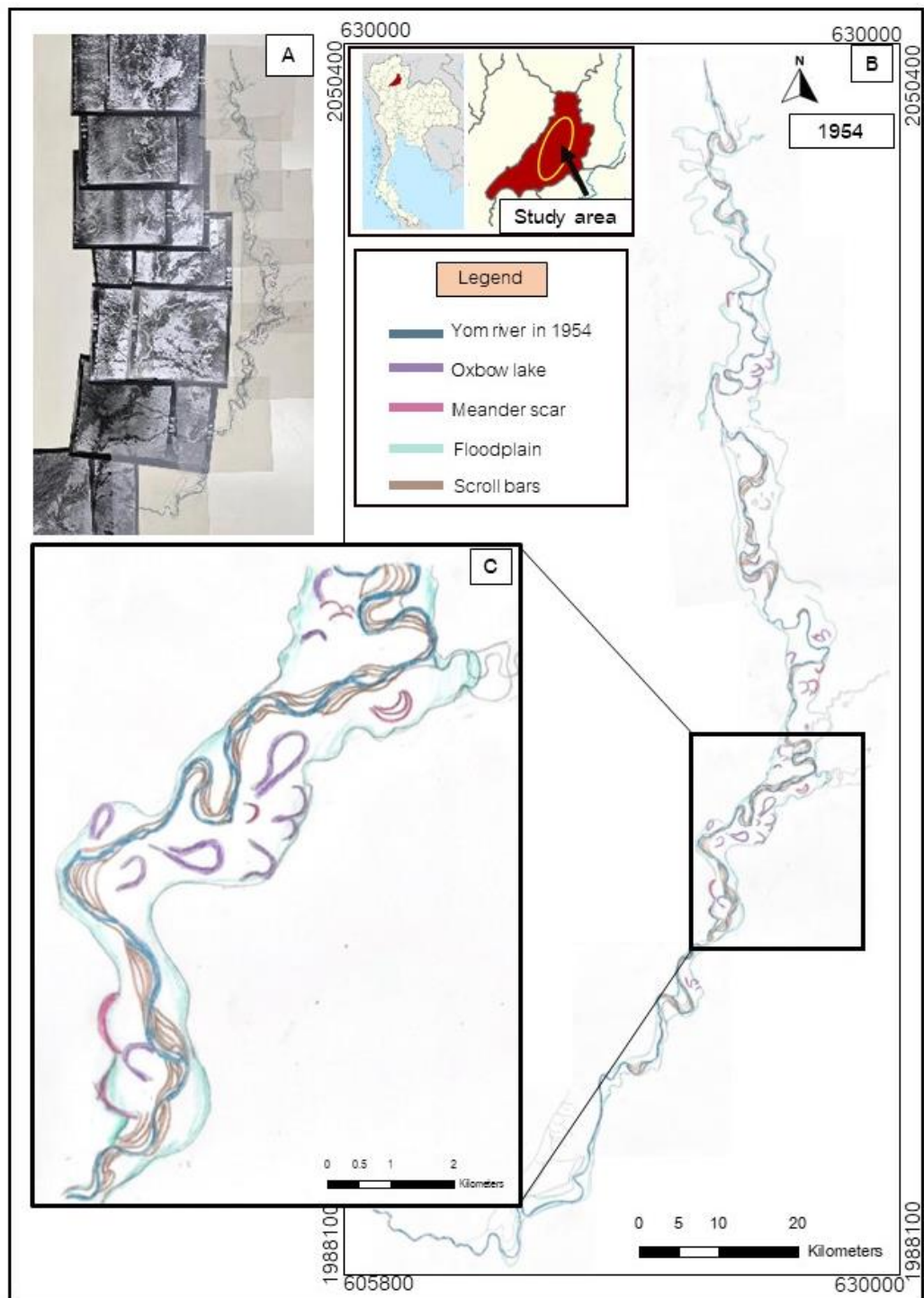


Figure 21 Aerial photographs of 1954 period and interpretation map (A) .
 The geomorphological changes interpretation via using a mirror stereoscope (B) .
 The rich zone of channel migrations in the middle part of study area (C).

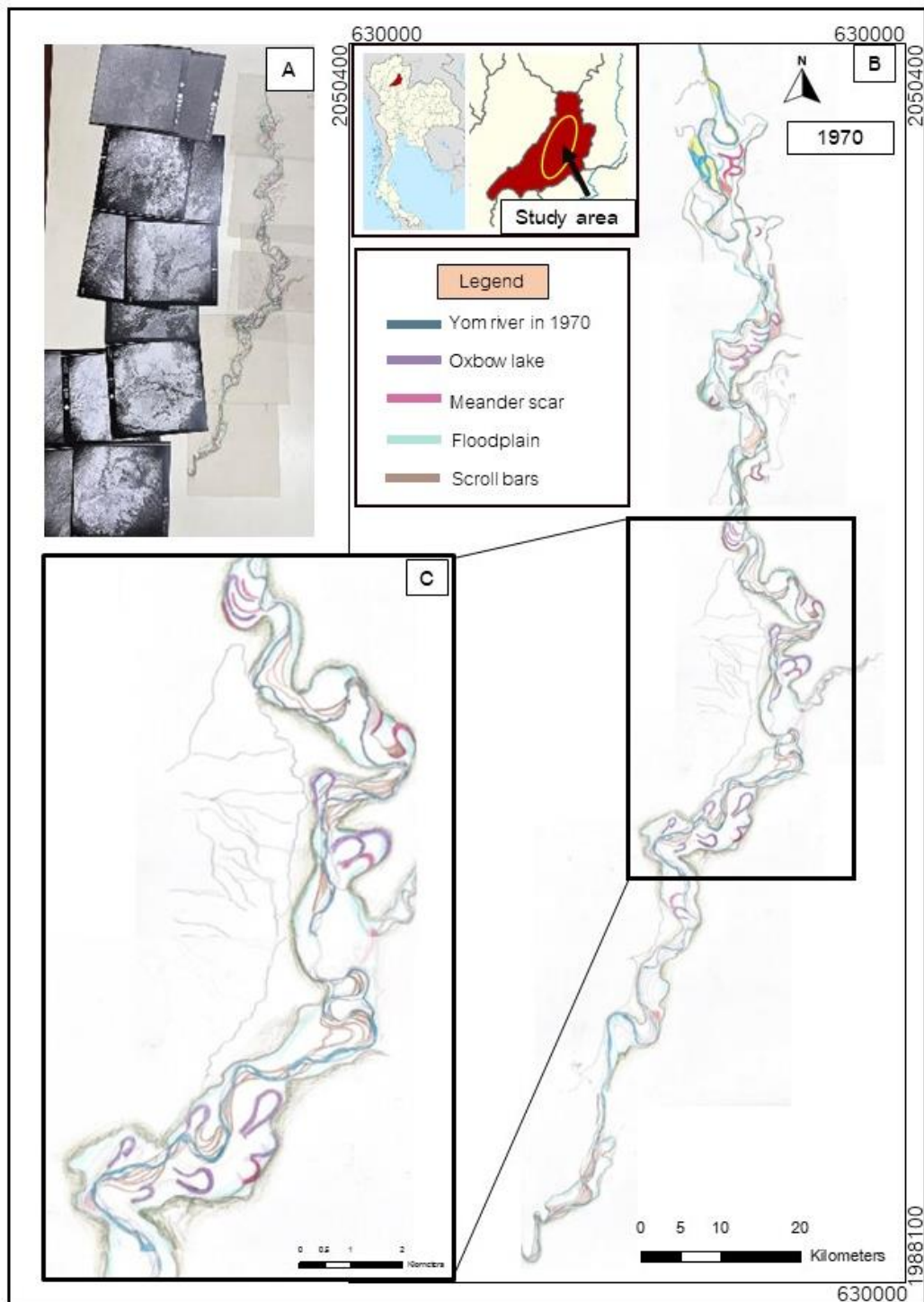


Figure 22 Aerial photographs of 1970 period and interpretation map (A) .
 The geomorphological changes interpretation via using a mirror stereoscope (B) .
 The rich zone of channel migrations in the middle part of study area (C) .

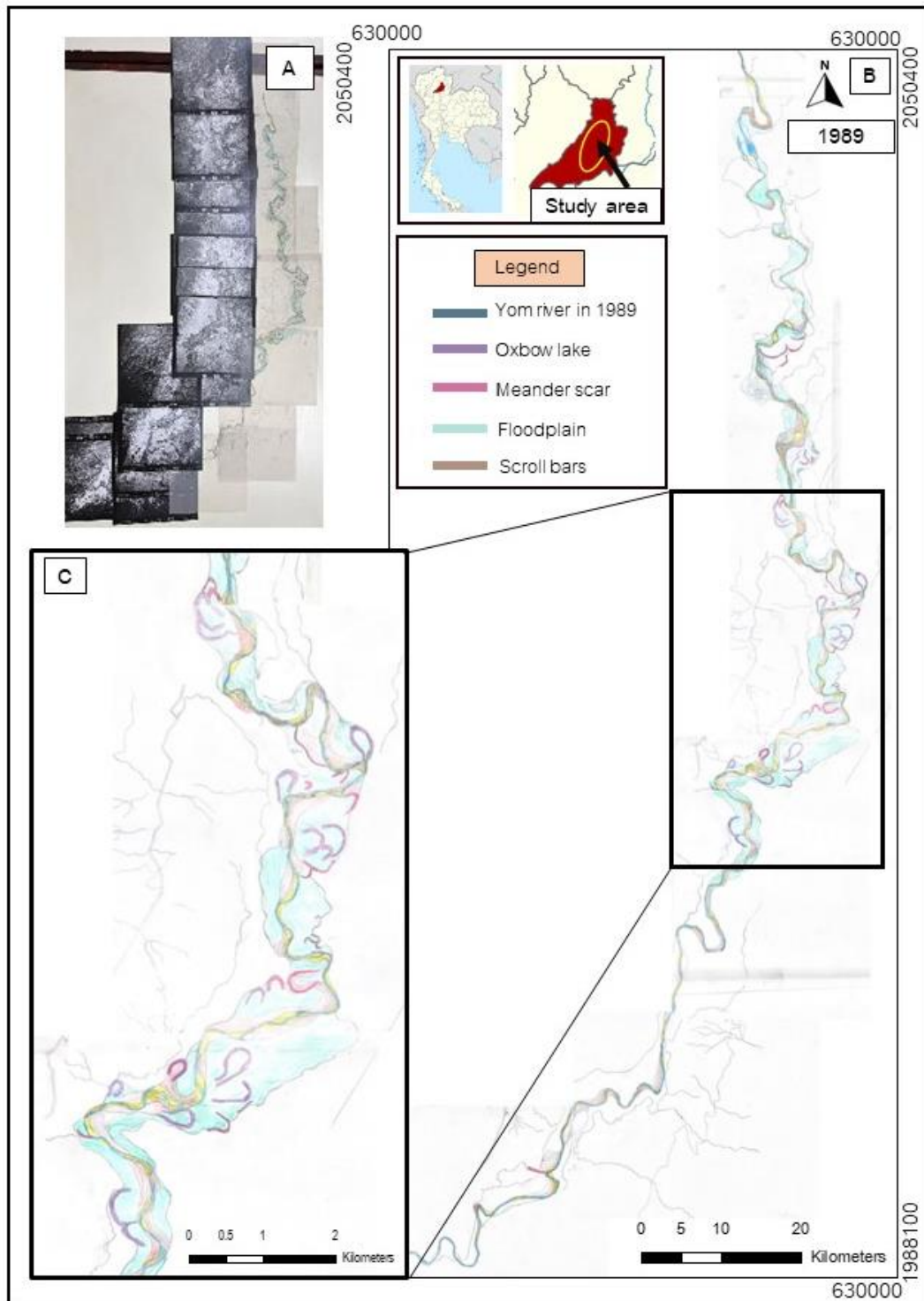


Figure 23 Aerial photographs of 1989 period and interpretation map (A) .
 The geomorphological changes interpretation via using a mirror stereoscope (B) .
 The rich zone of channel migrations in the middle part of study area (C) .

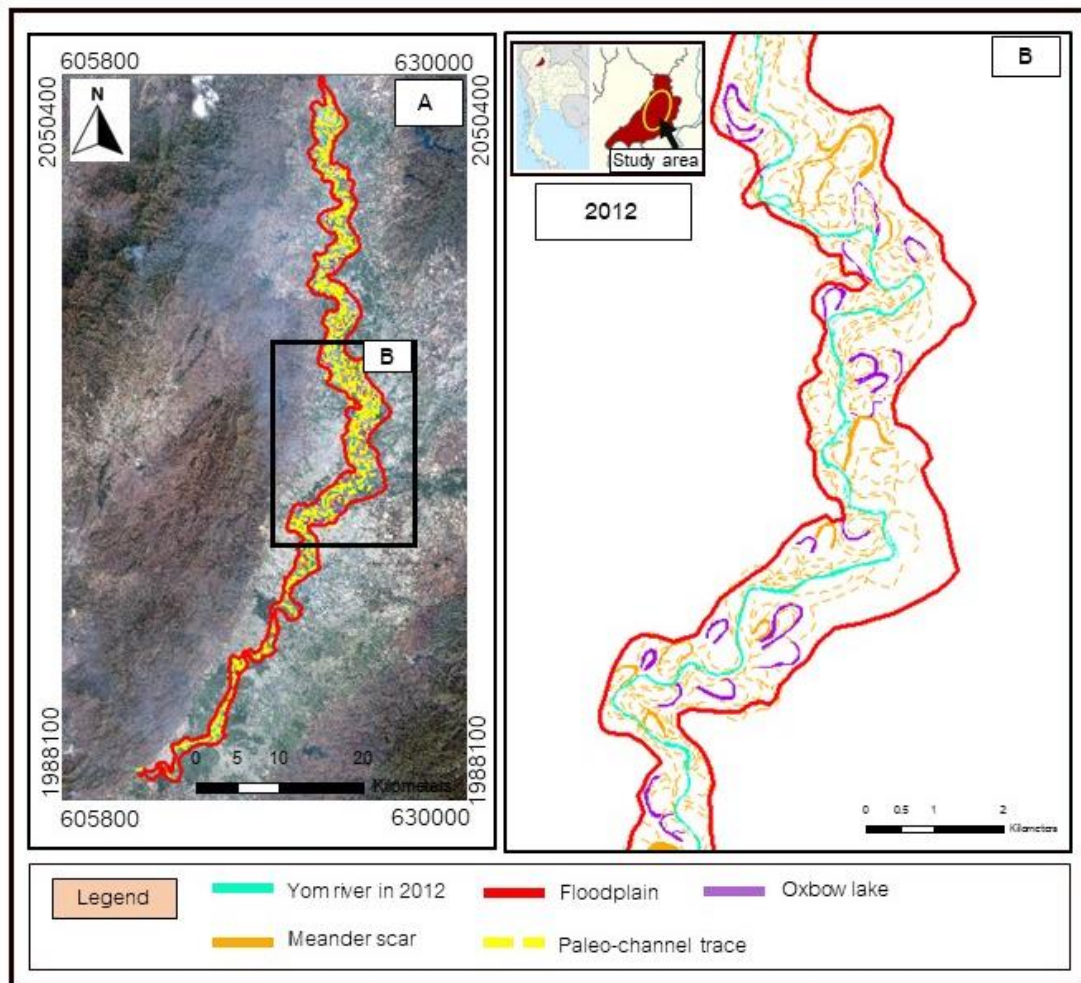


Figure 24 A satellite image of 2012 and geomorphological changes interpretation via using Google Earth (A). The rich zone of channel migrations in the middle part of study area (B).

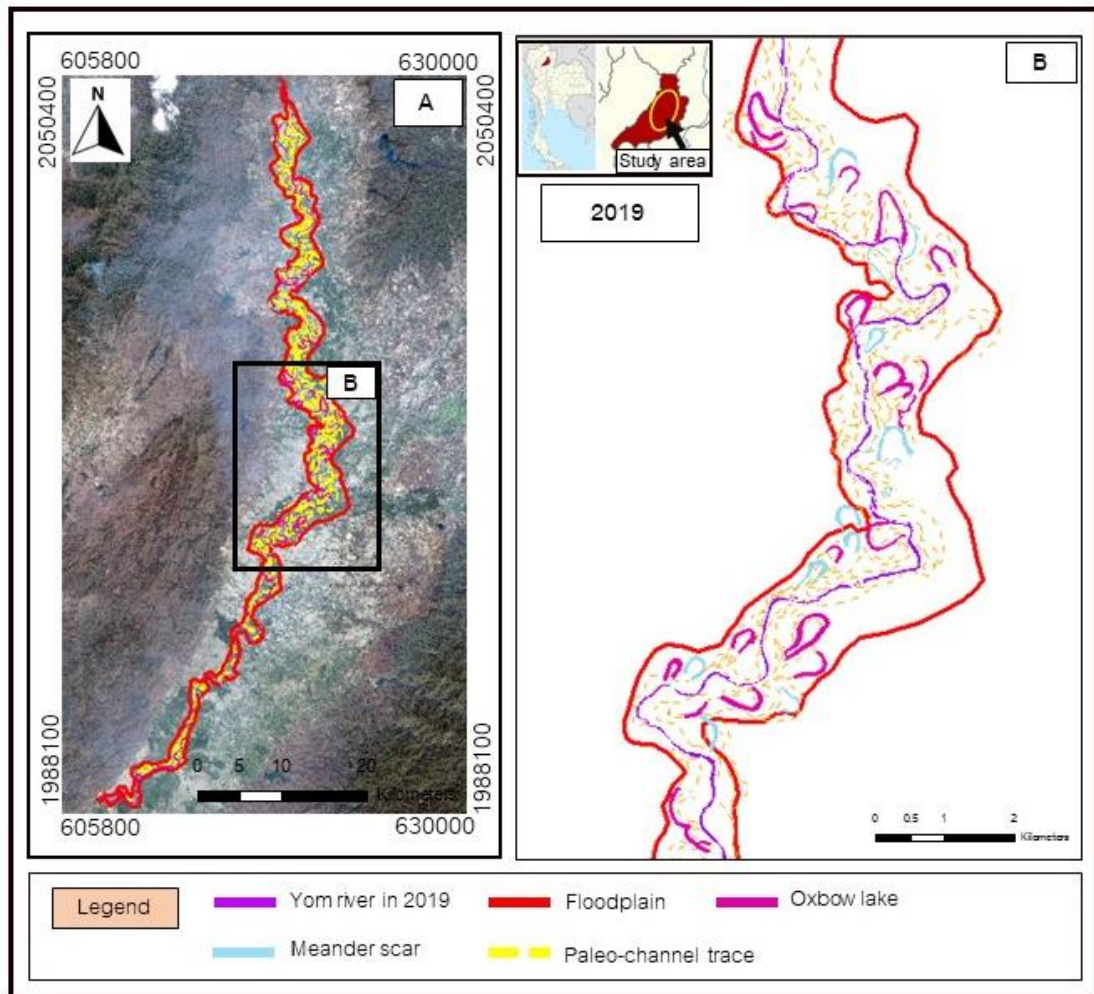
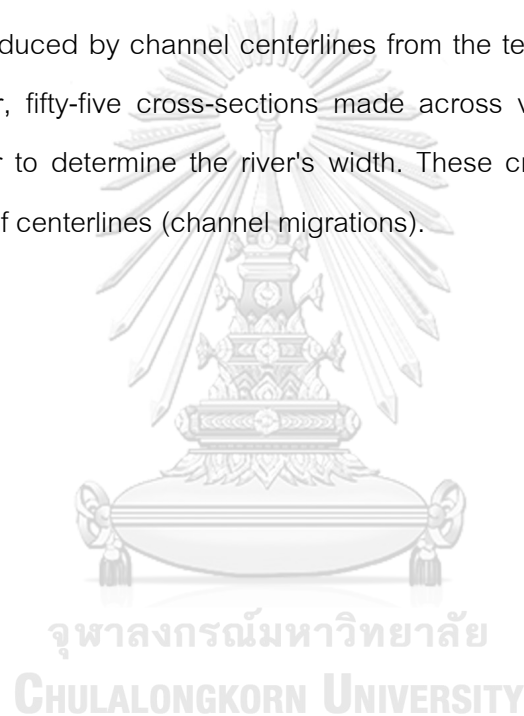


Figure 25 A satellite image of 2019 and geomorphological changes interpretation via using Google Earth (A). The rich zone of channel migrations in the middle part of study area (B).

3.1.2.2 Geomorphic Criteria Calculation

Channel width (W), channel length (L), sinuosity index (SI), the radius of curvature (Rc), and channel migrations are five geomorphic parameters that were used to analyze trends. Each criterion has its own resources and details that have been beneficial for determining how geometry has changed throughout time. In order to compare recent channels and paleo- (abandoned channels), the sinuosity index (SI), the radius of curvature (Rc), channel width (W), and channel migration rate were measured using the measure tool for distance measurement on ArcGIS 10.4.1. Channel length (L) was produced by channel centerlines from the temporal vector layer of river courses. Moreover, fifty-five cross-sections made across various river sections were measured in order to determine the river's width. These cross-sections represent the lateral movement of centerlines (channel migrations).



3.1.2.2.1 The Sinuosity index (SI)

Sinuosity indexes can use to describe measuring channel stability. SI coefficient is 1.05 but not more than 1.25, a river is sinuous. 1.25 to 2, it shows a meandering river. Up to 2, it is highly meandering. The river channel can transform itself, if SI is about 2 (highly meander), it will be modified into less sinuosity (Hooke, 2007b). The distance of down valley and channel length were applied to aerial photos and satellite images (Figure 20). Both values are measured by using Measure Tool from ArcMap 10.4.1. This study measures SI across five-year periods in the same thirty locations (1954-2019).

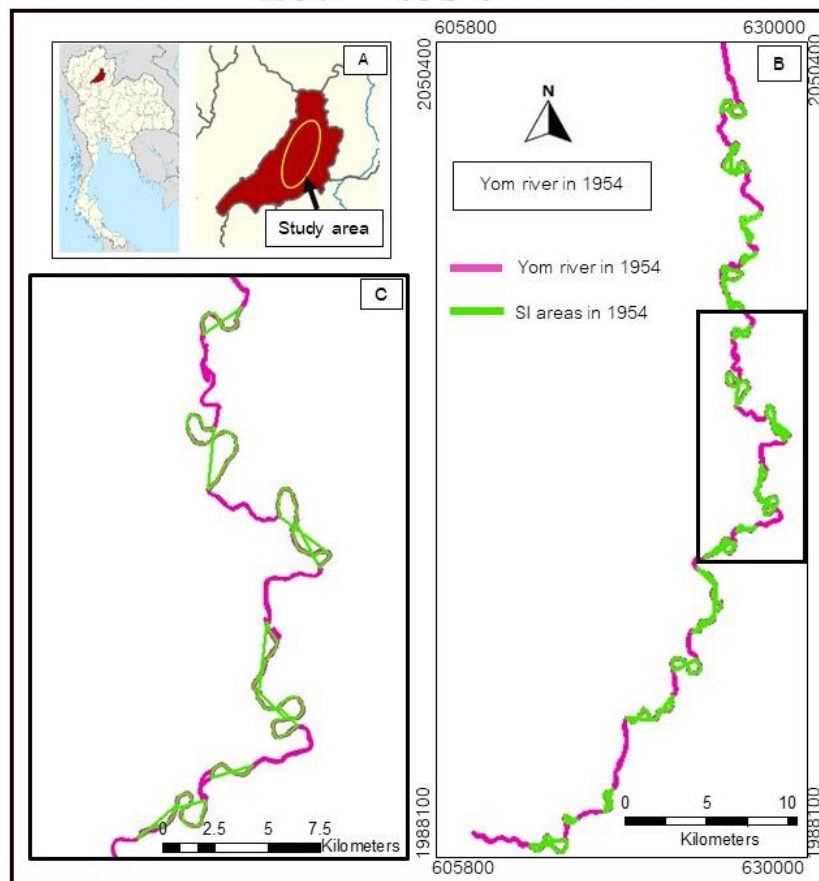


Figure 26 Map shows SI measure in 1954 period. The index map of the study area from Thailand and Phrae Province (A). The measurement of Sinuosity index in 1954 shows all thirty locations along the Yom River in the study area (B). Each location was measured in two values (Channel length divided by down valley length) (C).

3.1.2.2.2 The radius of curvature (Rc).

One of the metrics used to determine a river's curve is the radius of curvature or Rc. Sinuosity is inversely correlated with the radius of curvature (Rc), which determines how "tight" a single meander bend is. Calculating the Rc involves finding the radius of a circle that fits the meandering arc that extends from the bank-full channel's border to the junction of two lines that perpendicularly bisect the tangent lines of each meander departure point. Sinuosity and Rc have an inverse relationship. The river bends will be near to one another if the Rc value is high. A wider bend, on the other hand, will display a low Rc value. Areas 1 and 3 of the curve's one and only precisely full bend will be examined in this investigation over a period of five measurements (from 1954 to 2019). Nevertheless, due to the cut-off at the curve, area 2 could only be measured for three years (Figure 41).

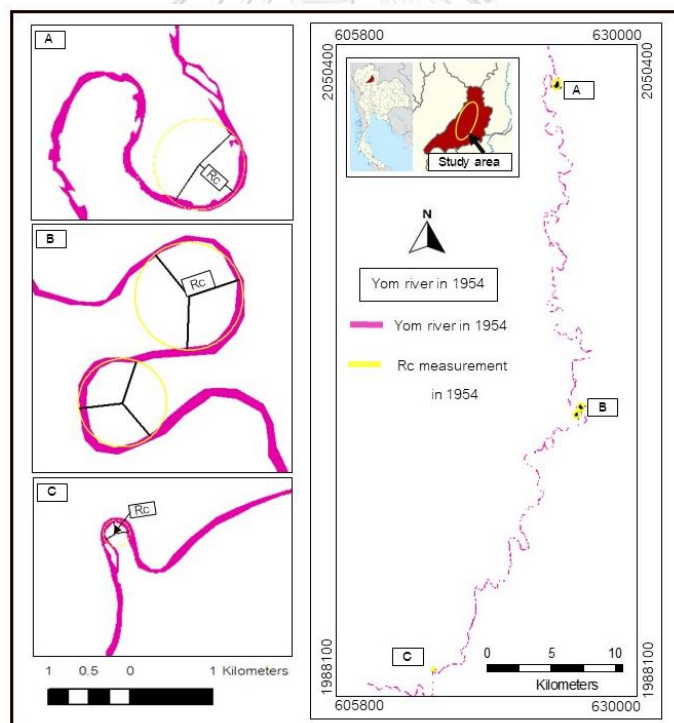


Figure 27 The map shows the locations of measurements Rc values in 3 locations from the study area. Rc measurement at river bend in the upper part of study areas (A). Rc measurement at bend in the middle part of study areas (B). Rc measurement at lower bend in study areas (C).

3.1.2.2.3 Channel width (W)

Bank deposition narrows the channel, whereas bank erosion has the opposite effect. Hence, achieving the equilibrium river width requires balancing opposite bank accretion and bank erosion. Although there may still be periodic oscillations, there are no long-term trends (narrowing or widening) in the width of the river in this case. When the banks advance and subside, the river changes flow. This work on width measurements in each value reveals a channel's stage and evolution features as well as the cross-sectional distance of a channel. Fifty-five fixed cross-sections were used to measure the channel's width, and each cross-section is spaced about two kilometers apart along the length of the river each year (Figure 28).

3.1.2.2.4 Centerline migration rate

The vector layer of channel polygons creates the centerline from generation in ArcGIS program's tool, which is the midpoint between the left and right banks. Meander migration rates were monitored and computed over five time periods (1954, 1970, 1989, 2012, and 2019). The river's centerline motion was counted at 53 for each cross-section (along the same cross-section line as the width measurement illustrated in Figure 28), and the rate of migration for the various sites was computed over time.

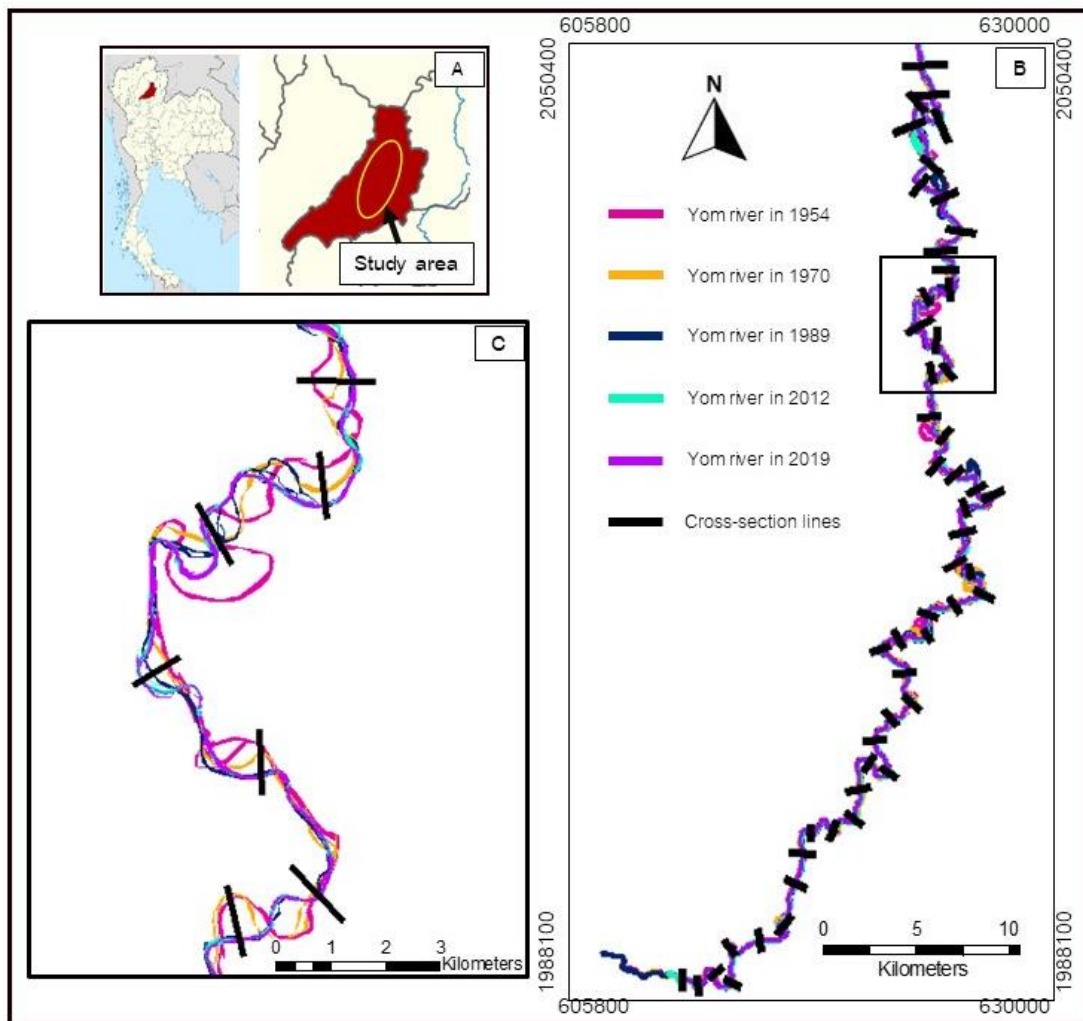


Figure 28 The map shows the channel width and centerline migration. The index map of the study area from Thailand and Phrae Province (A). The measurement of R_c were measured on fifty-three fixed cross-sections and each cross-section is spaced about two kilometers apart along the length of the river each (B). Each location was measured in the same cross-section line (C).

3.1.2.2.5 Channel length (L)

In large-scale maps, it is measured along the geometric axis or the line of maximum depth. A stream's length is determined by measuring the length of the stream channel from the beginning to a particular location or to the outlet. The centerlines of the channel, which were derived from the temporal vector layer of river courses, are where the length of the Yom rivers in the research area is measured, halfway between the left and right sides were generated from the channel polygon. Rather than the river channel lateral migration, the meander bend cut-off and neck cut-off is the cause of the faster rate of length change. (Bag et al., 2019) (Figure 29).

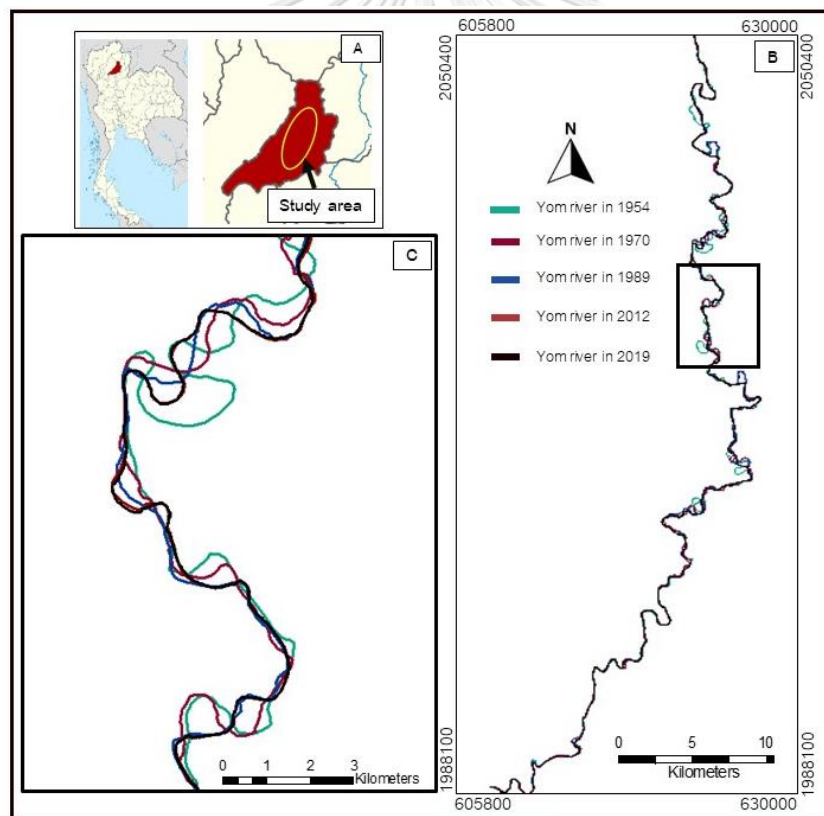


Figure 29 This map illustrates the channel length Study area map index (A). The length has been measured along the midline between the left and right banks of the channel polygon (B). The middle part of study area shows the migration through the midline obviously.

3.2 Field investigation

Analyzing the accuracy of aerial picture interpretation is the objective of this effort. Also, in the shallow geophysical survey, electrical resistivity tomography (ERT) and ground penetrating radar (GPR) were used to study the depth of the channel deposits for the behavior and direction of the river, furthermore, it constructed the radar facies from the lithological classes of the GPR and ERT. For a confirmed geophysical survey, sediment samples were taken from boreholes in various landforms to further determine the kind of sediment, sediment investigations were conducted. All of the data were then combined and correlated as a result.

3.2.1 Study area and sites

A layer of Cenozoic silt with a thickness of approximately two kilometers makes up the Yom River, which mostly runs from north to south through the Phrae basin, which has an area of 1,100 square kilometers. Its latitudes are from 18°00'N to 18°30' N and longitudes from 100° 05' E to 100° 20'E, respectively. The majority of the rocks enclosing the basin are from the Triassic Lampang group, which is composed of shale, mudstone, and limestone; Carboniferous-Permian rocks could also be found in some locations. Limestone, shale, and chert from the Permian era are less common to the east and west (Figure 1).

The geomorphic map displays the sites of the shallow geophysical survey (ERT and GPR) and sediment samples shown in Figure 30. The Paleo-channels (meander scars), point bar, and floodplain were all investigated using six resistivity survey lines, two GPR survey lines, and five boreholes.

The first location is in Ban Long Lue Bun. The point bar and meandering scar are covered by the 235 meters and 140 meters resistivity survey lines, respectively.

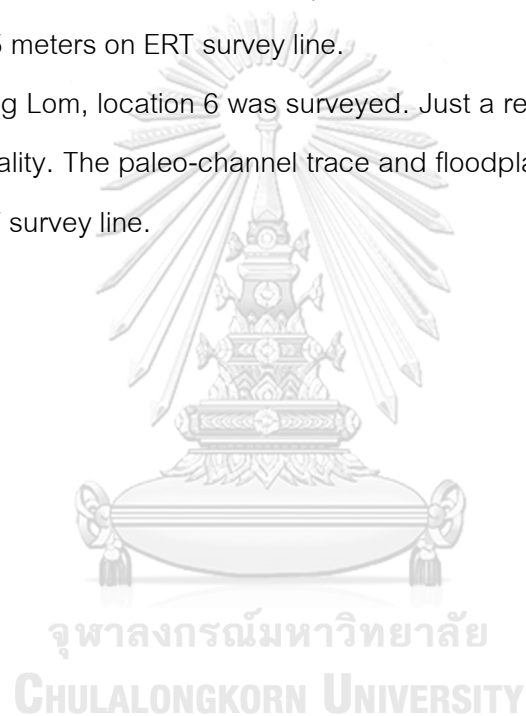
Surveying was performed at Location 2 in Ban Huai Mai. The longest GPR survey, measuring 410 meters, and the longest resistivity survey line, measuring 470 meters, both explore floodplain and paleochannel traces.

Ban Huai Kan was used to assess Location 3. Just a resistivity survey was used to study this site. The paleochannel trace and floodplain are both covered by the 235 meters on ERT survey line.

At Ban Ton Nun, location 4 was investigated. Only a resistivity survey was used to study this location. The paleochannel trace and floodplain are both covered by the 235 meters on ERT survey line.

Surveying was completed at Location 5 in Ban Ton Kha. Just a resistivity survey was used to explore this area. The floodplain, Meander scar, and point bar are all included in the 235 meters on ERT survey line.

In Ban Nong Lom, location 6 was surveyed. Just a resistivity survey was used to investigate this locality. The paleo-channel trace and floodplain are both covered by the 235 meters on ERT survey line.



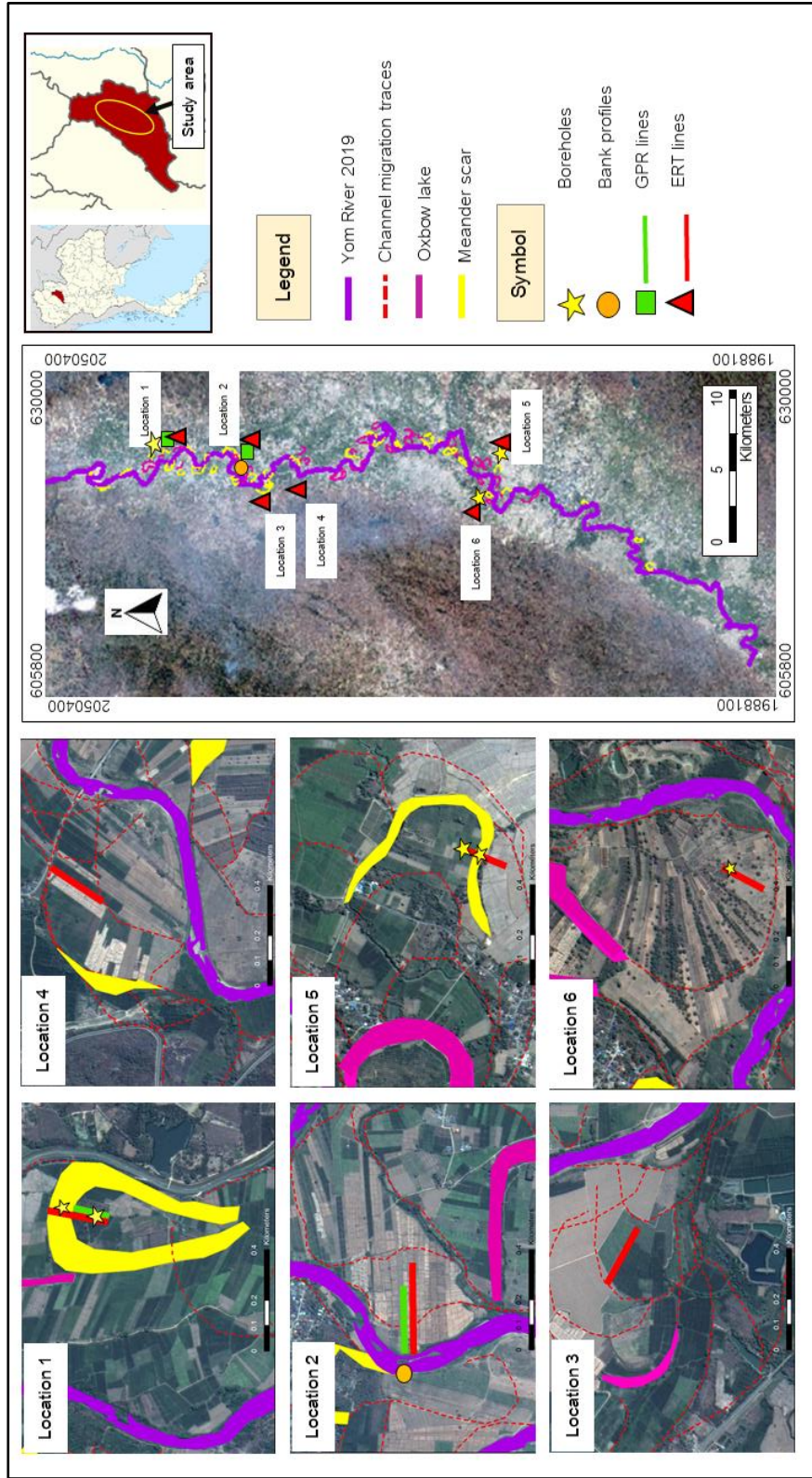


Figure 30 The geomorphic map displays the sites of the shallow geophysical survey (ERT and GPR) and sediment samples. The Paleochannels (meandered scars), point bar, and floodplain were all investigated using six resistivity survey lines, two GPR survey lines, and five boreholes from six locations.

The sediment boreholes were gathered as close as possible to the survey lines using a manual hand auger. One bank profile of the Yom River describes the investigation at the opposite bank from location 2. (Ban Hui Mai). Also, the sample sediments were dug as deeply as possible by hand auger following resistivity survey lines and approximately ground-penetrating radar lines in order to correlate each site's stratigraphy and lithology. The minimum borehole depth is two meters whereas the maximum is four meters. Each sample were then obtained at a depth of twenty centimeters from each borehole, going from top to bottom on the hand auger, placed in a zip-lock bag, and returned to the lab for grain size analysis.



Figure 31 The sediment samples were taken from boreholes (Left). The river bank profile near the Yom River (Right).

3.2.2 Geophysical survey

3.2.2.1. Ground penetrating radar (GPR)

Ground penetrating radar (GPR) is a non-invasive technique mostly used for subsurface research ((Cassidy & Jol, 2009) and (Neal, 2004)). High-frequency electromagnetic (EM) waves in the range of 10-1000 MHz are used in GPR to detect changes in the shallow sub-surface's dielectric characteristics (Neal, 2004) . In this study, geomorphologic units interpreted from aerial photographs and satellite pictures were used for geomorphological change surface interpretation, in addition to, the shallow subsurface sedimentary layers using ground penetrating radar (GPR) with the GSSI-SIR System-20. Antennas tuned to the 100 MHz frequency were used for the GPR. Fieldwork investigation is shown in Figure 32.



Figure 32 The GPR investigation lines from 2 locations in fieldwork investigation.

3.2.2.2. Electrical Resistivity Tomography (ERT)

Although the GPR survey method may quickly collect data and supply high-resolution profile photos in shallow layers, it is limited to use in certain conditions from high-conductivity materials such as clay soils and soils that are salt contaminated. As a result, the sedimentary subsurface profiles from Electrical Resistivity Tomography (ERT), which can operate in a wider range of settings, were visualized using the Electrical Resistivity Survey. Electrical resistivity has the purpose of measuring the subsurface state using a 2D resistivity approach. It will either utilize a low-frequency alternating current (LFAC) generator or a direct current (DC) generator to detect the electric potential difference from subsurface sediments. A dipole-dipole electrode array survey is used in this work. The paleo-channel shape is clearly distinguishable since dipole-dipole configurations were utilized with a short electrical line and sensitivity to vertical shift. According to (Baines, 2002), resistivity may be used to assess the physical features of sediments based on their mineral composition, pore size, and inter-pore fluid, as well as their differential conductivities between floodplain and channel sediments. Based on the apparent resistivity measured after fieldwork and analyzed using the specialized resistivity program RES2DINV, the resistivity profiles have been interpreted. This software uses the conditioned least squares smoothing procedure, and the inversion process will define the values of resistivity for each value of the observed and estimated apparent resistivity and build an underground model using rectangular prisms (Wahid et al., 2015). The fieldwork investigation (Figure 33).

3.2.3 Sediment characteristic analysis

The majority of the samples taken from boreholes were clastic sediments, hence the dry sieve method was used to investigate this approach. Following the dry sieving process, particles were weighed in each size and categorized according to Folk's approach of gravel, sand, and mud to identify the sedimentary type (Figure 34) (Folk, 1954). These lithological logs were scaled, and ERT and GPR profiles were merged.



Figure 33 Resistivity investigation lines (Red lines) in six locations where located of paleochannels, floodplains and point bars on the map on figure 30. Location 1(A), Location 2 (B), Location 3 (C), Location 4 (D), Location 5 (E) and Location 6 (F).

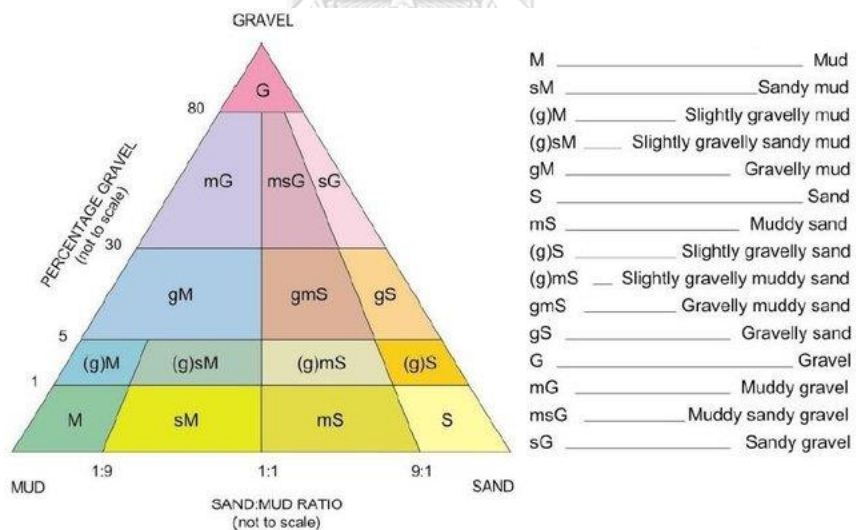


Figure 34 Classification by sediment class (derived from Folk, 1954) from Georgia Bayliss-Brown, 2012 (Bayliss-Brown, 2012).

CHAPTER 4

Result

4.1 Geomorphological map

Comparing geomorphological changes throughout the previous five periods was achieved using ArcGIS 10.4.1 software (1954, 1970, 1989, 2008, and 2019). Channel migration, neck cut-offs, oxbow lakes, and meander scars are examples of how geomorphology has changed over the past 65 years (from 1954 to 2019) in aerial photographs and satellite images. There are several meander changes in the upper and middle parts, but there are only a few geomorphological remnants in the lower area. Figures 35 to 39 display the interpretation outcomes for the years 1954, 1970, 1989, 2012, and 2019.

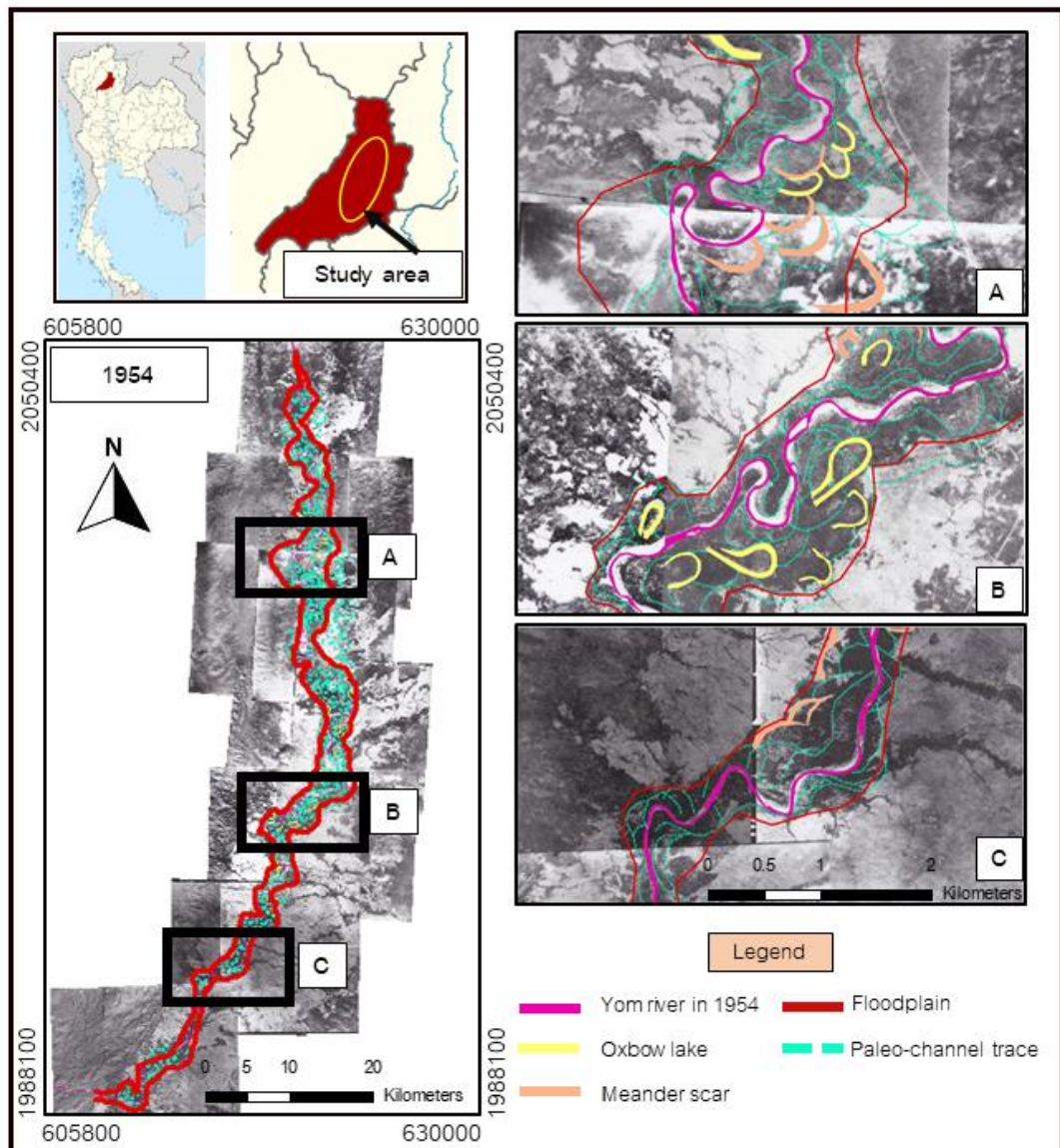


Figure 3.5 The interpretation of Geomorphological map of Study area in 1954. The channel migration traces were illustrated on the upper and middle part of study area (A and B), whereas the lower part was shown lack of traces (C).

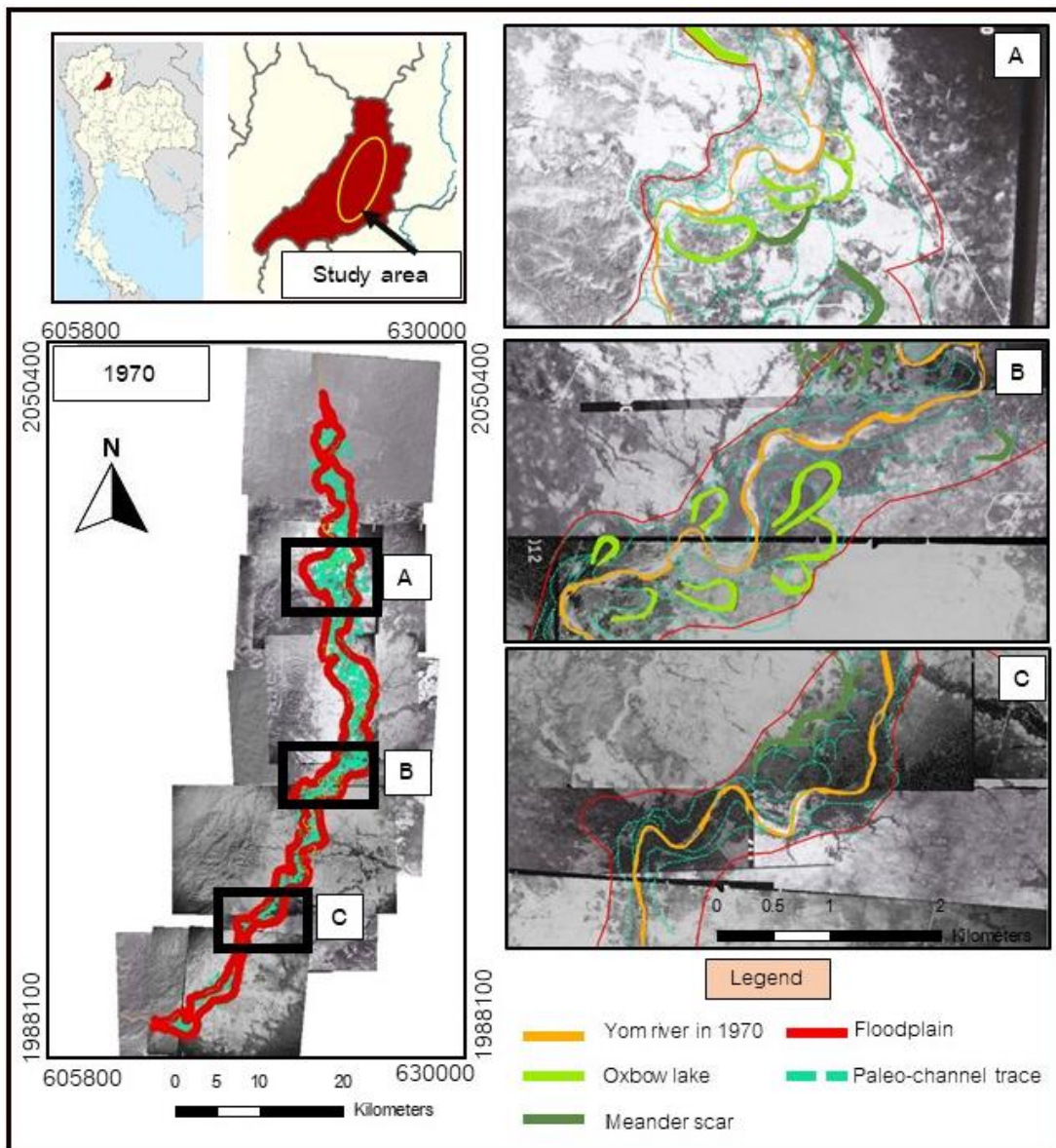


Figure 36 The interpretation of Geomorphological map of Study area in 1970. The channel migration traces were illustrated on the upper and middle part of study area (A and B), whereas the lower part was shown lack of traces (C).

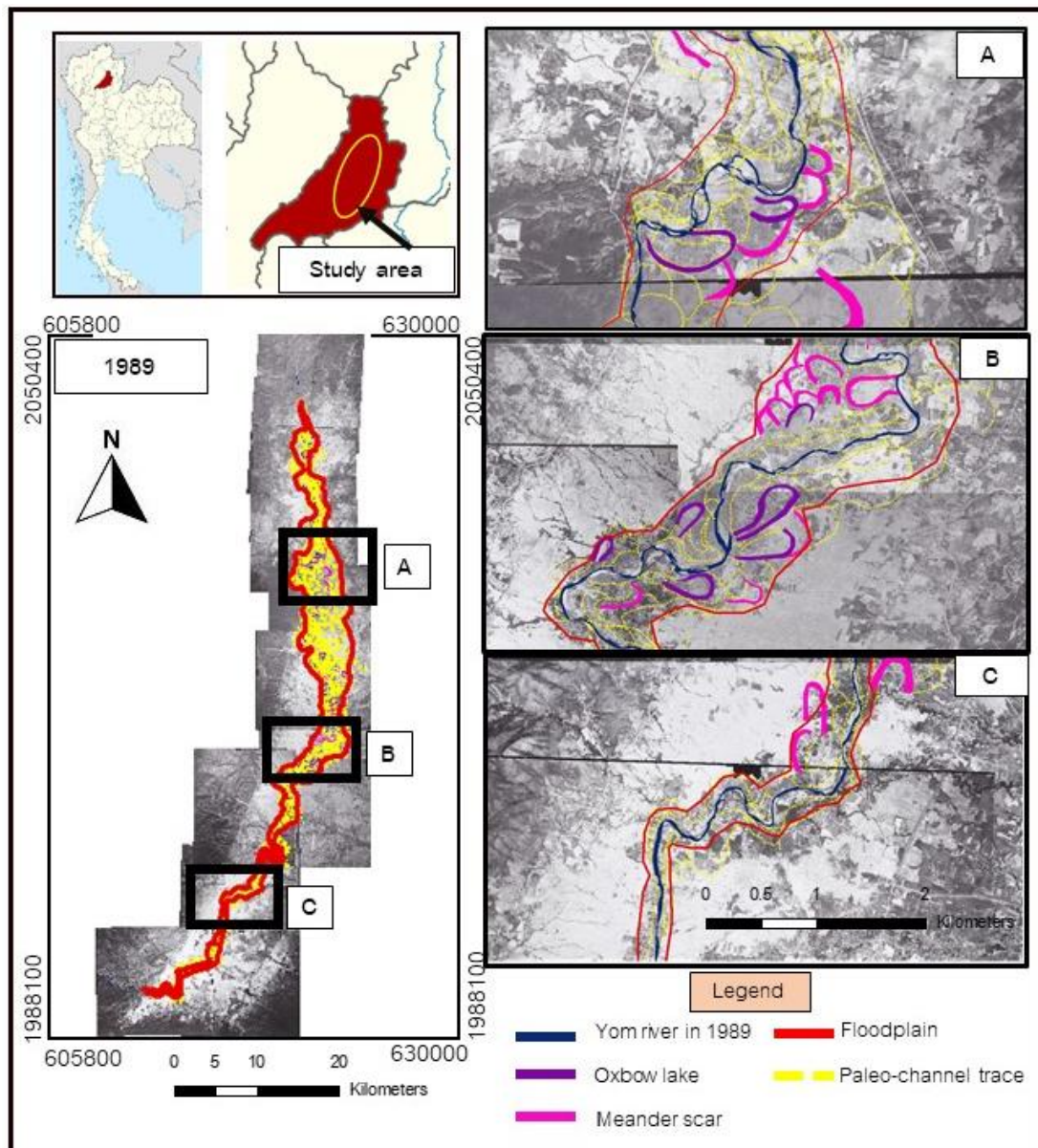


Figure 37 The interpretation of Geomorphological map of Study area in 1989. The interpretation of Geomorphological map of Study area in 1989. The channel migration traces were illustrated on the upper and middle part of study area (A and B), whereas the lower part was shown lack of traces (C).

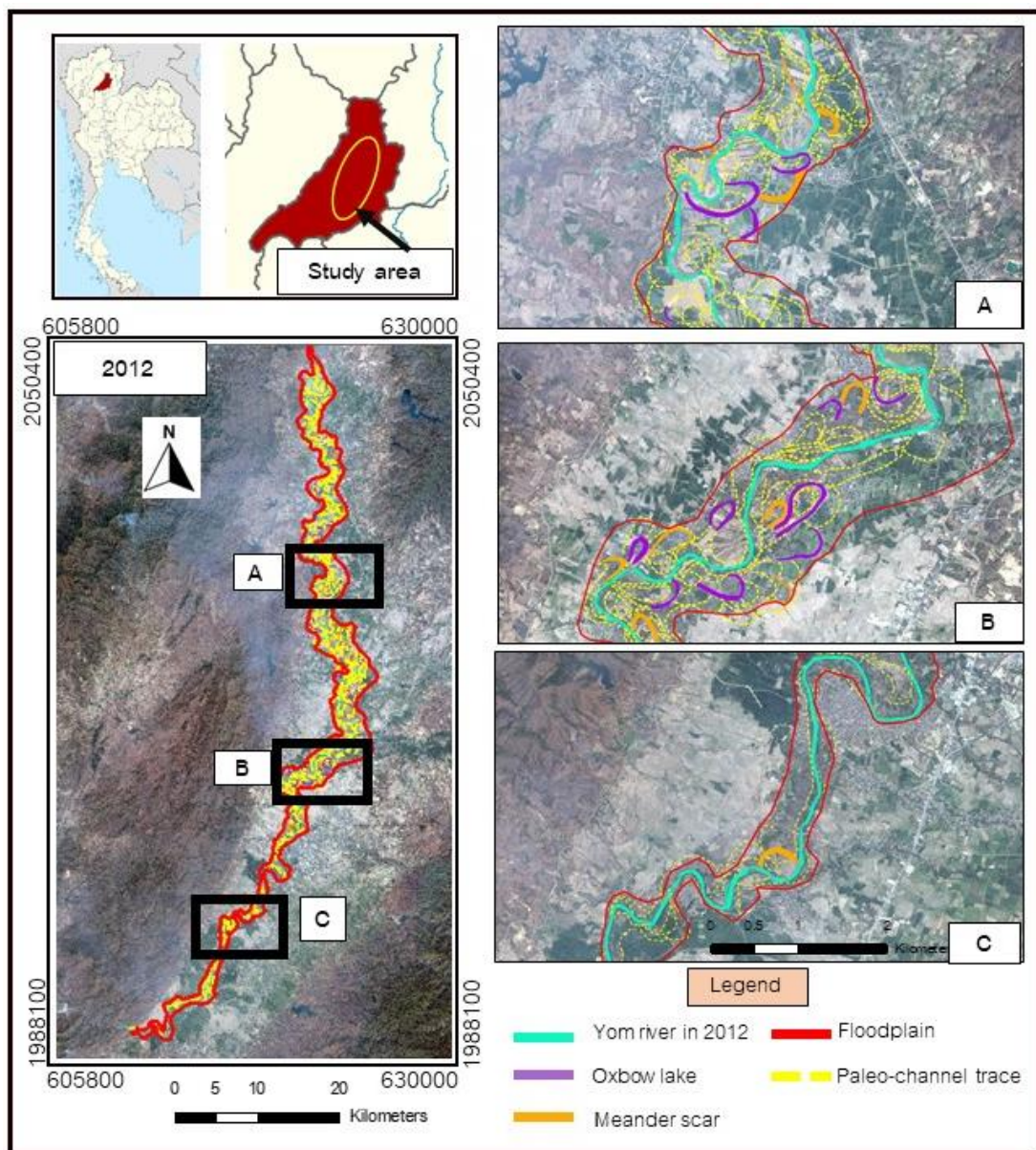


Figure 38 The interpretation of Geomorphological map of Study area in 2012. The channel migration traces were illustrated on the upper and middle part of study area (A and B), whereas the lower part was shown lack of traces (C).

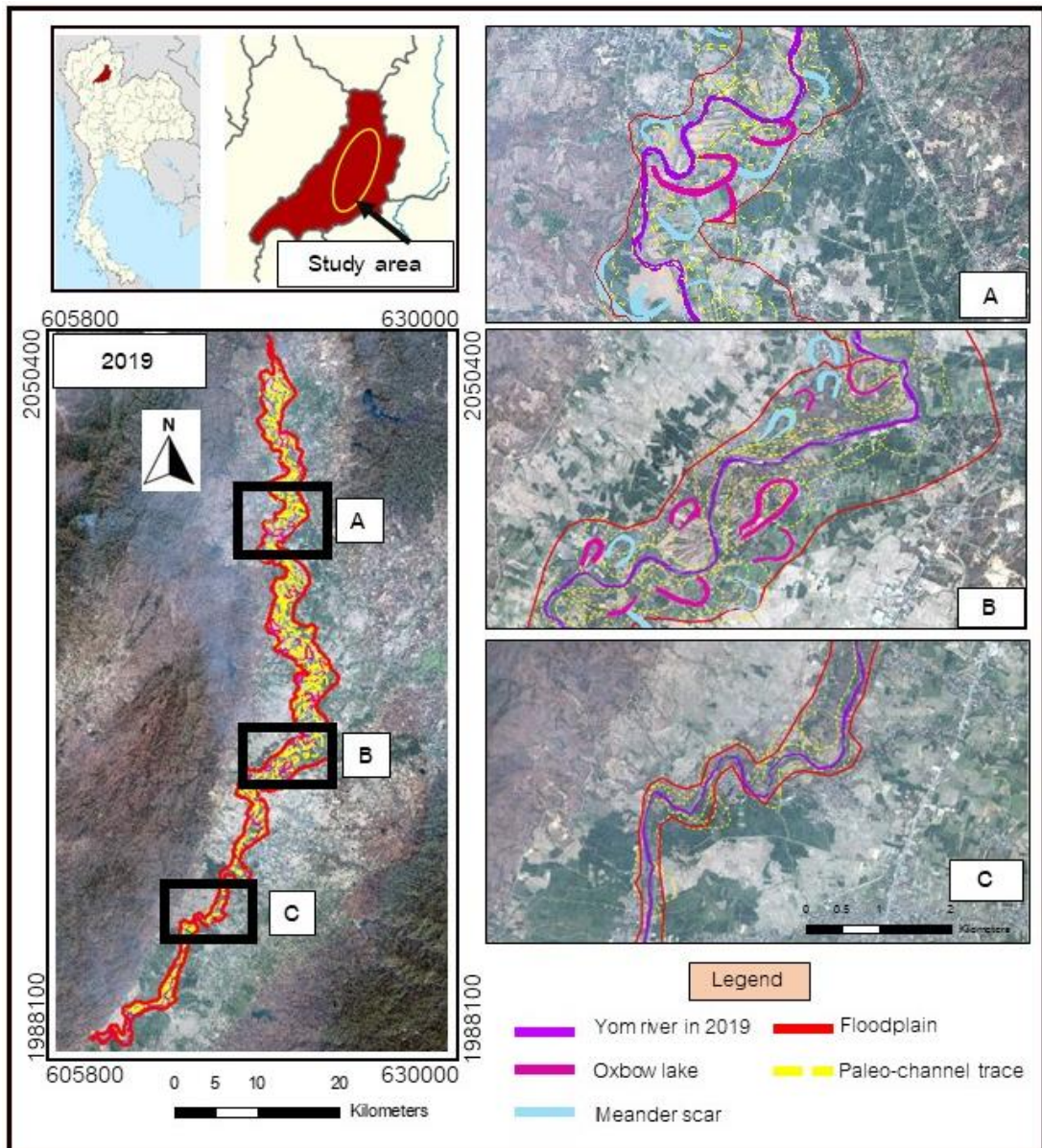


Figure 39 The interpretation of Geomorphological map of Study area in 2019. The interpretation of Geomorphological map of Study area in 1954. The channel migration traces were illustrated on the upper and middle part of study area (A and B), whereas the lower part was shown lack of traces (C).

4.2 Geomorphological criteria analysis

4.2.1 Sinuosity Index (SI)

Given the SI measurements used in this study, they varied from 1.95 to 1.50 from 1954 to 2019. The sinuosity value was significantly highest in 1954 at 1.95, and the lowest in 2019 is 1.50, As the total sinuosity values of the Yom River have decreased over time as seen in Figure 40, it is plausible to assume that the river had erosion and deposition between 1954 and 2019. Moreover, SI values from the past to the recent illustrate in meander river type (SI of the meander is 1.25 to 2).

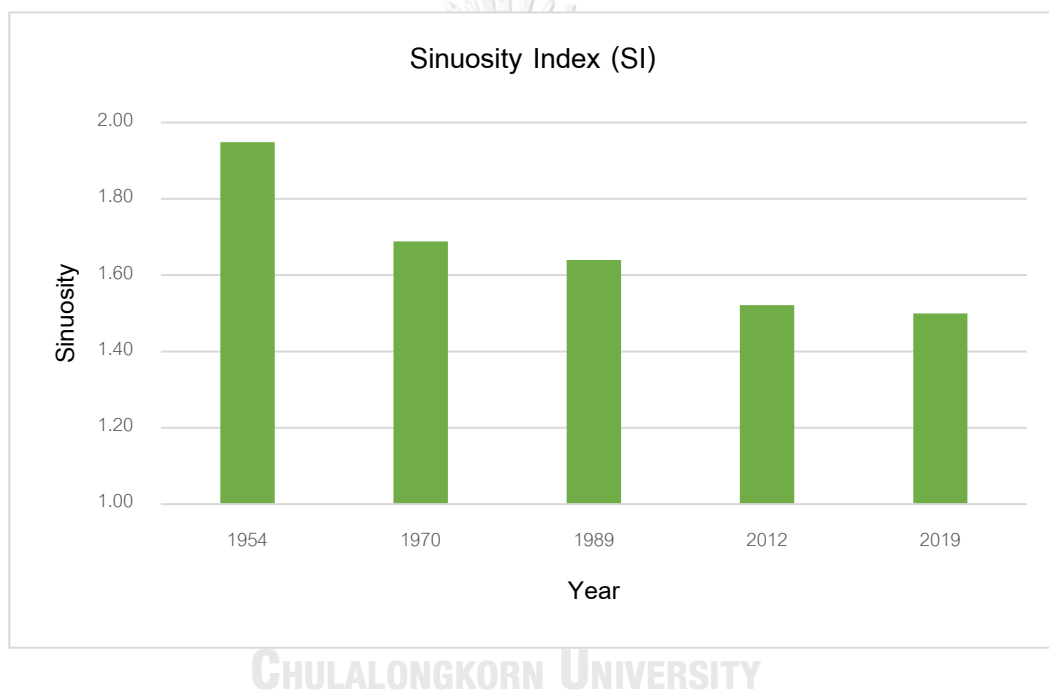
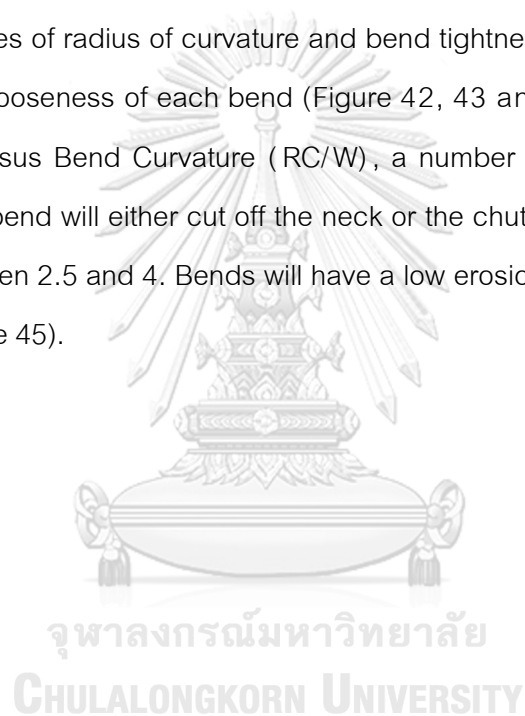


Figure 40 The graph of SI values from 1954 to 2019 shows the decreasing trend.

4.2.2. The Radius of curvature (Rc)

The Rc is the thickness value of the bend; if the value is high, the river bends will be close to each other. A wider bend, on the other hand, will have a low Rc value. Areas 1 and 3 of the curve, which were recorded throughout 5 periods (1954 to 2019), are the only fully complete bends that will be measured in this research. Area 2 was only monitored during specific years due to cut-off channels. According to Figure 41, RC had measurements from three distinct locations that the measurement able bends covered the whole research area.

The changes of radius of curvature and bend tightness ratio (Rc/W) can specify the tightness and looseness of each bend (Figure 42, 43 and 44). Moreover, Meander Migration Rate versus Bend Curvature (RC/W), a number that falls between 1 and 2 indicates that the bend will either cut off the neck or the chute. Bends will erode quickly if values are between 2.5 and 4. Bends will have a low erosion rate if values increase by more than 5 (Figure 45).



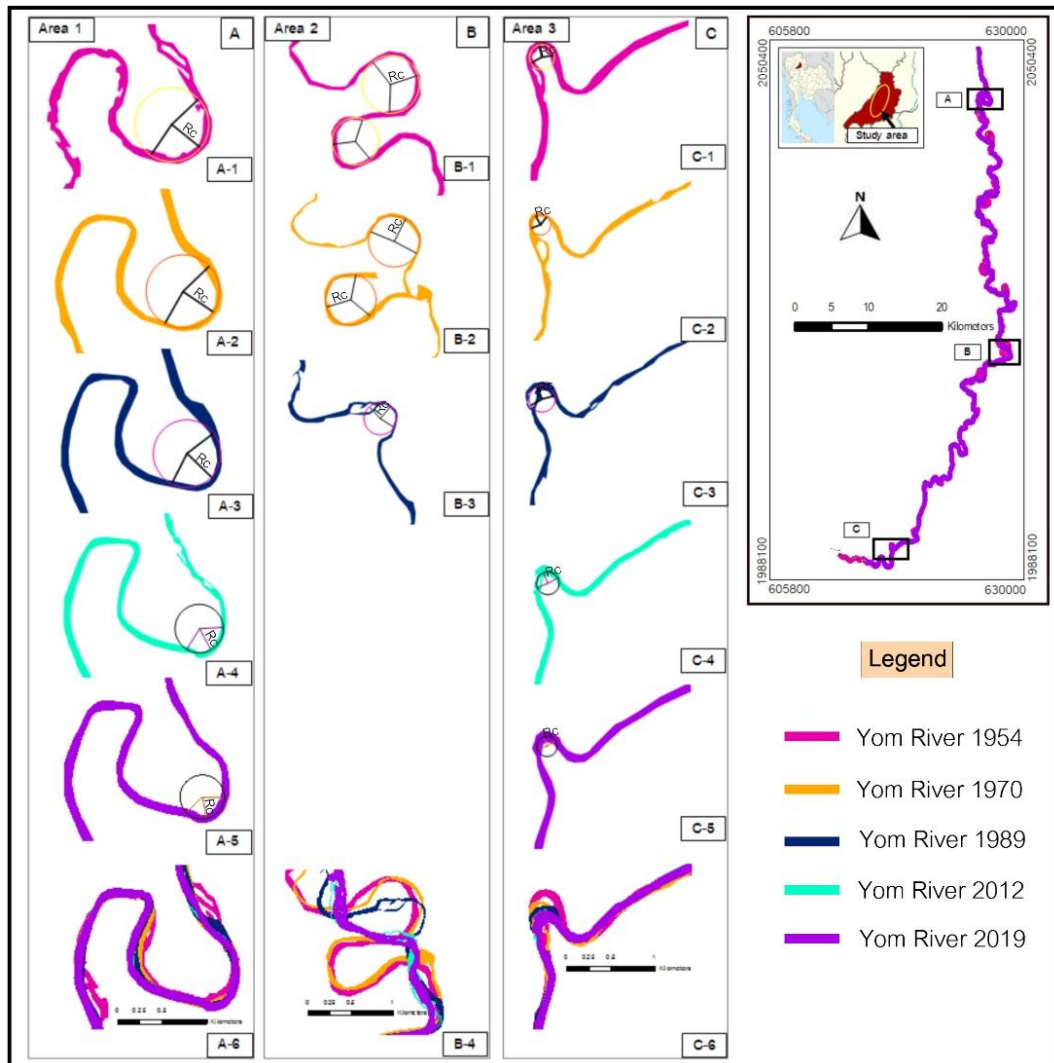


Figure 41 Rc had measurements from 3 locations from 1954-2019. The Rc measurement of Bend 1 from 1954 to 2019 (A-1 to A-5) and total Yom River change in bend 1 (A-6). The Rc measurement of Bend 2 from 1954 to 1989 (B-1 to B-3) and total Yom River change in bend 2 (B-4). The Rc measurement of Bend 3 from 1954 to 2019 (C-1 to C-5) and total Yom River change in bend 3 (C-6). Through this investigation, it was possible to see exactly evaluation at Bend 2 had changed since it was cut off 35 years earlier.

Bend 1	1954	1970	1989	2012	2019
Rc	416.9615	409.164	374.8866	267.7326	247.575
Rc/W	7.476449	5.501734	5.848465	4.64491	4.362554

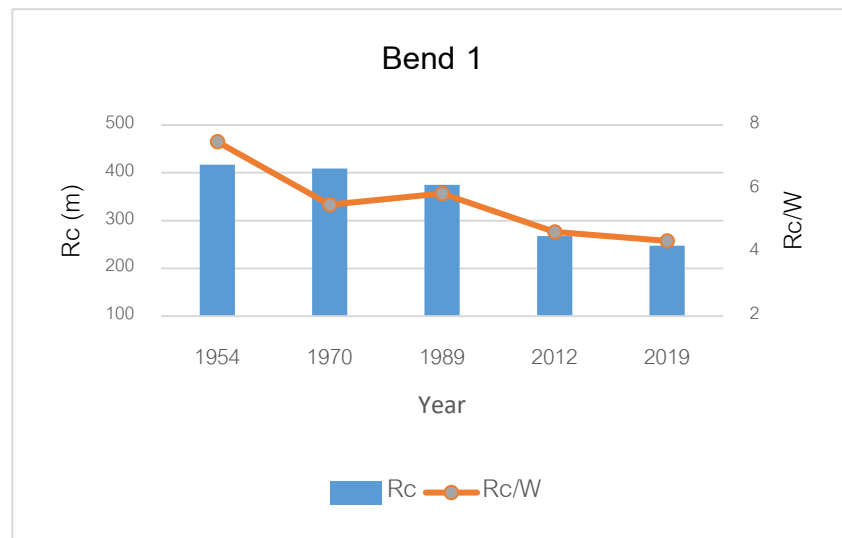
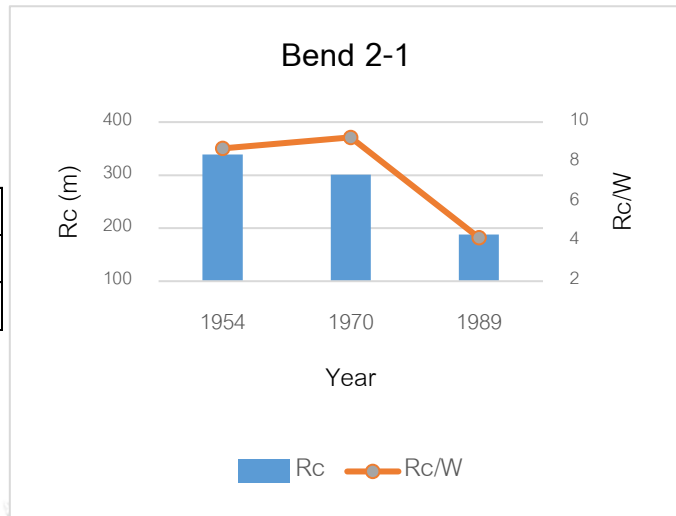
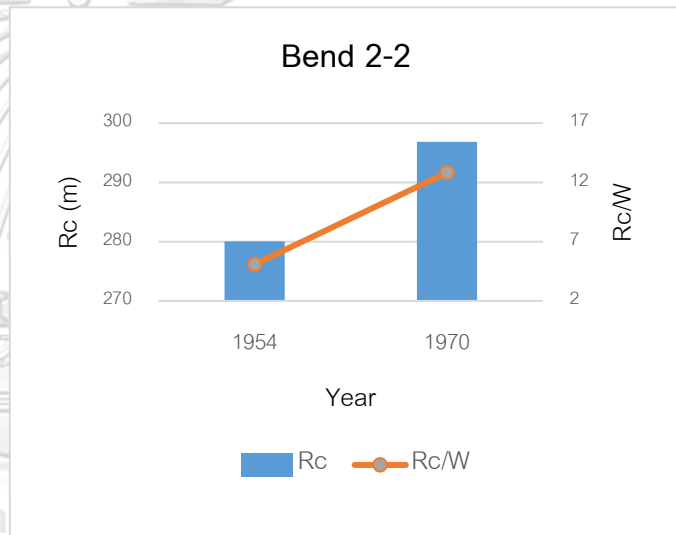


Figure 42 The changes of radius of curvature and bend tightness ratio (Rc/ W) at Bend1 was decreasing from 1954 to 2019.

Bend 2-1	1954	1970	1989
Rc	339.0796	301.0775	188.2538
Rc/W	8.672112	9.232675	4.186209



Bend 2-2	1954	1970
Rc	280.0453	296.8696
Rc/W	5.08526	12.8182



CHULALONGKORN UNIVERSITY

Figure 43 The changes of radius of curvature and bend tightness ratio (Rc/ W) at Bend 2. Bend 2-1 was slightly rose up from 1954 to 1970 and a sharp drop from 1970 due to the chute cut-off as the Bend 2-2 radius of curvature and bend tightness ratio (Rc/W) was increased from 1954 to 1970 and then the bend was cut-off (Figure 41).

Bend 3	1954	1970	1989	2012	2019
Rc	138.5218	115.968	114.1706	118.6386	113.3808
Rc/W	2.821792	1.887807	1.215098	1.363506	1.022739

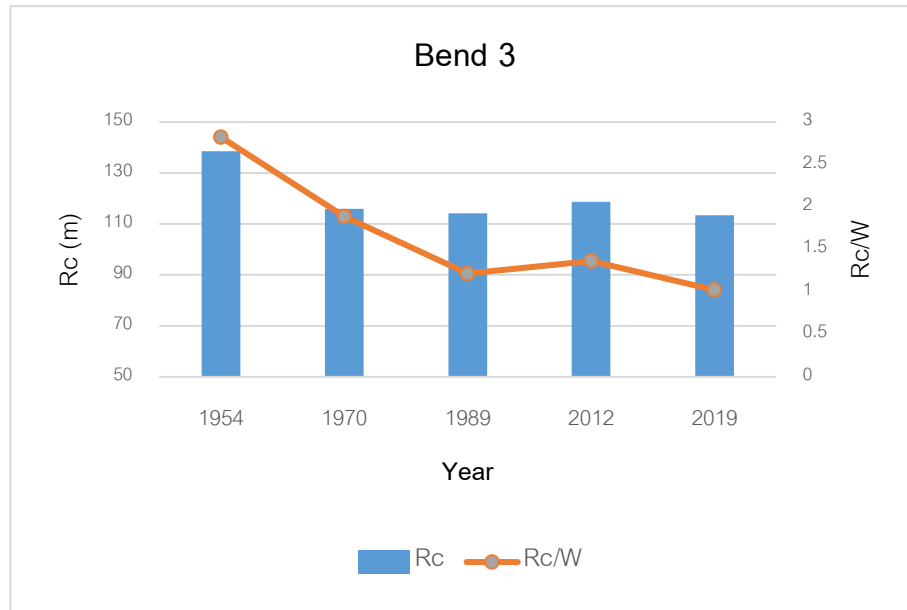


Figure 44 The changes of radius of curvature was varied and bend tightness ratio (Rc/W) at Bend 3 was decreasing from 1954 to 2019.

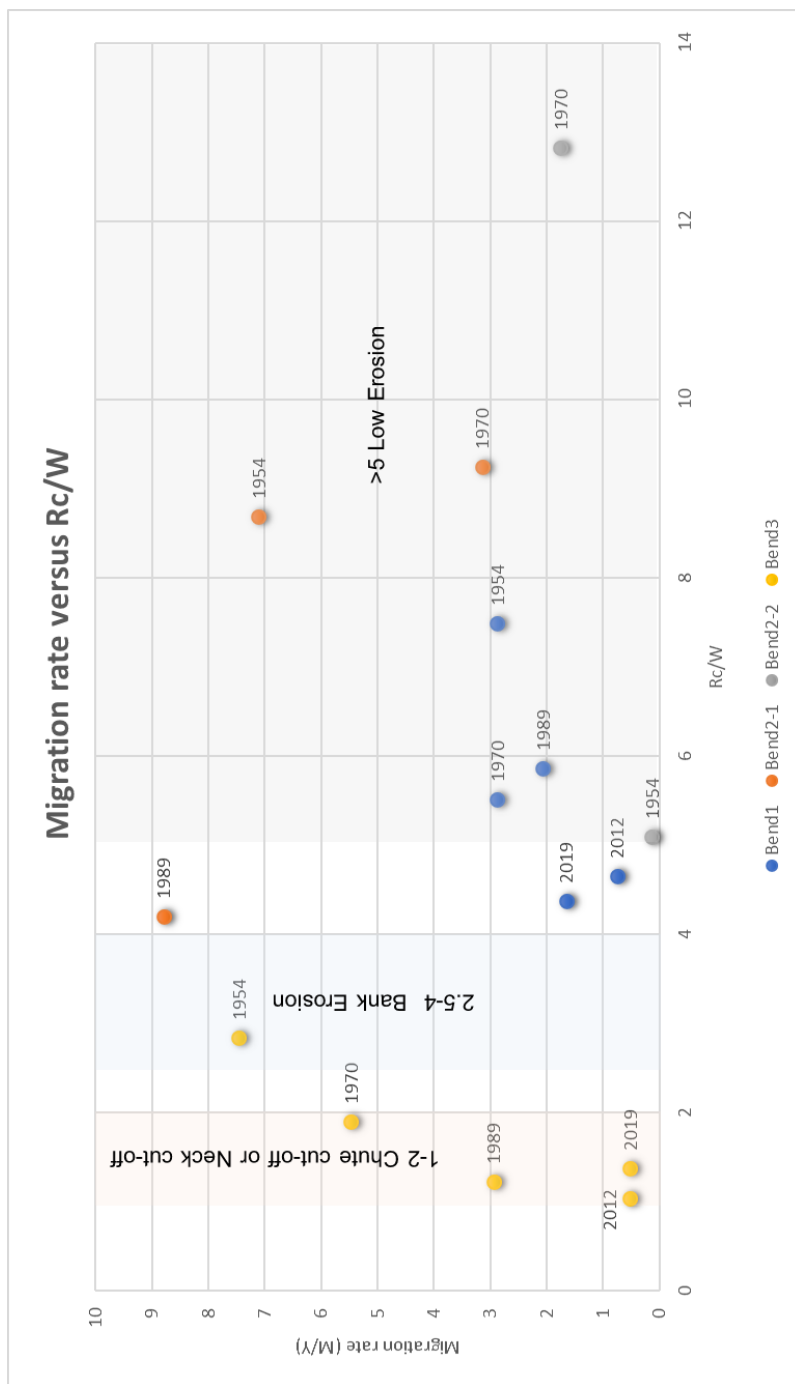


Figure 45 Meander Migration Rate versus Bend Curvature (Rc/W), a number that falls between 1 and 2 indicates that the bend will either cut off the neck or the chute. Bends will erode quickly if values are between 2.5 and 4. Bends will have a low erosion rate if values increase by more than 5, According to the

4.2.3 Channel Width (W)

According to the results of measuring Fifty-three values along the river in five periods (Figure 46), the average channel width in 1954, 1970, 1989, 2012, and 2019 is 59.70 meters, followed by 64.72 meters, 58.13 meters, 59.14 meters, 58.25 meters, and 58.23 meters, respectively. The width of the Yom channel has been slightly reduced from 1954 to 2019 but when compare to paleochannel width, it has changed dramatically from 90.10 meters to 58.23 meters. In addition to The width of this channel classified is medium size since paleo to recent is 20 to 200 meters (Miall, 2013).

Width						
Year	Paleochannel	1954	1970	1989	2012	2019
Average	90.10	64.72	58.13	59.14	58.25	58.23

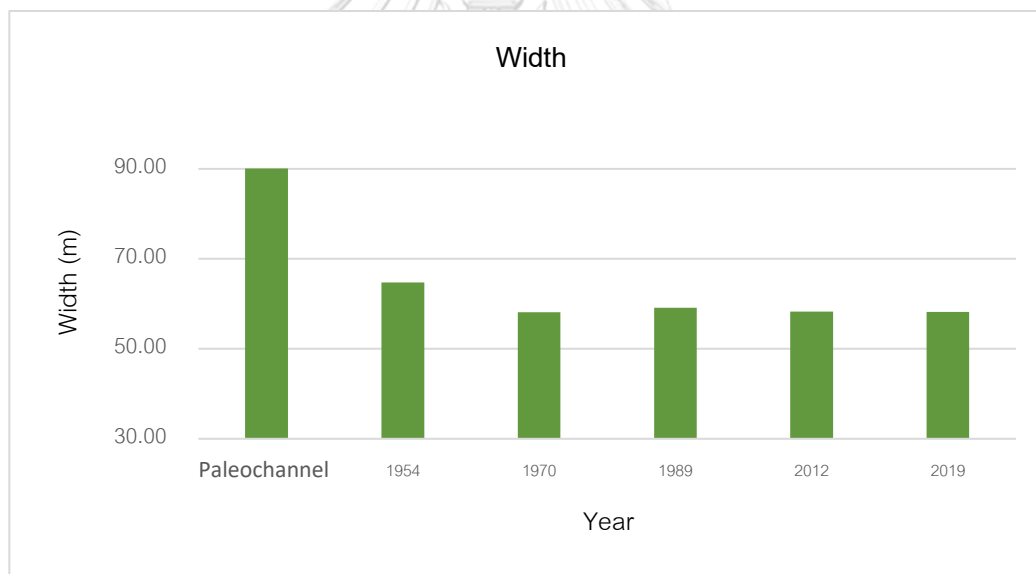


Figure 46 The graph of Yom channel width has been slightly reduced from 1954 to 2019 but when compare to paleo-channel width, it has changed dramatically from 90.10 meters to 58.23 meters.

4.2.4 Channel length (L)

The midline between the left and right banks of the channel polygon is where the Yom River's channel length was measured. The largest channel length for the whole research period was in 1954 (127.93 kilometers), while the shortest was in 2012 (110.19 kilometers). demonstrates how the length of the river stream decreased overall by 17.74 kilometers from 1954 to 2012 and then slightly grew from that year to 2019 by 2.02 kilometers (Figure 47).

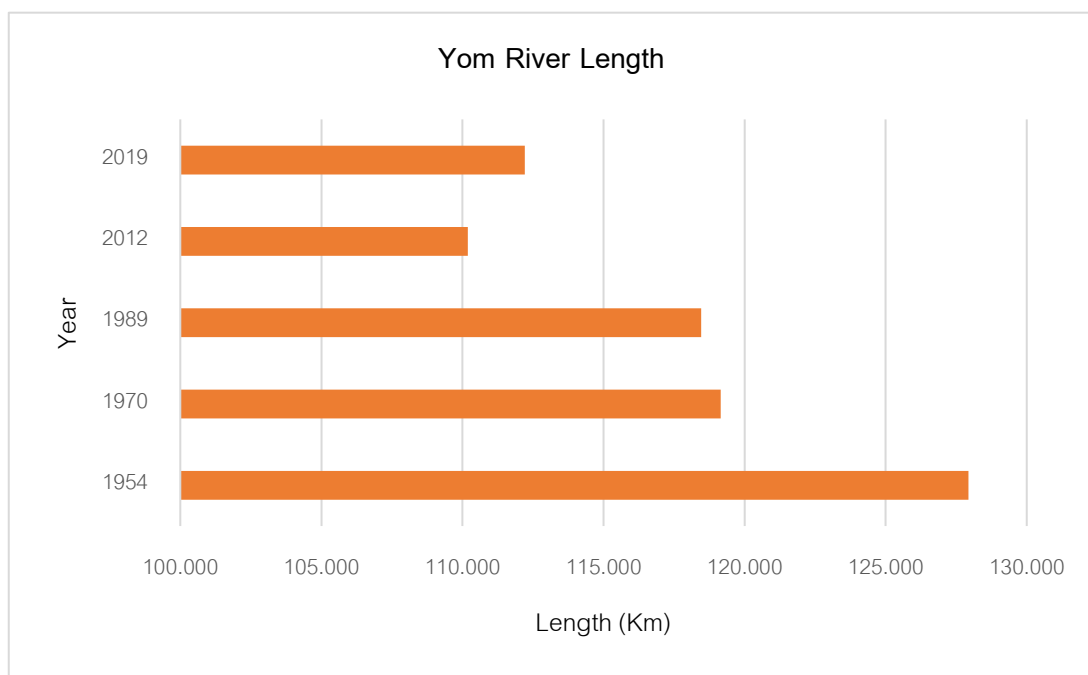


Figure 47 The graph shows compared to the length of Yom River from 1954 to 2019 was dropped due to neck cut-off and chute cut-off.

4.2.5. Channel centerline migration from 1954 to 2019

The centerline lies halfway between the left and right banks. From 1954 through 2019, the global centerline migration rates each year has varied. The centerline moved eastward at a rate of around 0.46 meters per year between 1954 and 1970. (Left side of the river). On the other hand, the centerline changed to the west (right bank of the river) throughout the time periods 1970 to 1989, 1989 to 2012, and 2012 to 2019, respectively, as indicated in the graph. In Figure 41 and 42 that every value of migration was plotted.

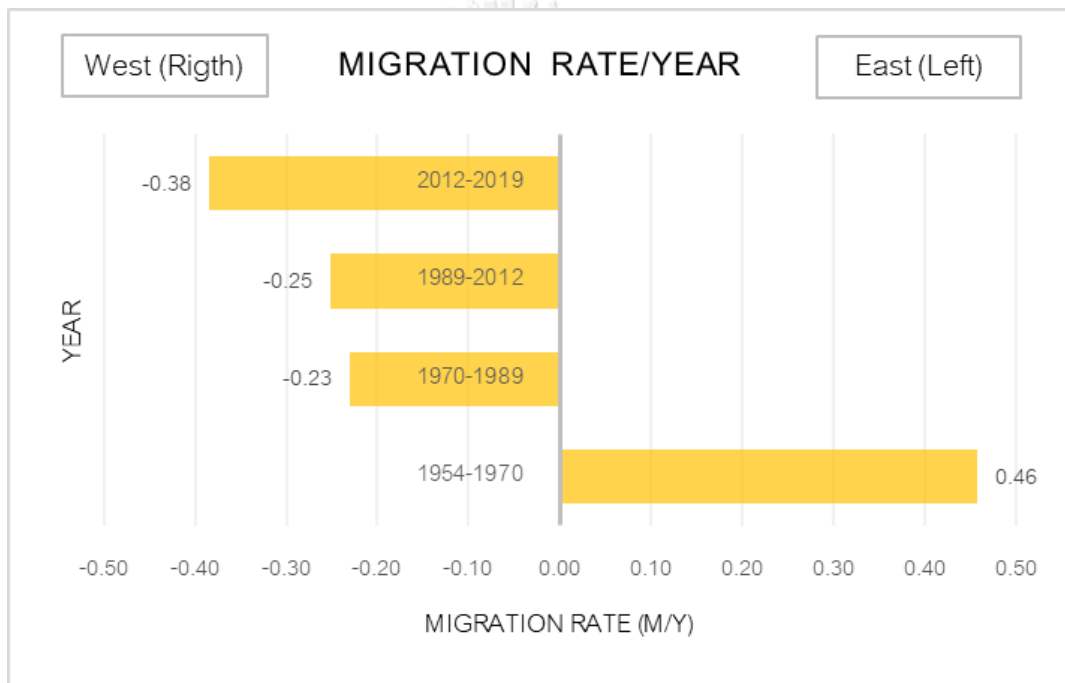


Figure 4 8 The graph shows migration rate / year of Yom River since 1954 to 2019. The River migration to the West (right bank of the river) throughout the time from 1970 to 2019, In contrast to 1954 to 1970, the River was migrated to the East.

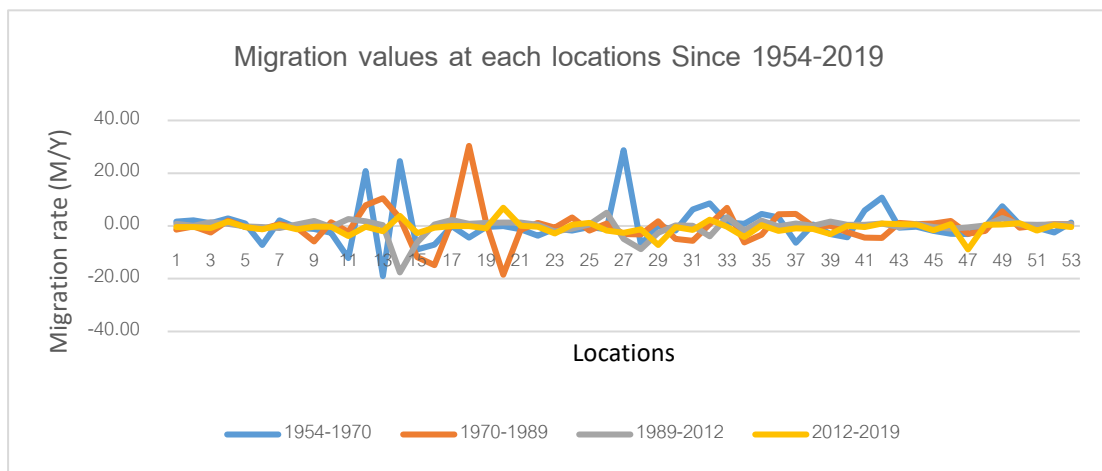


Figure 49 The graph shows all values of migration rate/year in each location from fifty-three cross-sections were plotted. In the obviously different values chances display to the dramatically of migrations due to cut-off.

4.3 Sedimentological data analysis

4.3.1 Grain-size analysis from Boreholes data

Sediment samples taken from boreholes and a profile were processed, and each sample was correlated to morphological characteristics such as a river bank profile, floodplain, or paleo-channel. The sites of the sediment sample were identified on a map in Figure 30.

For the purpose of collecting sediment samples, each geomorphological attribute was sampled using a hand auger in this study. Moreover, sediments from the river bank profile were gathered with the intention of researching the previous fluvial stratigraphy. The five cores from the three locations of meander scars (paleochannels) and floodplains were gathered for the drilling data. A hand auger was used to gather samples from each sample at a depth of 20 cm, which were then put into plastic zip-lock bags.

Two samples representing floodplain and paleochannel along the resistivity line were taken at the first site location (Figure 30) for grain size measurement, however, only the floodplain sample was taken from the GPR line. For the second site (location 5), which is situated on a paleochannel (meander scar) and floodplain along a resistivity line, an additional two samples were taken. The floodplain from the third site (location 6) is where the last sample and resistivity line was taken. These data were used to compare the correlations between shallow geophysical field surveys and sediment size (Resistivity and GPR investigations).

The majority of the samples taken from boreholes were clastic sediments, hence the dry sieve method was used to investigate this approach. Following the dry sieving process, particles were weighed in each size and categorized according to Folk's approach of gravel, sand, and mud to identify the sedimentary type.

1) Site 1 from location 1: Paleochannel and floodplain (at Ban long Lue Bun), two hand-dug boreholes (LLB-1 and LLB-2). The coordinates of LLB-1 at the paleochannel (meander scar) are 18.450590N and 100.175892E degrees in latitude and longitude, respectively. The core depth is 200 centimeters in total. Mud makes up every stratum of the sediment. LLB-2 is situated at a latitude of 18.451062N degrees and a longitude of 100.176403E degrees in the Yom River valley. The core depth is 300 centimeters in total. There are two distinct sedimentary categories that it lies underneath. The sediment levels between 20 and 100 centimeters are primarily made up of mud, while the sediment layers between 100 and 300 centimeters are entirely made up of sandy mud.

2) Site 2 from location 5: Floodplain connected with meander scars (Ban Ton Kha) where 2 boreholes (TK-1 and TK-2) were collected from the floodplain and meander scar respectively similar to location 1 . The coordinates of TK-1 in the floodplain are 18.190361N degrees latitude and 100.161556E degrees longitude. The core depth is 400 centimeters in total. The sediment layers are mostly made up of muddy sand interspersed with a layer of sand between 100 and 120 centimeters in depth from depths of 20 to 160 centimeters. In addition, there are layers of sandy gravel that are 40 centimeters thick and 10 centimeters thick, respectively, in depths between

160 and 300 centimeters, with gravelly sand interspersed between the layers of sandy gravel. There is mostly muddy sand (total thickness is 60 cm) at a depth of 300–400 centimeters in this area, which was interspersed with sand gravel and gravelly sand (each thickness is 20 cm). In latitude 18.189748N degrees and longitude 100.161308E degrees, TK-2 is situated in a mud-filled paleo-channel (meander scar) that was formerly part of the Yom River.

3) Location 3 : The floodplain (Ban Nong Lom) , which is situated at latitude 18.198453N degrees and longitude 100.152707E degrees, provided one borehole sediment (NL-1) for collection. The core is 220 centimeters deep overall. All of this stratigraphic logging is depicted as having a fining upward characteristic, with the higher logging (depths of 20 to 80 centimeters) being made up of mud, overlaid on layers of muddy sand (20 centimeters thick) , and sand (10 centimeters thick) , gravelly sand (20 centimeters thick), and sandy gravel (20 centimeters thick). These five boreholes lithological analyses were shown in Figure 51.

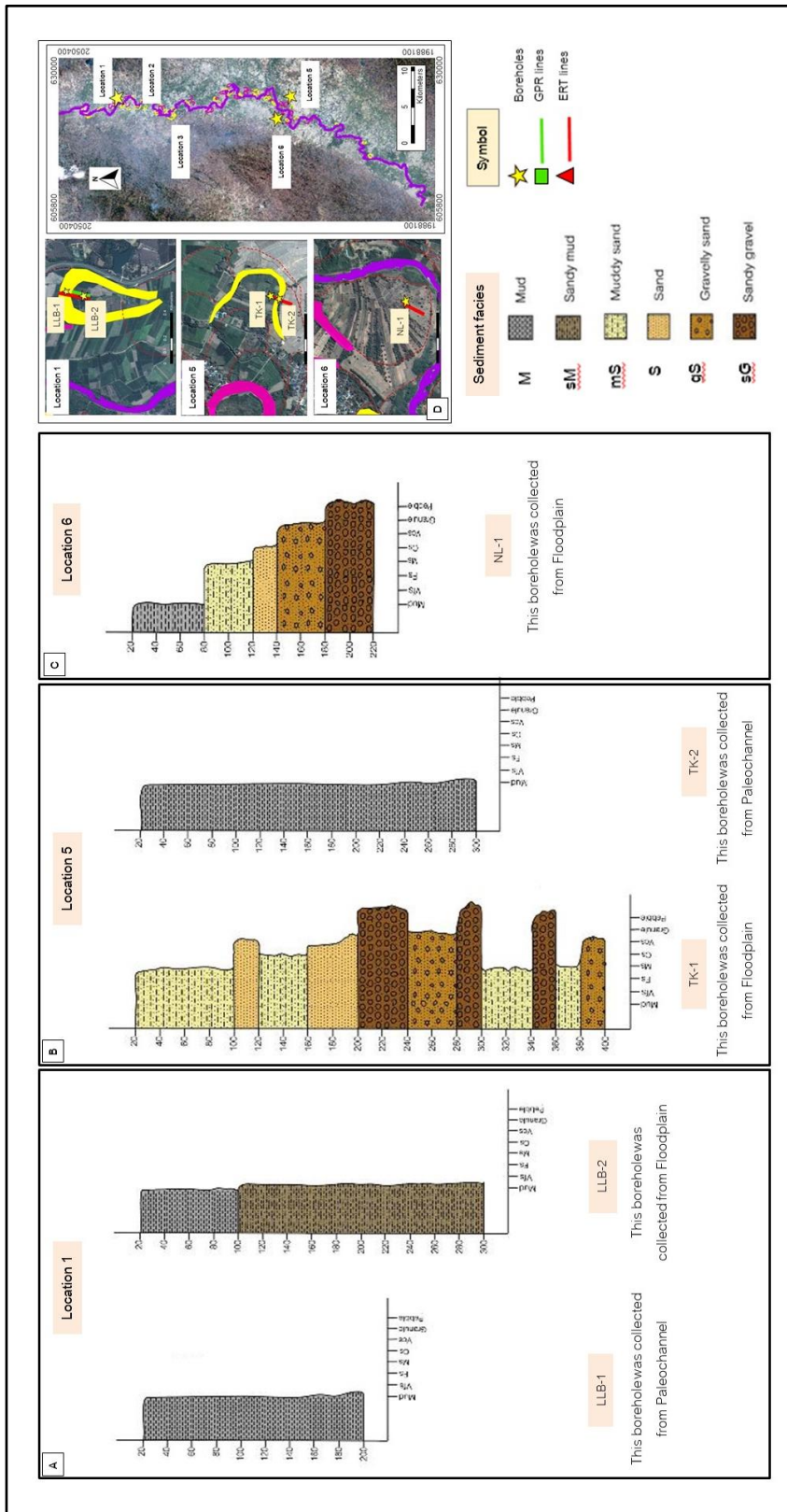


Figure 50 Five boreholes lithological analyses from 3 locations in study area. The first site was collected two boreholes from location 1 (A). The second site was collected two boreholes from location 5 (B). The third site was collected one borehole from location 6 (C).

4.3.2 River Bank profiles

The river profile from this study represents to sedimentology and stratigraphy of paleo-fluvial succession that profile has shown perfect profile on one site at Ban Huai Mai (which is on the other side of the river from location 2 of the site of geological investigations) (Figure 52).

The bank river profile of the Yom River is located at a latitude of 18.394520N degrees and a longitude of 100.155969E degrees. The height of the river bank is approximately 5 to 6 meters. The upper layer is topsoil which mainly consists of brown clay and silt from the surface to an estimated 40 centimeters. All of this stratigraphy logging profile is shown as a fining upward character on 3 sequences, which each sequence is composed of mud and sandy mud on the upper profile (depth from 40-100 centimeters) , overlaid on gravelly sand and sandy gravel (thickness is about 20 centimeters). The bank profile shows on Figure 52.

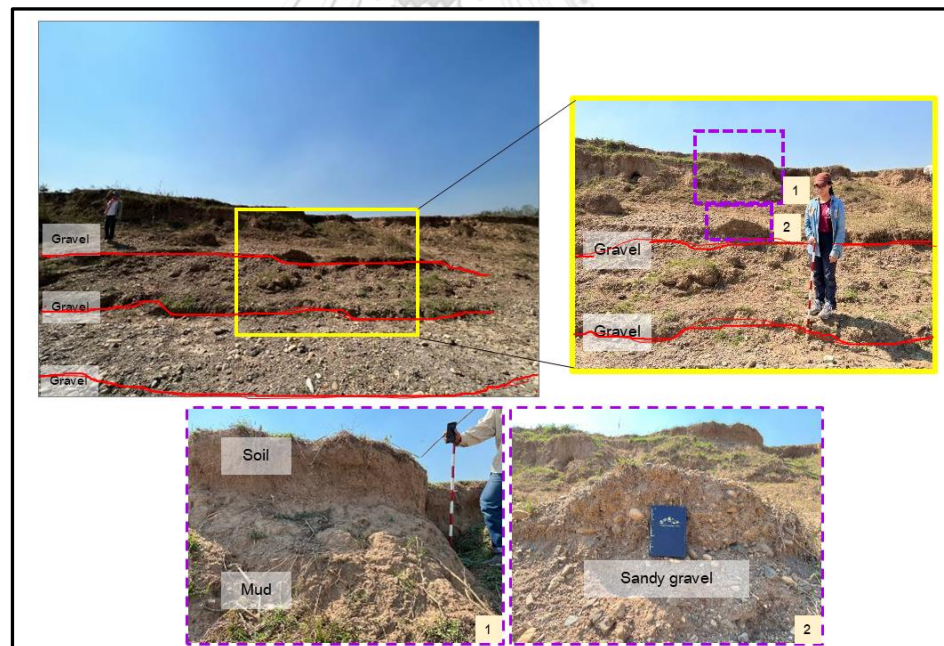


Figure 51 The river profile from this study represents to sedimentology and stratigraphy of paleo-fluvial succession that profile has shown perfect profile on one site at Ban Huai Mai.

4.4 Electrical Resistivity Tomography (ERT) profiles

Six resistivity survey lines and two GPR survey lines were investigated along paleochannels (meandered scars), point bars, and floodplains.

Location 1 is located near Ban Long Lue Bun. The 235 meters resistivity survey line covers a meandered scar, point bar, and floodplain shown in Figure 53.

The result of resistivity was separated into two zones which are the low resistivity zone, and the moderate resistivity zone (Figure 53). From the sediment analysis of location 1, the layer is from 0 to -2 meters. represents a low resistivity value of about 7.25-42.8-ohm meter. where present in 3 areas, the first place is meander scar feature (horizontal from 20 to 96 meters, vertical depth from 0 to -10 meters), the second area is floodplain (horizontal from 150 to 235 meters vertical from 0 to -4 meters), and the last is all vertical subsurface (depth from -20 to -50 meters). This zone relates to the sedimentary analysis from LLB-1 and LLB-2, It is all composed of mud, and sandy mud.

The resistivity value shows moderate resistivity about 42.8-162-ohm meter. where present in 2 areas, the first area is meander scar feature (horizontal from 0-96 meters and depth from -10 to -20 meters), and this zone is shown in floodplain area were separated to 2 parts (horizontal from 96 to 150 meters, vertical from 0 to -20 meters and horizontal from 150 to 235 meters, vertical from -4 to -25 meters). This zone relates to the sedimentary analysis from TK-1, It is all composed of four associations with muddy sand, sand, gravelly sand, and sandy gravel.

Location 2 was surveyed at Ban Huai Mai. The longest resistivity survey line 470 meters displayed on the map and the longest 470 meters resistivity survey; investigates the floodplain and point bar. The result of resistivity was separated into two zones which are low to moderate resistivity zone, and the moderate to high resistivity zone (Figure 54). As a low to moderate resistivity value is about 3.18-47.8-ohm meter. that is present at the bottom of the profile inversion (vertical depth estimate from -15 to -50 meters), This zone relates to the sedimentary analysis from LLB-1 and LLB-2, It is all composed of mud, and sandy mud.

Whereas the resistivity value shows moderate to high resistivity about 47.8-366-ohm meter., were present on floodplain and point bars feature (horizontal from 0 to 235 meters and vertical depth from 0 to -15 meters). Moreover, the zone shown on the right bottom profile was horizontal from 350 to 380 meters, and vertical depth from -40 to -50 meters in a semi-circle shape. This zone relates to the sedimentary analysis from the bank profile and NL-1, It is all composed of five associations of mud, muddy sand, sand, gravelly sand, and sandy gravel.

Location 3 was surveyed at Ban Huai Kan. This area was only investigated in a resistivity survey. The 235 meters resistivity survey line covers the floodplain and previous channel trace. The result of resistivity was separated into two zones which are the low resistivity zone, and the moderate resistivity zone (Figure 55). As a low resistivity value is about 0.282-44.4-ohm meter. that is present at the bottom of the profile inversion (vertical depth estimate from -20 to -50 meters), This zone relates to the sedimentary analysis from LLB-1 and LLB-2, It is all composed of mud, and sandy mud. Otherwise, the resistivity value shows moderate resistivity about 44.4-104-ohm meter., present on the floodplain and previous channel trace feature (vertical depth from 0 to -20 meters). This zone relates to the sedimentary analysis from TK-1, It is all composed of 4 associations with muddy sand, sand, gravelly sand, and sandy gravel.

Location 4 was surveyed at Ban Ton Nun. This area was only investigated in a resistivity survey. The 235m-resistivity survey line covers the floodplain and the previous channel trace. The result of resistivity was separated into two zones which are low to moderate resistivity zone, and the moderate to high resistivity zone (Figure 56). As a low to moderate resistivity value is about 5.51-47.1-ohm meter., which is present at the bottom zone of the profile inversion (vertical depth from -15 to -50 meters), This zone relates to the sedimentary analysis from LLB-1 and LLB-2, It is all composed of mud, and sandy mud which is characteristic sediment similar to floodplain deposition, moreover, this zone shows the u-shape geometry at the left, middle, and right side of low resistivity zone.

The resistivity value shows moderate to high resistivity about 47.1-235-ohm meter., This zone relates to the sedimentary analysis from TK-1, and NL-1, It is all composed of five associations with muddy sand, sand, gravelly sand, sandy gravel, and gravelly sand.

Location 5 was surveyed at Ban Ton Kha. This area was only investigated in a resistivity survey. The 235 meters resistivity survey line covers the floodplain, meander scar, and point bar. The result of resistivity was separated into two zones which are the low resistivity zone, and the moderate resistivity zone (Figure 57). This zone relates to the sedimentary analysis from LLB-1 and LLB-2, It is all composed of mud, and sandy mud. As a low resistivity value is about 5.07-47.1-ohm meter., it shows on the bottom and the top of the ERT profile (in horizontal from 45-235 meters and vertical from 1.5 to -10 meters, and -20 to -50 meters), moreover, it shows the trapezoid shape on the northern part (left zone of profile cross-section).

Since the resistivity value shows moderate to high about 52.4-302 ohm meter., were present on a floodplain, point bar, and subsurface. This zone was separated into two parts, the surface zone on a floodplain and the subsurface zone (horizontal from 18 to 50 meters, vertical from 0.5 to -25 meters and horizontal from 150 to 235 meters, vertical from -10 to -30 meters, respectively). This zone relates to the sedimentary analysis from TK-1, and NL-1, It is all composed of five associations with muddy sand, sand, gravelly sand, sandy gravel, and gravelly sand.

Location 6 was surveyed at Ban Nong Lom. This area was only investigated in a resistivity survey. The 235 meters resistivity survey line covers the floodplain and point bars. The result of resistivity was separated into two zones which are moderate to high resistivity zone (resistivity value 18.3-175-ohm meter.), and the very high resistivity zone (resistivity value 175-953 ohm meter.) (Figure 58). From the borehole on the left side of the ERT profile cross-section, the lithology from the moderate to a very high zone is NL-1 characteristic sediment which is composed of 5 associations with muddy sand, sand,

gravelly sand, sandy gravel, and gravelly sand (shown on vertical depth 0 to -15 meters). This area has an extremely high resistivity value different from other sites due to very drought on sediments. However, the characteristic of lithology can interpret as fluvial deposits such as paleo-channel. As the moderate to high zone (shown on vertical depth from -15 to -50 meters)., This zone relates to the sedimentary analysis from TK-1, It is all composed of four associated.



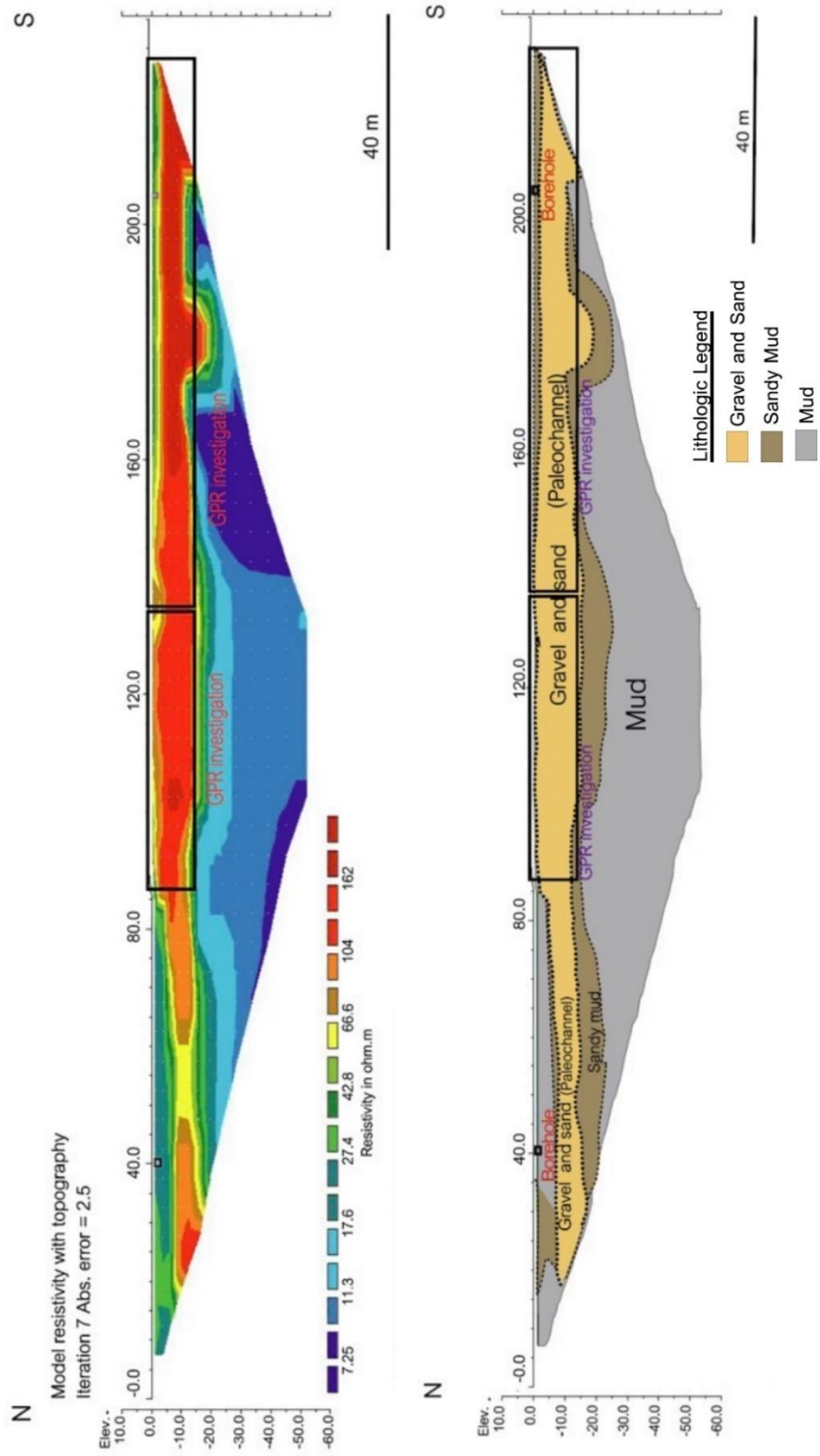


Figure 52 The 235 m-resistivity survey line covers a meandered scar, point bar, and floodplain show inversion model of ERT from interpretation base on boreholes data and resistivity values at location 1.

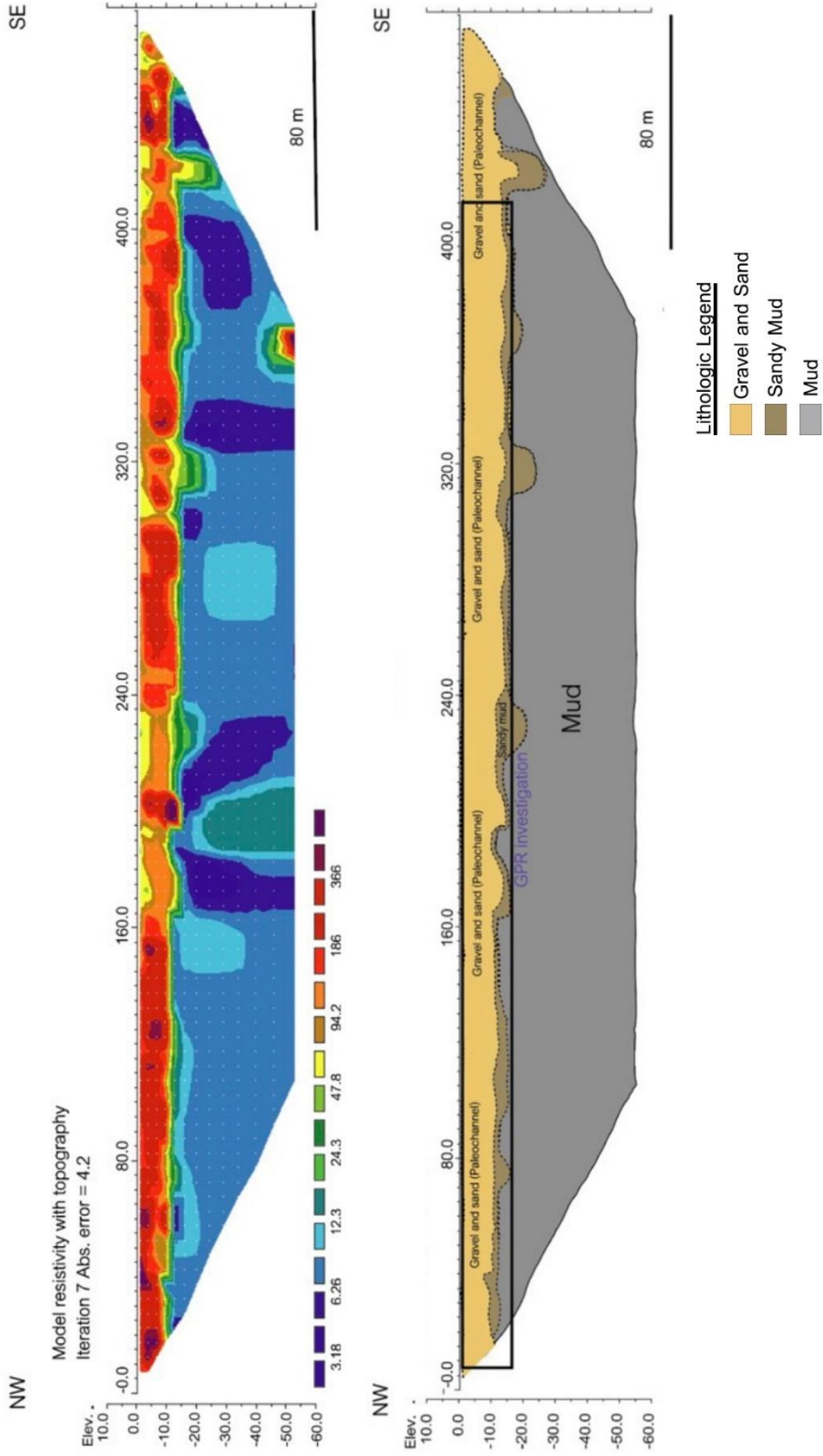


Figure 53 The 470m-resistivity survey; investigates the floodplain and point bar show inversion model of ERT from interpretation base on boreholes data and resistivity values at location 2.

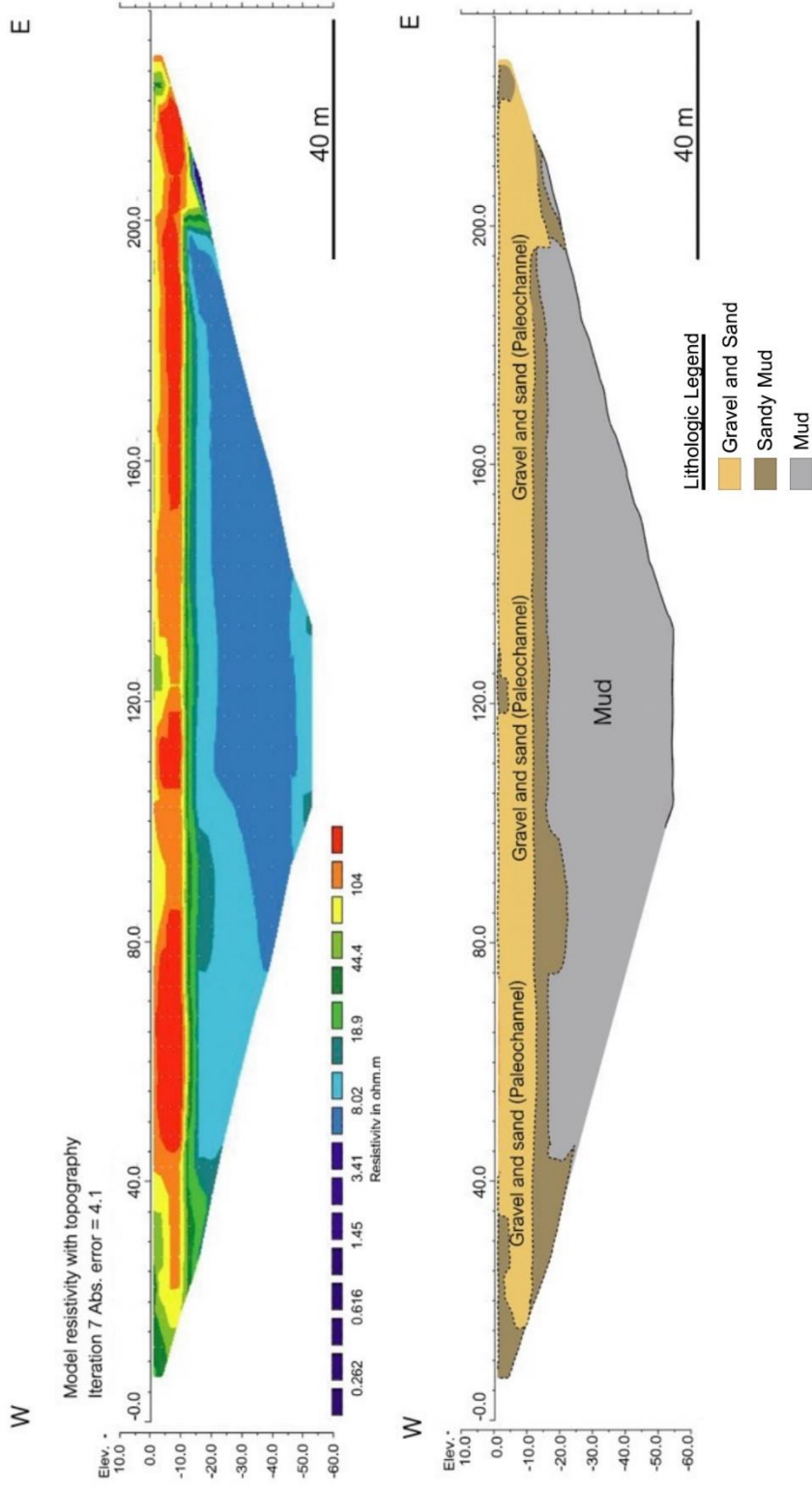


Figure 54 The 235m-resistivity survey line covers the floodplain and previous channel trace show inversion model of ERT from interpretation base on boreholes data and resistivity values at location 3.

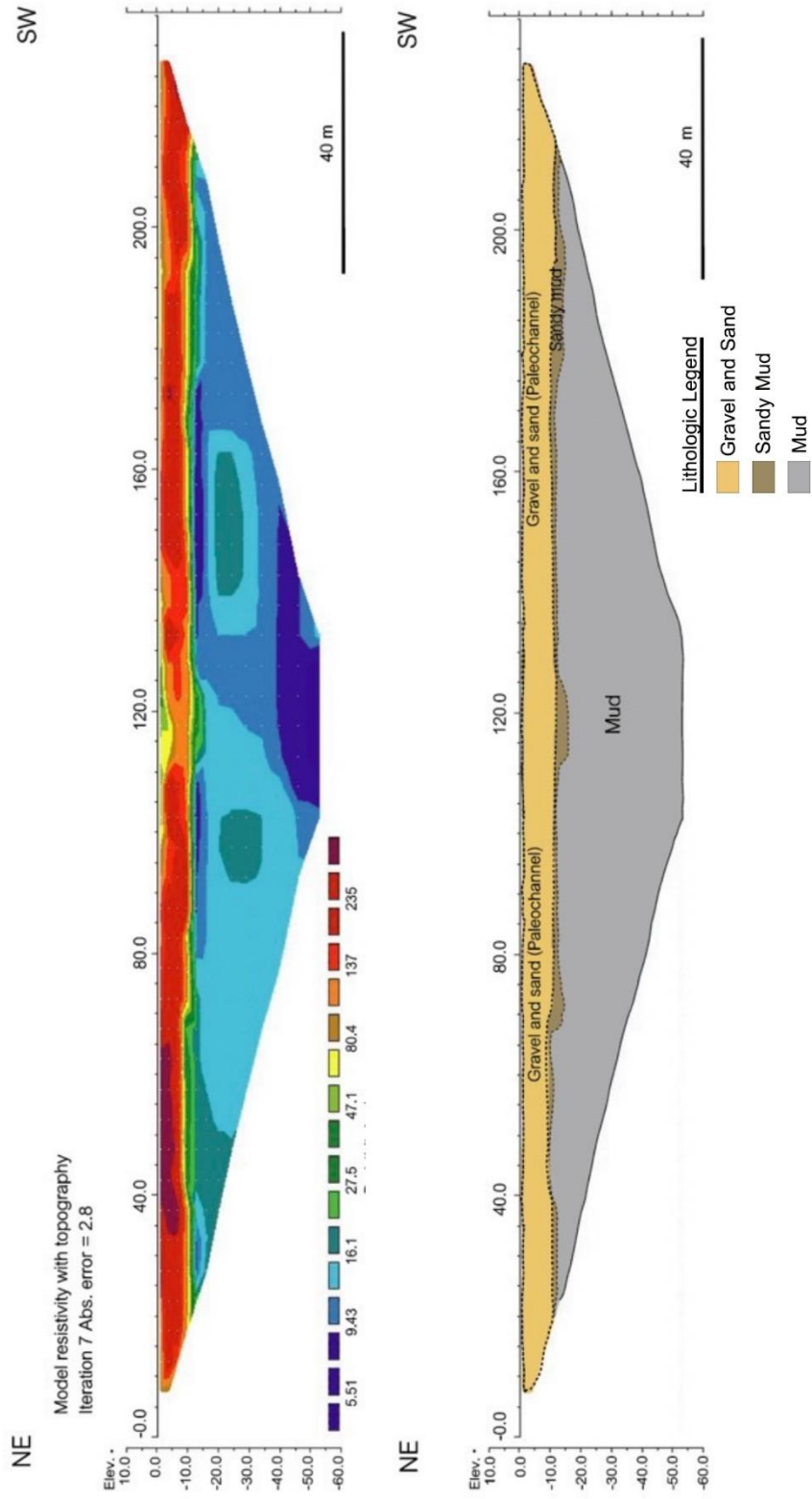


Figure 55 The 235m-resistivity survey line covers the floodplain and the previous channel trace show inversion model of ERT from interpretation base on boreholes data and resistivity values at location 4.

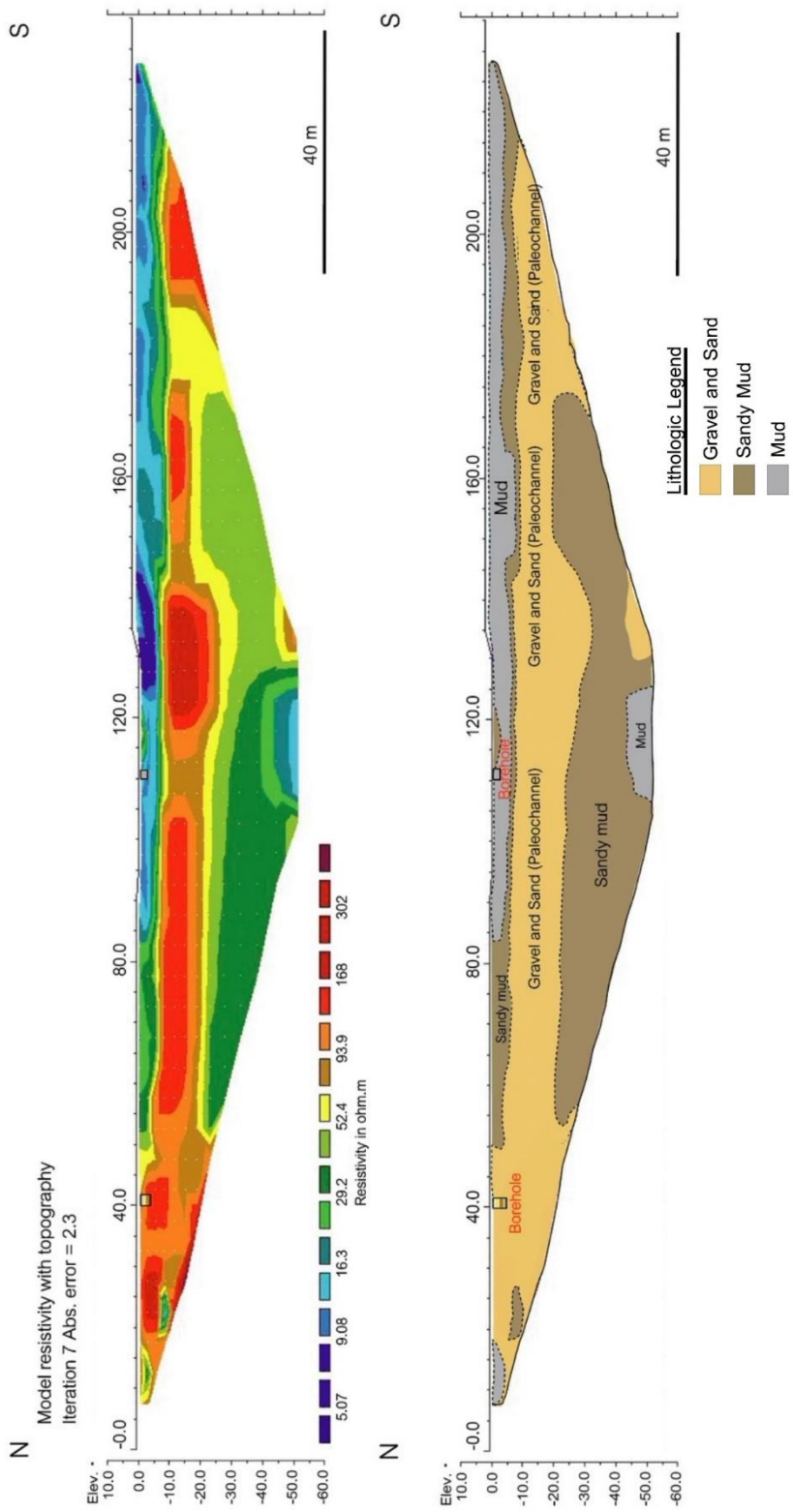


Figure 56 The 235m-resistivity survey line covers the floodplain, meander scar, and point bar show inversion model of ERT from interpretation base on boreholes data and resistivity values at location 5.

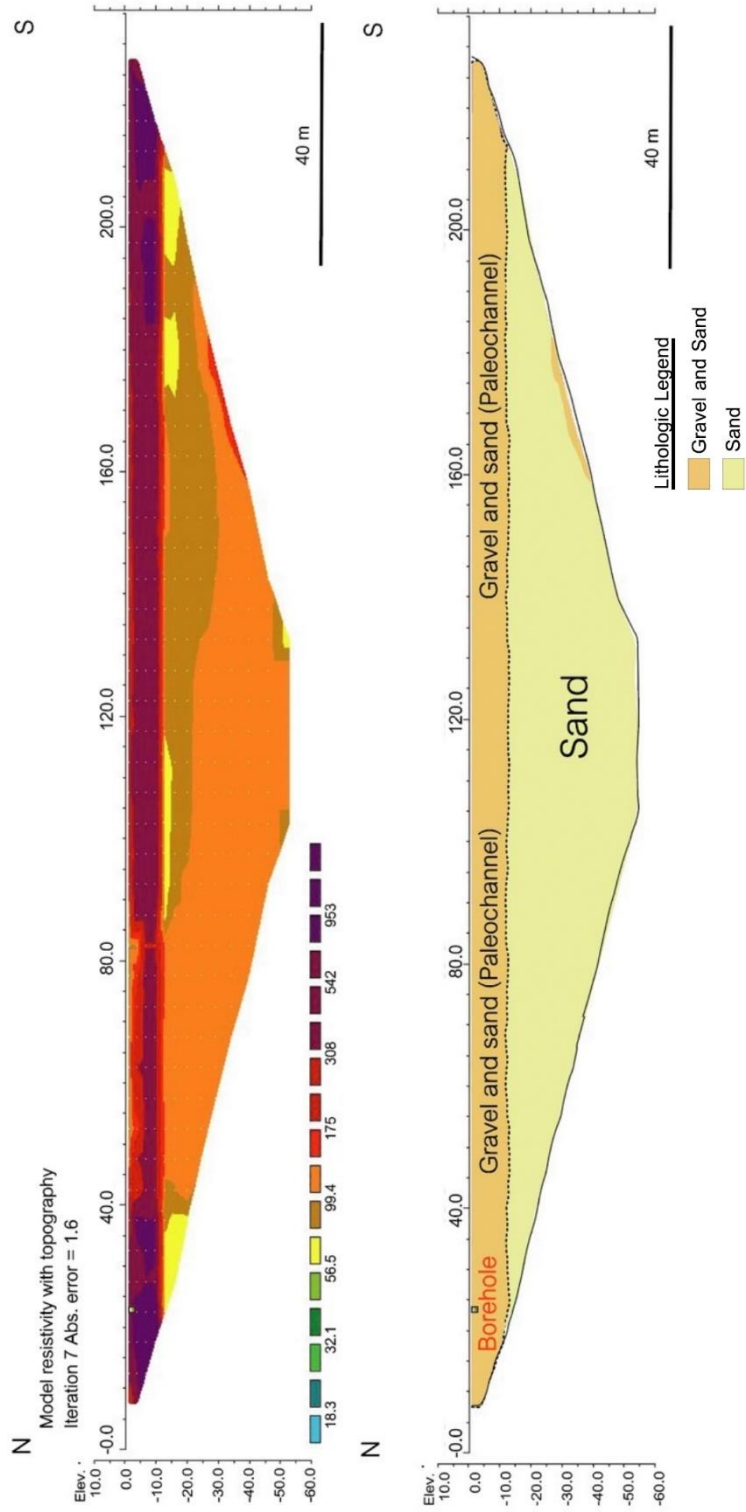


Figure 57 The 235m-resistivity survey line covers the floodplain and point bars show inversion model of ERT from interpretation base on boreholes data and resistivity values at location 6.

4.4.1 Ground Penetrating Radar

GPR profiles are located in Figure 30, this study investigated GPR on 2 sites (Location 1 and 2). Location 1 is located in Ban long Lue Bun which is surveyed on a point bar and floodplain, it will be separated into 2 lines because of the continuity area. Based on Location 2 Ban Huai Mai, the main targets of the investigation are paleochannel and floodplain.

1) Location 1: Ban long Lue Bun

The result of GPR from location 1 surveyed on the floodplain and point bar, 140 meters-GPR survey line be separated into 2 lines each line in 48 meters and 97 meters, respectively.

The profile of the 48 meters-GPR survey line (Figure 5 9) shows a maximum depth of 15 meters. From the surface to the depth of 3 meters, mud layers show whereas the parallel can be observed from the upper part. The depth of 10 meters sediment layer dips northward into the dried channel, due to lithology, sedimentary, and structure from GPR data, it can assume that this part is the old point bar that has been accumulated into the paleochannel. In 2.5 to 10 meters found concave-up (channel shape) it can assume that is the paleochannels and scroll bars.

The profile of the 97 meters-GPR survey line (Figure 53) shows a maximum depth of 15 meters There have 3 different zones that can be distinguished depending on the contrast of the GPR signal. The upper zone of GPR profile presents parallel mud layers from surface to 2.5 meters. In the middle zone from depth 2.5 to 11 meters, the profile shows a discontinuous reflection pattern in some parts showing a concave-up curve and inclined pattern, which can assume to small paleochannel, scroll bar and lateral migrations. The lower zone of profile displays poor reflectivity because the sediment layer cannot be observed from water saturated in depth from 11 to 15 meters.

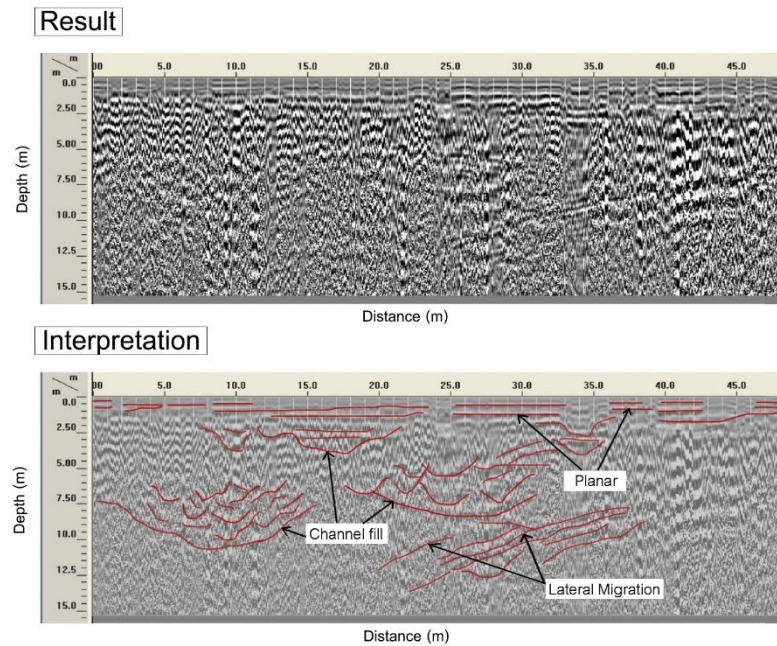


Figure 58 The result of GPR was used 100 MHz antenna from location 1 surveyed on the floodplain and point bar, this profile of the 48 meters-GPR survey line shows a maximum depth of 15 meters.

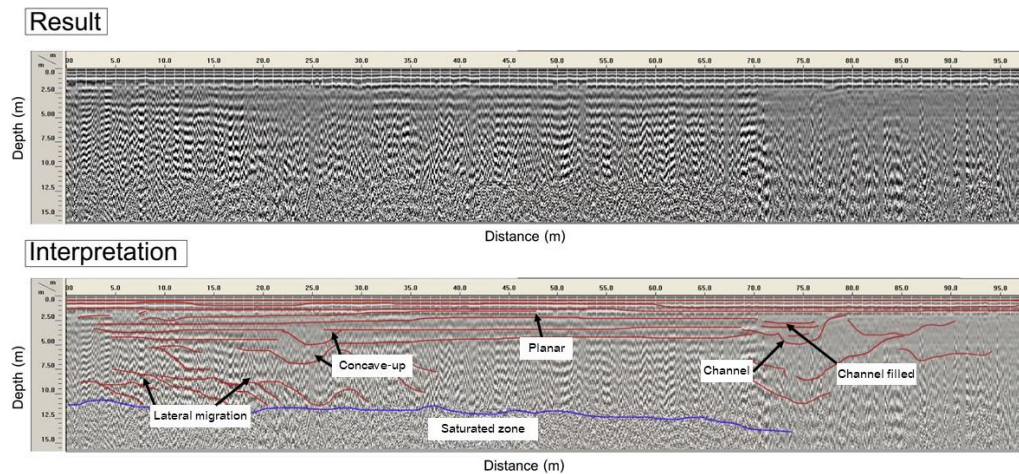


Figure 59 The result of GPR was used 100 MHz antenna from location 1 surveyed on the floodplain and point bar, the profile of the 97 meters-GPR survey line shows a maximum depth of 15 meters. there have 3 different zones that can be distinguished depending on the contrast of the GPR signal.

2) Location 2: Ban Huai Mai

The result of GPR from location 2 surveyed on the floodplain and paleo channel the longest 410 meters-GPR survey (Figure 30). This GPR profile was can observe from surface to 5 meters in vertical depth because of the poor reflective signal. In Figure 61, this profile can obvious the concave shape (width in 20-40 meters and depth in 2-5 meters, approximately) , From geometry and lithology interpretation with ERT, it can assume to be paleochannel. Although this profile can interpret the shape of paleochannel, the structure in detail is unclear to observe, in some concave shape has parallel and incline line, which can assume to be parallel and cross -bedding deposits in the fluvial system.

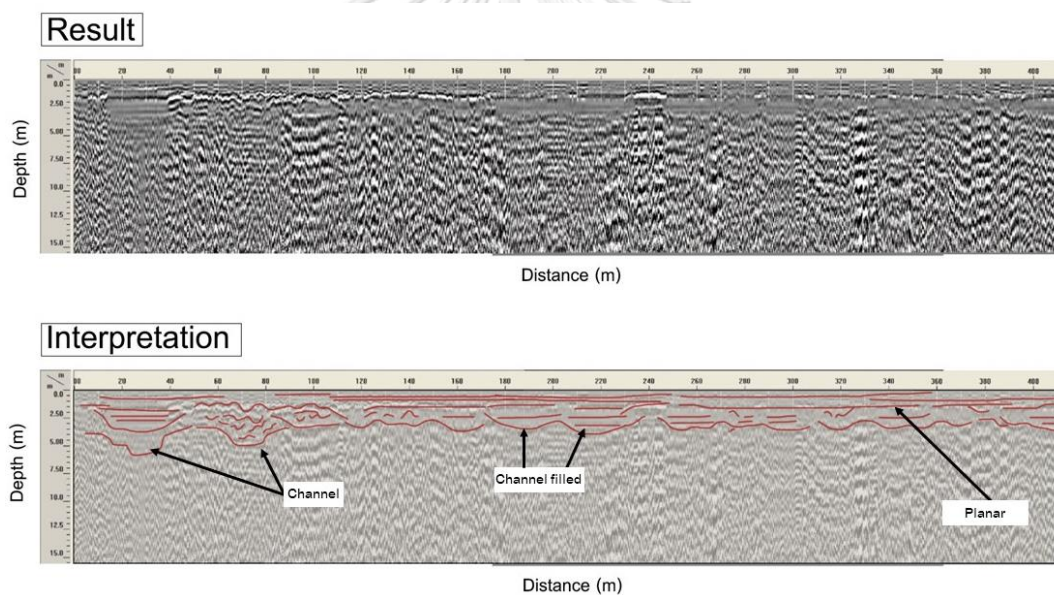


Figure 60 The result of GPR was used 100 MHz antenna from location 2 surveyed on the floodplain and paleo channel the longest 410 meters-GPR survey. This GPR profile was can observe from surface to 5 meters in vertical depth because of the poor reflective signal.

CHAPTER 5

Discussion

This study analyzed aerial photos, satellite images, and topography maps from various periods to determine the geomorphological changes in the region. This study will concentrate on channel sinuosity (SI), bend radius of curvature (Rc), width (W), length (L), and channel migration rates that can help to understand the natural processes of the river as these geomorphological criteria were used to determine the differences in the geomorphology changes over 65 years. Also, ground-penetrating radar and electrical resistivity investigations are used to find the structure and sediment deposits of paleochannels without disrupting the subsurface sediment layer. This study's objectives are to examine the upper Yom River's geomorphological changes and the impact of channel deposit thickness on the behavior and course of the river.

The study of the Upper Yom River's geomorphological evolution in Phrae Province is separated into two main sectors: 1. The alteration in the Yom River's features throughout a 65-year research period by looking at changes in the topographical surface and on the ground. 2. The evaluate sediment characteristics and subsurface structure, geophysical methods including GPR and ERT will be used to study the subsurface of paleochannels. This data will then be compared with sediment boreholes and bank profile data.

As a consequence, the outcomes of this research will be divided into two sections in this chapter: the results from the analysis of geomorphological change from aerial photographs and the results from the use of geophysical techniques to examine sediment layers and ancient underground fluvial depositional structures.

5.1 Geomorphological Changes from aerial photographs

5.1.1. Geomorphological map

In order to compare the geomorphological changes across the previous five time periods (1954, 1970, 1989, 2008, and 2019), ArcGIS 10.4.1 was utilized. Between 1954 and 2019, channel migration (lateral migration) was visible in aerial photographs and satellite photos as a result of the oscillation of the meandering river produced by erosion and deposition along the riverbank, which led to chute cut-off and neck cut-off to maintain balance. The chute cut-offs often have higher stream power, trace close to the meandering discrimination limit, and are linked with more noticeable spatial width changes (Kleinhans & van den Berg, 2011). As a result of their propensity to meander over their floodplain, meandering rivers frequently leave behind a pattern of scroll bars and cut-off lakes (Parker et al., 2011).

The expression "floodplain" refers to an alluvial landform that is relatively flat, near a river channel, and occasionally flooded. In addition, meander bends in the same channel do not necessarily have characteristics in common with one another (Schmudde, 1997), and differences in bank dynamics can occur both within rivers as well as between them (Hooke, 2007a); (Alho & Mäkinen, 2010). According to (Lotsari et al., 2014), the sites of bend erosion change across meander bends of various planform types, and depending on whether the floodplain is flat or steep-sided, the topography of the surrounding area can affect the creation of numerous channel remains.

The upper and middle areas of the research location exhibited more cut-off remnants than the lower part due to the floodplain area being flat and broader than the lower in all five prior times, as seen by the meander scar and oxbow lake. Maps and cross-sections of the floodplain at the upper, middle, and lower sections are given for comparison (Figure 62), whereas the lowest part has a small floodplain and human habitation close to the Yom River, which is the reason for limiting the flow of the river and lack of remnants.

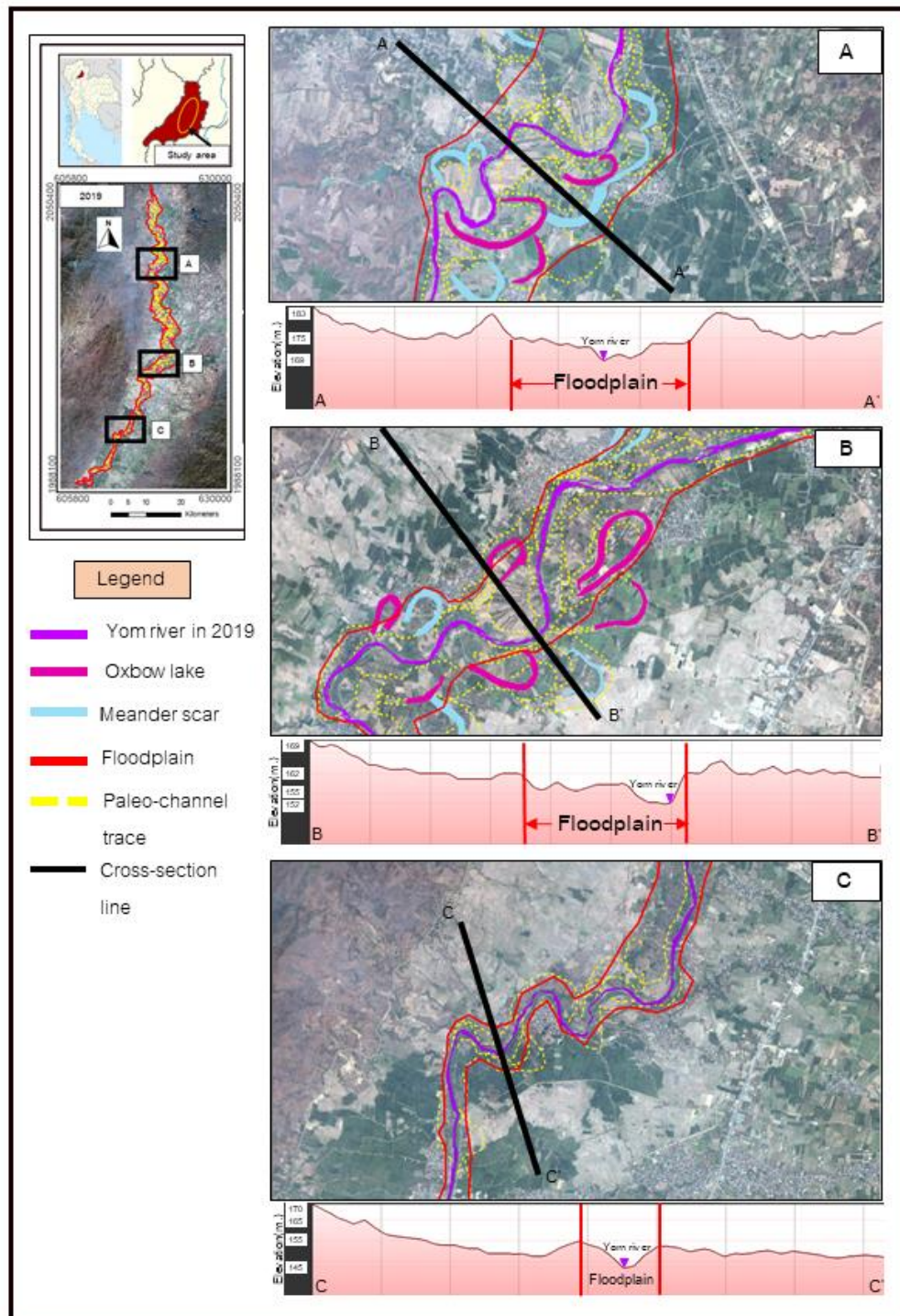


Figure 6.1 Maps and cross-sections of the floodplain at the upper (A), middle (B), and lower sections (C) are given for comparison.

5.1.2. The change in geomorphic criteria

The meander planform of affected rivers has been the subject of several additional investigations. In terms of causes, a variety of other human impacts have been identified, such as reservoir construction and land-use modifications in the catchment and/or the floodplain that result in changes to the controlling variables (flow and sediment discharge) (e.g., (Kiss et al., 2008); (Ollero, 2010); (Magdaleno & Fernández-Yuste, 2011); (Yousefi et al., 2016). For example, (Kiss & Blanka, 2012) and (Suizu & Nanson, 2018) found that fluctuations in hydrological regimes associated with climate changes or indirectly associated with human influences may have significant effects on meander shape. However, because the interpretation of cause-and-effect relationships of cumulative impacts is frequently constrained, it is typically challenging to distinguish between natural and human causes (Downs & Piégay, 2019).

The five parameter planforms of channel width (W), length (L), sinuosity index (SI), the radius of curvature (Rc), and centerline migration rate/year (M/Y) will be discussed in this study's discussion of the causes of these changes. The measure could take notice of changes to channel behavior and development (Williams, 1984). From the past to the present, all parameters have tended to decline. These specifics are described.

5.1.2.1. Channel width (W)

The channel width is reduced by bank accretion, but bank erosion has the reverse effect. Hence, the equilibrium river width can only be achieved if opposite bank accretion and bank erosion are balanced out. bank erosion happens during or soon after flood events, whereas bank accretion occurs during high flow stages (deposition) and low flow stages (consolidation and plant cover) and is typically significantly slower. The width of Yom channel has been slightly reduced from 1954 to 2019 but when compare to paleo-channel width, it has changed dramatically caused of bank deposition increasing from time to time by human activities e.g. Land-use changes may have many

potential effects on either sediment supply or runoff. Deforestation may increase the sediment supply through augmentation of soil erosion, and decrease runoff because of higher evapotranspiration, whereas the opposite patterns generally occur during periods of reforestation. (García-Martínez & Rinaldi, 2022), Based on previous studies (Boonyawat and Susanpoontong, 1996) ; (Department of Water Resources (DWR), 2005); (Royal Irrigation Department (RID), 2010), changes in land use in the Yom River since 1973 are summarized in Table 2. Land use in the Yom River basin was classified into four major groups including agricultural, forest, urban, and water-covered. Most of the land use areas are agricultural areas and forest. During the period 1973e1993, the agricultural area increased from 24 to 44% of the total area (1.02% per year). Meanwhile, the forest area decreased from 75 to 54% (1.05% per year). These reasons are the main cause of changing in width of study area.

Type of land use	Percentage of land use					
	1973 ^a	1982 ^a	1989 ^a	1993 ^a	2001 ^b	2009 ^c
Agricultural area	23.85	34.37	39.47	44.19	44.71	46.05
Forest	75.29	64.65	59.12	53.83	51.48	49.28
Urban area	0.86	0.98	1.37	1.75	2.51	3.53
Water covered area	–	–	0.03	0.19	0.47	1.15
Other	0.01	–	0.01	0.04	0.83	–

^a From Boonyawat and Susanpoontong (1996).

^b From DWR (2005).

^c From RID (2010).

Table 2 Percentage of land use in the Yom River basin in 1973, 1982, 1989, 1993, 2001, and 2009. From (Namsai et al., 2020).

5.1.2.2. Changing in length (L) and sinuosity index (SI)

These two parameters can provide changes in a river caused by chute cut-off and neck cut-off. Chute cutoffs in meandering rivers can develop in a variety of ways, including Swales on the floodplain surface that can redistribute overbank flows and incise until producing a cutoff and an embayment upstream of a point bar that forms by localized bank erosion, often during floods, causing downstream extension of the embayment ultimately leading to cut-off. (Van Dijk et al., 2012). Earlier studies accomplished in 1981, 1995, 2006, and 2011 indicated that severe flood occurrences were correlated with significant sediment loads in the Yom River (Namsai et al. 2020). As a result, there are no records of flood events in the studied area before 1981.

Rainfall plays a major role in rainfall-runoff interactions, which is essential to the evaluation of floods and droughts (Chattopadhyay & Edwards, 2016). Based on Kunkel and Andsager (Kunkel et al., 2003), the increased frequency of severe precipitation events in the United States may have contributed to hydrological flood events. In addition, in between 1921 and 2015, annual rainfall data were discovered in the upper and lower reaches of the Yom River basin to have an insignificantly rising trend (Mama et al., 2018). The Yom basin's rainfall trends between 1921 and 2015 show an increase in rainfall, according to the research. There may be flood occurrences, which are predicted to produce flood events, but which are not recorded and analyzed between 1954 and 1981. The Yom River in the study area was cut off as a result of this.

5.1.2.3. Relationships between R_c/W and channel migrations

The important ratio of the radius of channel curvature to channel width (R_c/W), which is reached by an increasing meander bend, influences controls on the ensuing direction and rate of meander migration, was identified by (Hickin, 1974) Furthermore, the tightness and looseness of a bend could be determined by the relationship between the radius of curvature and channel width (R_c/W). Lower numbers clarify the tight bends, whereas higher values specify the loose bends. The study demonstrates a direct correlation between migration rate and the tightness index (R_c/W), with lower tightness values corresponding to slower rates of bend migration (Beg et al., 2019). When migration rates are plotted versus R_c/W , a number that falls between 1 and 2 indicates that the bend will either cut off the neck or the chute. Bends will erode quickly if values are between 2.5 and 4. Bends will have a low erosion rate if values increase by more than 5 (Nanson & Hickin, 1983). According to the graph (Figures 42 to 44) other bends have a value rise of more than 4, which indicates low erosion rates, and bend number 3 may be cut off. According to the information in Figure 45, the Upper and middle portions of the Yom River in the research region have decreasing rates of erosion since these sections have already cut themselves off, whereas the lower portion has been actively bending.

5.2 GPR radar facies of fluvial deposit

Based on radar reflection patterns in the study area, radar facies were mainly interpreted from locations 1 and 2. Radar facies from fluvial deposits can be divided into five facies by using references in the interpretation part from (Shukla et al., 2008); (Neal, 2004); (Okazaki et al., 2015); (Skelly et al., 2003); (Beres et al., 1999); (Hickin et al., 2009); (Overmeeren, 1998) and (Jol and Bristow, 2003) (Table 3).

Facies 1, Sand lamination to a thick bed or sheet flood is an example of horizontal sand bedding, as are layered horizontal bedding (Shukla et al., 2008).

Facies 2, These facies were also regarded as a moderately dipping bed of lateral migration process on point bars. The deposit interface abruptly terminates. (Neal, 2004)

Facies 3, These facies range in size from tiny to big, are channel-shaped, and typically include an erosion interface. The border is often an erosion interface, small- to large-scale, channel-shaped, and (Okazaki et al. , 2015) ; Variable dip reflection surrounded by a concave reflection (Skelly et al., 2003). The width of the curved is vary from 3 but not more than 30 m.

Facies 4: A structure of disorganized, discontinuous reflection (Neal, 2004) ; massive sheet or lens channel fill (Beres et al. , 1999) ; Cobbles and buried logs are examples of point sources with a high density (Hickin et al., 2009; Okazaki et al., 2015).

Facies 5: The zone of attenuated energy from sediments with high clay content or highly conductive dissolve minerals in groundwater (the "water-saturated zone") is represented by the reflection free, which has the impact of weakly defined reflection and absence of penetration profile. (Beres et al. , 1999) , Weak reflection resulting from attenuation of electromagnetic waves (Van Overmeeren, 1998); (Neal, 2004), and poor uniform sediment or resolution (Jol and Bristow, 2003).



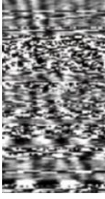

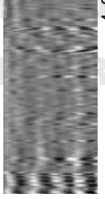

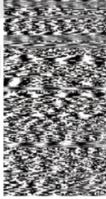

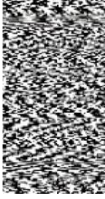

Facies	Reflection geometries	Radar reflection	Reflection configuration	Descriptions
I	Continuous, parallel (planar)	 3x35 m.		Sand lamination to a thick bed or sheet flood is an example of horizontal sand bedding, as are layered horizontal bedding (Shukla et al., 2008).
II	Inclined	 3.5x7 m.		These facies was also regarded as a moderately dipping bed of lateral migration process on point bars. The deposit interface abruptly terminates. (Neal, 2004)
III	Channel fill, concave-up	 4x20 m.		These facies range in size from tiny to big, are channel-shaped, and typically include an erosion interface. The border is often an erosion interface, small- to large-scale, channel-shaped, and (Sowik, 2011; Okazaki et al., 2015); Variable dip reflection surrounded by a concave reflection (Skelly et al., 2003)
IV	Chaotic	 4x10 m.		A structure of disorganized, discontinuous reflection (Neal, 2004); massive sheet or lens channel fill (Beres et al., 1999); Cobbles and buried logs are examples of point sources with a high density (Hickin et al., 2009; Okazaki et al., 2015).
V	Reflection free	 4x18 m.		The zone of attenuated energy from sediments with high clay content or highly conductive dissolve minerals in groundwater (the "water saturated zone") is represented by the reflection free, which has the impact of weakly defined reflection and absence of penetration profile. Beres et al. (1999), Weak reflection resulting from attenuation of electromagnetic waves (Overmeeren, 1998; Neal, 2004), and poor uniform sediment or resolution (Jol and Bristow, 2003).

Table 3 Based on radar reflection patterns in the study area, radar facies were mainly interpreted from locations 1 and 2.

Radar facies from fluvial deposits can be divided into 5 facies.

5.3 Relationship between fluvial sediment and ERT lithological classes

Based on this relationship, the lithological classification may be determined from all the information gathered. Fluvial deposits range in thickness from 5 to 20 meters deep, and both vertical and horizontal shifts are plainly visible. based on the results of the resistivity profile. Table 4 displays the sediment from on-site boreholes as well as the apparent resistivity data from ERT surveys.

At Location 1 (Figure 53), two zones were identified. The low resistivity zone consisted of mud and sandy mud, indicating recent and paleo floodplain deposits. The moderate resistivity zone exhibited associations of muddy sand, sand, gravelly sand, and sandy gravel, suggesting a paleo-channel and past point bar deposition.

Location 2 (Figure 54), featured a low to moderate resistivity zone composed of mud and sandy mud, indicating an old floodplain. However, areas within the resistivity profile displayed moderate to high resistivity, suggesting the presence of a paleochannel and paleo-point bar deposition.

At Location 3 (Figure 55), a low resistivity zone comprised mud and sandy mud, signifying an ancient floodplain deposit. The moderate resistivity zone contained associations of muddy sand, sand, gravelly sand, and sandy gravel, indicating a paleochannel and paleo-point bar.

Location 4 (Figure 56), showcased a low to moderate resistivity zone composed of mud and sandy mud, resembling floodplain deposition. The resistivity profile exhibited a U-shape geometry resembling a channel, potentially representing ancient lakes or meander scars. Additionally, moderate to high resistivity values and associations of muddy sand, sand, gravelly sand, sandy gravel, and gravelly sand suggested the presence of a paleochannel and paleo-point bar.

At Location 5 (Figure 57), the low resistivity zone represented floodplain deposits, while the resistivity profile suggested the division into a surface zone and subsurface zone, both exhibiting associations of muddy sand, sand, gravelly sand, sandy gravel, and gravelly sand. These zones were interpreted as paleochannels and old point bars.

Location 6 (Figure 58) , exhibited a moderate to high resistivity zone with associations of muddy sand, sand, gravelly sand, sandy gravel, and gravelly sand. The lithology suggested fluvial deposits, particularly a paleo-channel, and the moderate to high zone primarily consisted of sand, indicative of a point bar feature.

The integration of stratigraphy and sediment characteristics described by boreholes and six resistivity profiles from an ERT survey allows us to distinguish between ERT lithological classes of subsurface sediments in the research location. Table 4 defines the resistivity values for the lithological classes. The association between sediment particle size and their electrical resistivity characteristics led to the deduction of three lithological classifications. Mud, Sandy Mud, Sand and Gravel showed that their respective resistivity ranges were 0-18-ohm meter, 18-47-ohm meter, and 47-953-ohm meter. This association between their physical characteristics and apparent resistivity may be used in ERT surveys in nearby areas or along other rivers.

In conclusion, the resistivity analysis conducted at various locations revealed valuable information about the subsurface characteristics. The distinct zones identified in each location, based on resistivity values and lithological compositions, indicated the presence of floodplain deposits, paleochannels, and paleo-point bars. These findings provide insights into the geological history and deposition processes of the studied areas, contributing to a better understanding of their sedimentary environments and potential implications for future geological studies and land management decisions.

Resistivity (Ω .m.)	ERT Lithological classifications
0-18 Ω .m.	Mud
18-47 Ω .m.	Sandy Mud
47-953 Ω .m.	Sand and gravel

Table 4 The sediment from on-site boreholes as well as the apparent resistivity data from ERT surveys in this study area.

CHAPTER 6

Conclusion

6.1 Conclusions

The analysis of the geological interpretation of aerial photographs from earlier periods, geomorphic criteria, sediment analysis, electrical resistivity tomography (ERT), and ground penetrating radar (GPR) was used in the study of the geomorphological change of the upper Yom River in Phrae Province between 1954, 1970, 1989, 2012, and 2019. This study's findings may be summarized as follows.

Conclusions of the assessment of aerial photographs and satellite images from the 1954 to 2019 time periods led to the geological interpretation. Channel migration, neck cut-off, oxbow lakes, and meander scars are examples of the changing geomorphology that has occurred during the past 65 years (from 1954 to 2019). Due to the flatness and broader of floodplain area, the upper and middle portions of the research site had more cut-off remnants than the lower section.

Channel width (W), channel length (L), sinuosity index (SI), radius of curvature (Rc), and channel migrations are five geomorphic metrics that were used to compare changes. The width (W) of the Yom River's paleochannel has altered dramatically in recent years because of continuous increases in bank deposition brought on by human activities. Changes in land use might have a variety of impacts on runoff or the supply of sediment. The channel's longest length was 127.93 kilometers in 1954, while its shortest length was 110.19 kilometers in 2012. Between 1954 and 2019, it varied between 1.95 and 1.50 according to SI measurements. In 1954, the sinuosity rating was its greatest (1.95), while in 2019, it was at its lowest (1.50). Yom River's total length and sinuosity measurements reflect a downward tendency from the past to the present, indicating that it was frequently cut off at the neck and chute during several floods. In addition, the upper and middle portions of the Yom River in the research region have decreasing rates of erosion because these sections have already cut themselves off, whereas the

lower portion has been actively bending due to the migration rates versus R_c/W values. R_c/W shows lower tightness values corresponding to slower rates of bend migration.

Six resistivity survey lines, two GPR survey lines, five boreholes, and a river bank profile were explored from sedimentology and geophysics field investigation along paleochannels (meandered scars), point bars, and floodplain. Folk's categorization method was used to assign a classification to the sediments from each landform. According to the results of the grain size analysis, the types of sediment deposits from each landform include mud, sandy mud, muddy sand, sand, gravelly sand, and sandy gravel in the example of point bars and paleo-channels, and mud and sandy mud in the occurrence of floodplains and meandering scars.

The last analysis is the outcome of ERT and GPR, the lithological categorization of this study's results may be determined from the ERT profile. Both vertical and horizontal changes were clearly visible in the fluvial deposit, which ranged in thickness from 5 to 20 m. like the floodplain, the point bar, and the paleo channel. Additionally, the five types of radar facies seen in river deposits are Continuous (Parallel), Inclined, Concaved-up (Channel fill), Chaotic, and Reflection Free.

6.2 Recommendation

The goal of this research was to examine how the Yom River's geomorphology has changed over time, both from the surface and as seen in aerial and satellite images. The pattern of The river's transformation can be seen using data from the last 65 years, but if additional data from earlier decades can be analyzed and more techniques are used to forecast future trends, the better and more thorough will be this river's change. Additionally, GPR and ERT are used in conjunction with other geophysical instruments in the study of river changes in the paleo from the subsurface, which can reveal changes in the structure and type of sedimentary.

The thickness of the sediment in the paleo fluvial may now be determined, which may be helpful for resource management in the future. This study examined the soil structure using a 100 MHz GPR antenna that could only be scanned up to a certain depth (often 15 m). It was discovered from the stratigraphy of river sediments that both the internal structure and the sediment properties changed throughout time. less than the antenna's frequency range is possible. Consequently, the study to gather more precise data, recommends using GPR antenna surveys with a greater variety of frequencies. Further age dating of ancient sediments may also aid in improving our comprehension of the dynamics of this river.





APPENDIX

จุฬาลงกรณ์มหาวิทยาลัย
CHULALONGKORN UNIVERSITY

Location	Width																						
	1954	1954	1970	1970	1989	1989	2008	2008	2019	2019	Paleochannel												
1	79.82	80.12	81.38	80.44	94.25	92.13	93.74	93.37	45.90	47.39	45.10	46.13	54.06	53.75	53.76	53.86	51.83	50.65	51.53	51.34			
2	117.49	120.71	117.12	118.44	119.28	120.11	118.79	119.39	62.40	62.72	62.79	62.64	63.98	62.24	62.39	62.87	65.39	66.59	64.64	65.54			
3	100.83	100.83	100.83	100.83	117.05	115.13	115.55	115.91	56.71	54.40	58.83	56.65	72.40	71.97	69.95	71.44	82.76	82.73	82.69	82.73			
4	55.81	55.75	55.74	55.77	74.34	74.31	74.46	74.37	64.02	64.15	64.12	64.10	57.62	57.56	57.73	57.64	56.76	56.71	56.77	56.75			
5	75.04	75.02	74.91	74.99	74.72	74.74	74.60	74.69	91.07	91.17	91.23	91.16	56.29	53.13	53.13	54.19	72.12	70.03	70.37	70.84			
6	100.32	99.73	100.70	100.25	76.69	78.71	78.11	77.84	91.59	90.50	90.92	91.00	78.81	78.92	80.09	79.27	78.64	77.54	78.91	78.36			
7	29.66	29.70	28.82	29.39	64.89	62.87	63.13	63.63	44.02	43.47	44.01	43.83	45.65	45.65	45.65	45.65	37.17	37.13	36.44	36.91			
8	30.00	30.08	29.44	29.84	52.75	53.86	53.67	53.43	56.37	56.38	56.74	56.49	37.12	37.12	36.64	36.96	52.79	50.16	52.76	51.90			
9	87.22	87.22	87.22	87.22	64.43	64.43	64.43	64.43	76.21	75.25	75.43	75.63	46.32	46.41	46.04	46.26	40.69	39.87	40.63	40.40			
10	111.04	111.04	111.04	111.04	58.38	56.25	56.90	57.17	51.38	51.73	51.33	51.48	60.93	61.18	59.77	60.63	52.82	53.98	51.40	52.73			
11	64.47	64.47	64.47	64.47	67.98	68.88	67.98	68.28	64.39	63.53	63.85	63.92	48.98	43.01	47.92	46.64	24.58	26.59	26.74	25.97			
12	60.36	59.96	59.45	59.92	50.80	51.16	51.29	51.08	33.04	31.85	30.75	31.88	40.83	40.26	39.74	40.27	66.26	65.09	66.75	66.03			
13	47.98	46.40	48.51	47.63	62.59	64.82	63.50	63.64	39.16	38.70	39.00	44.42	45.36	44.69	44.83	43.24	42.21	43.46	42.97				
14	63.84	64.54	62.08	63.49	83.00	84.44	83.61	83.88	57.25	57.64	54.84	56.58	44.22	41.71	41.92	42.62	74.53	75.12	76.56	75.40			
15	71.98	72.60	72.54	72.37	26.26	26.21	26.15	26.21	24.97	23.96	23.74	24.22	47.63	45.27	44.80	45.90	34.67	35.36	35.07	35.03			
16	56.81	55.88	56.73	56.47	27.69	28.68	27.60	27.99	79.69	79.79	79.69	79.72	46.67	44.73	46.52	45.97	44.70	44.70	45.39	44.93			
17	58.64	57.05	58.83	58.17	63.84	63.84	63.89	63.86	44.87	45.27	45.31	45.15	57.70	59.64	59.64	58.99	54.31	54.65	54.07	54.34			
18	41.17	41.26	41.26	41.23	37.51	38.31	38.44	38.09	56.35	57.34	55.55	56.42	49.51	48.84	49.54	49.30	42.66	42.00	43.28	42.64			
19	47.19	46.85	47.68	47.24	27.25	27.28	28.06	27.53	66.64	67.37	67.23	67.08	55.27	54.13	55.99	55.13	46.86	47.26	46.93	47.02			
20	44.03	43.07	43.79	43.63	22.44	22.40	22.41	22.42	25.56	26.23	26.74	26.18	51.71	51.73	50.60	51.35	36.23	36.14	35.99	36.12			
21	50.62	49.87	49.91	50.14	30.98	30.94	29.83	30.58	44.08	43.30	43.36	43.58	78.93	79.53	79.88	79.45	73.59	74.20	74.51	74.10			
22	41.97	41.81	41.73	41.84	22.99	21.88	22.10	22.32	50.11	49.06	49.20	49.46	44.53	44.38	44.13	44.35	55.00	54.16	55.92	55.03			
23	59.37	59.46	59.01	59.28	27.61	26.08	26.33	26.67	53.31	53.09	53.83	53.41	69.12	69.17	69.51	69.27	52.59	52.59	52.59	52.59			
24	73.49	74.40	73.97	73.95	45.62	45.46	45.46	45.51	28.57	26.50	26.41	27.16	67.33	66.69	65.68	66.57	77.38	76.45	76.47	76.77			
25	52.32	52.31	53.28	52.64	30.59	30.69	30.67	30.65	56.18	54.85	55.86	55.63	73.29	74.07	73.29	73.55	52.40	52.86	52.46	52.57			
26	58.79	59.00	57.42	58.41	55.08	55.03	54.18	54.76	66.69	65.35	65.95	65.99	56.47	54.61	52.96	54.35	73.39	74.03	73.45	73.62			
27	66.66	67.09	67.11	66.96	52.12	51.99	51.15	51.75	54.90	54.02	54.21	54.38	64.74	66.43	62.66	64.61	82.28	81.86	81.68	81.94			
28	39.14	38.82	39.33	39.10	32.14	32.92	32.75	32.61	44.79	45.11	45.01	44.97	43.87	45.00	44.49	44.45	46.21	46.21	45.88	46.10			
29	55.42	54.90	54.89	55.07	23.12	23.15	23.20	23.16	46.50	46.49	46.63	46.54	52.00	51.77	52.06	51.94	49.94	49.56	51.06	49.86			
30	60.80	60.11	60.34	60.42	82.09	82.50	82.53	82.37	49.19	49.23	49.09	49.17	58.61	59.48	59.82	59.30	50.43	50.80	51.01	50.88			
31	82.36	82.51	82.87	82.58	64.34	63.07	63.23	63.54	89.90	88.46	89.61	89.32	46.45	46.61	45.45	46.17	56.52	54.39	55.74	55.55			
32	49.64	50.29	50.42	50.12	58.06	60.56	59.26	59.30	56.99	56.47	56.16	56.54	59.72	60.61	60.60	60.31	41.08	41.08	41.08	41.08			
33	114.93	115.60	116.61	115.72	49.72	50.68	51.13	50.51	68.93	69.69	67.93	68.85	62.50	62.50	62.50	62.50	44.25	44.08	44.07	44.13			
34	55.64	55.40	55.54	55.53	66.83	66.71	66.70	66.75	51.46	51.30	51.52	51.43	48.62	49.05	49.27	48.98	65.63	66.14	65.19	65.65			
35	78.82	78.93	78.14	78.63	82.78	83.07	82.58	82.80	42.23	43.02	42.33	42.53	71.34	73.40	72.55	72.43	89.74	91.25	90.79	90.59			
36	58.11	58.92	58.18	58.40	36.84	37.88	37.41	37.38	107.53	108.44	107.94	107.97	62.88	62.22	61.78	62.29	78.53	78.50	78.43	78.49			
37	42.19	42.86	41.57	42.20	40.81	42.99	41.03	41.61	93.63	93.38	93.47	93.49	55.51	55.97	56.54	56.01	49.83	50.24	49.90	49.99			
38	64.56	63.70	64.32	64.19	48.41	48.42	47.83	48.22	63.10	64.15	64.67	63.97	60.06	60.08	59.42	59.85	42.51	42.35	42.67	42.51			
39	121.38	120.31	120.86	120.85	107.14	108.02	106.30	107.15	61.43	60.77	60.46	60.89	61.69	61.58	61.62	61.63	56.65	56.45	56.96	56.69			
40	55.80	54.72	56.42	55.64	108.47	109.06	108.22	108.58	41.97	41.95	41.62	41.85	40.95	40.30	41.04	40.76	39.68	39.65	39.87	39.73			
41	72.86	73.49	73.97	73.44	91.76	90.71	90.81	91.03	39.74	38.82	40.07	39.54	48.88	49.27	50.43	49.52	44.61	46.04	45.88	45.51			
42	49.14	49.83	49.90	49.62	52.31	53.60	52.74	52.88	49.43	49.46	49.38	49.42	50.85	51.77	50.84	51.15	40.06	40.54	40.90	40.50			
43	51.76	52.88	52.10	52.25	71.64	72.00	71.29	71.64	39.22	40.09	40.27	39.86	41.48	41.51	41.37	41.45	36.09	35.70	36.59	36.12			
44	36.59	36.59	35.83	36.34	50.63	50.87	50.52	50.67	51.21	51.12	51.25	51.19	62.94	62.07	62.84	62.61	43.89	43.82	43.50	43.74			
45	58.73	58.70	58.70	58.71	61.35	61.94	61.25	61.51	79.00	78.16	78.57	78.58	48.99	49.20	49.35	49.18	40.90	41.03	41.26	41.06			
46	82.86	83.21	82.96	83.01	62.19	61.96	62.10	62.08	83.33	83.13	83.00	83.15	62.23	62.57	62.54	62.45	47.95	48.00	47.96	47.97			
47	77.89	78.77	78.56	78.40	51.70	50.05	51.59	51.12	45.86	45.00	44.98	45.28	77.44	78.83	80.87	79.05	126.51	126.51	126.52	126.51			
48	43.76	43.67	43.52	43.65	52.26	53.00	52.14	52.47	45.47	45.35	44.90	45.24	67.67	67.93	68.57	68.06	76.76	76.13	76.75	76.55			
49	49.14	49.00	49.14	49.09	61.69	61.44	61.16	61.43	93.95	93.95	93.97	93.96	87.23	86.57	87.23	87.01	110.91	110.77	110.91	110.86			
50	62.86	62.86	62.86	62.86	46.74	46.74	46.74	46.74	77.75	77.95	77.65	77.78	80.03	80.23	79.94	80.07	59.26	59.34	59.14	59.24			
51	50.09	50.77	50.92	50.59	52.33	52.69	52.45	52.49	64.21	64.35	64.29	64.28	67.11	67.34	67.57	67.34	64.17	64.26	64.36	64.26			
52	86.35	86.08	86.02	86.15	62.27	62.46	62.07	62.27	71.35	71.36	71.75	71.49	63.50	63.55	63.55	63.53	71.33	71.46	71.56	71.45			
53	81.68	81.04	81.24	81.32	31.52	31.76	31.35	31.55	98.33	98.75	98.45	98.51	97.47	97.59	97.36	97.47	86.53	86.36	86.48	86.45			
Average				64.72				58.13				59.14				58.25				58.23	90.10		

Table 5 Shows the values from measure of river width since 1954 to 2019 and paleochannels.

Sinuosity															
Location	1954			1970			1989			2012			2019		
	Channel L.(AB)	Down Val L.(CD)	AB/CD	Channel L.(AB)	Down Val L.(CD)	AB/CD	Channel L.(AB)	Down Val L.(CD)	AB/CD	Channel L.(AB)	Down Val L.(CD)	AB/CD	Channel L.(AB)	Down Val L.(CD)	AB/CD
1	4,262	1634	2.61	4,624	1,526	3.03	4,667	1470	3.17	4557	1552	2.94	4524	1534	2.95
2	3,539	2006	1.76	2807	1988	1.41	2,982	2,038	1.46	2672	1831	1.46	2878	1998	1.44
3	2,212	1,617	1.37	1931	1621	1.19	3034	2126	1.43	2643	2058	1.28	2958	2163	1.37
4	2683	1549	1.73	2817	1455	1.94	1,857	1,426	1.30	3701	2272	1.63	2779	2342	1.19
5	3977	713	5.58	2,011	1,479	1.36	2,259	1,436	1.57	2396	1151	2.05	2317	1113	2.08
6	2,489	2,363	1.05	2,165	1,984	1.09	2461	2219	1.11	1961	1368	1.43	2425	1794	1.35
7	1,991	1,182	1.68	1,601	1,110	1.44	2,231	1,786	1.25	2044	1702	1.20	2118	1776	1.19
8	2,729	1,578	1.73	2,600	1,461	1.78	1873	1278	1.47	2117	1492	1.42	1872	1372	1.36
9	5,628	2,078	2.71	2,702	1,603	1.69	2752	1974	1.39	3098	2328	1.33	3661	2727	1.34
10	4,360	2,114	2.06	4374	2021	2.16	4884	1993	2.45	3631	2445	1.49	3634	2481	1.46
11	2,631	1,693	1.55	2829	1831	1.55	3078	1610	1.91	3359	1801	1.87	3170	1654	1.92
12	2,735	2,335	1.17	2604	2199	1.18	2660	2125	1.25	2295	1762	1.30	2429	1908	1.27
13	3,034	1,292	2.35	2782	1358	2.05	2,418	1314	1.84	2096	1629	1.29	2002	1632	1.23
14	3,696	867	4.26	3,551	1110	3.20	2,038	1,456	1.40	1606	1170	1.37	1743	1253	1.39
15	1,877	1,436	1.31	1985	1398	1.42	2,543	2,006	1.27	2437	2061	1.18	2358	2018	1.17
16	3,338	985	3.39	2644	1445	1.83	2937	1712	1.72	2626	1860	1.41	2698	1886	1.43
17	1,866	1,711	1.09	1,514	1,252	1.21	1866	1711	1.09	1686	1412	1.19	1854	1548	1.20
18	2,764	2,120	1.30	2,470	1,777	1.39	2451	1874	1.31	2358	1842	1.28	2246	1727	1.30
19	2345	1731	1.35	2,545	1,939	1.31	2186	1793	1.22	2100	1757	1.20	2029	1701	1.19
20	2036	1462	1.39	1,944	1,457	1.33	2052	1656	1.24	1991	1662	1.20	2172	1827	1.19
21	4,589	1,924	2.39	4,439	1,868	2.38	4970	1989	2.50	5277	2112	2.50	5206	2097	2.48
22	2,654	2,155	1.23	2,224	1,771	1.26	2584	1917	1.35	2715	2024	1.34	2733	1969	1.39
23	3,234	2,221	1.46	3,073	2,073	1.48	3181	2026	1.57	3075	1983	1.55	3111	1962	1.59
24	2,562	1,814	1.41	2,823	1760	1.60	2,716	1,687	1.61	2396	1576	1.51	2203	1522	1.45
25	1,917	876	2.19	1,820	838	2.17	1,786	881	2.03	1744	1061	1.64	1758	1042	1.69
26	3617	1683	2.15	3,645	1,698	2.15	3803	1740	2.19	3962	1802	2.20	4451	2238	1.99
27	3,088	1701	1.82	3,112	1,754	1.77	3052	1700	1.80	3115	1726	1.80	3152	1779	1.77
28	2980	1488	2.00	3,021	1,498	2.02	3776	1282	2.95	2218	1706	1.30	2240	1622	1.38
29	1857	1426	1.30	2488	2051	1.21	1857	1426	1.30	1493	1280	1.17	1434	1293	1.11
30	1951	1850	1.05	1473	1401	1.05	1951	1850	1.05	2007	1790	1.12	2010	1794	1.12
Average			1.95			1.69			1.64			1.52			1.50

Table 6 Shows the values from measure of SI since 1954 to 2019.

Right=Westward, Left=Eastward												
Year	1954-1970			1970-1989			1989-2012			2012-2019		
Locations	Right	Left	MG/year	Right	Left	MG/year	Right	Left	MG/year	Right	Left	MG/year
1		27.19	1.70	-26.50		-1.39		18.96	0.82	-2.74		-0.25
2		34.06	2.13	-3.40		-0.18		2.54	0.11	-2.58		-0.37
3		16.70	1.04	-46.27		-2.44		32.52	1.41	-5.81		-0.83
4		46.02	2.88		39.38	2.07		17.52	0.76		11.61	1.66
5		14.13	0.88	-7.10		-0.37	-4.70		-0.20	-2.76		-0.39
6	-115.23		-7.20	-21.47		-1.13	-9.38		-0.41	-8.90		-1.27
7		34.77	2.17		13.55	0.71	-17.27		-0.75		2.43	0.35
8	-10.21		-0.64	-12.33		-0.65		14.11	0.61	-9.16		-1.31
9	-19.18		-1.20	-111.92		-5.89		43.45	1.89	-2.02		-0.29
10	-41.19		-2.57		27.61	1.45	-8.17		-0.36	-1.62		-0.23
11	-195.17		-12.20	-43.14		-2.27		61.24	2.66	-20.15		-2.88
12		333.85	20.87		149.65	7.88		39.61	1.72	-2.32		-0.33
13	-304.17		-19.01		198.70	10.46		7.58	0.33	-13.96		-1.99
14		392.45	24.53		55.72	2.93	-405.12		-17.61		23.31	3.33
15	-143.48		-8.97	-224.62		-11.82	-143.34		-6.23	-19.44		-2.78
16	-114.07		-7.13	-281.15		-14.80		13.24	0.58	-4.92		-0.70
17	-0.42		-0.03		31.44	1.65		50.97	2.22			0.00
18	-70.84		-4.43		576.82	30.36		19.77	0.86	-0.71		-0.10
19	-7.09		-0.44		26.61	1.40		26.29	1.14	-6.54		-0.93
20	-0.22		-0.01	-351.34		-18.49		28.67	1.25		48.36	6.91
21	-19.77		-1.24	-28.68		-1.51		28.79	1.25		0.17	0.02
22	-59.57		-3.72		22.93	1.21		9.22	0.40	-1.98		-0.28
23	-15.56		-0.97	-13.44		-0.71	-49.43		-2.15	-19.95		-2.85
24	-27.18		-1.70		62.35	3.28	-23.53		-1.02		3.25	0.46
25	-7.33		-0.46	-32.70		-1.72		13.49	0.59		8.43	1.20
26	-20.70		-1.29		16.70	0.88		115.18	5.01	-12.02		-1.72
27		459.51	28.72	-57.67		-3.04	-113.70		-4.94	-18.32		-2.62
28	-113.71		-7.11	-59.76		-3.15	-202.46		-8.80	-8.91		-1.27
29		2.26	0.14		33.50	1.76	-60.28		-2.62	-20.13		-2.88
30	-28.34		-1.77	-93.06		-4.90		3.74	0.16	-2.97		-0.42
31		100.86	6.30	-106.07		-5.58		1.12	0.05	-10.25		-1.46
32		137.34	8.58		11.89	0.63	-90.76		-3.95		16.69	2.38
33		22.41	1.40		130.44	6.87		78.13	3.40	-2.34		-0.33
34		13.76	0.86	-118.01		-6.21	-39.53		-1.72	-19.58		-2.80
35		72.62	4.54	-62.77		-3.30		45.75	1.99		1.92	0.27
36		51.41	3.21		84.02	4.42	-5.02		-0.22	-13.40		-1.91
37	-101.70		-6.36		87.77	4.62		20.44	0.89	-6.50		-0.93
38		9.66	0.60	-3.18		-0.17		2.15	0.09	-8.18		-1.17
39	-49.19		-3.07		1.26	0.07		38.37	1.67	-11.87		-1.70
40	-68.07		-4.25	-44.19		-2.33		9.61	0.42		0.79	0.11
41		94.75	5.92	-84.47		-4.45		8.85	0.38	-3.17		-0.45
42		104.09	6.51	-85.46		-4.50		22.06	0.96		6.55	0.94
43	-9.78		-0.61		22.09	1.16	-8.80		-0.38		4.48	0.64
44	-4.84		-0.30		13.56	0.71		19.71	0.86		3.53	0.50
45	-30.87		-1.93		16.36	0.86	-8.76		-0.38	-11.65		-1.66
46	-47.03		-2.94		36.58	1.93	-22.43		-0.98		4.67	0.67
47	-49.63		-3.10	-55.15		-2.90	-11.84		-0.51	-6.19		-0.88
48	-4.05		-0.25	-35.65		-1.88		4.83	0.21		3.40	0.49
49		119.33	7.46		104.07	5.48		67.74	2.95		3.68	0.53
50		8.68	0.54	-12.22		-0.64		12.22	0.53		6.96	0.99
51	-10.58		-0.66		0.93	0.05		10.39	0.45	-11.96		-1.71
52	-39.36		-2.46		12.12	0.64		14.22	0.62		1.87	0.27
53		19.86	1.24		13.91	0.73		14.31	0.62	-2.78		-0.40
	-55.76	96.17	0.46	-74.88	68.85	-0.23	-68.03	26.19	-0.25	-8.70	8.45	-0.38

Table 7 Shows the values from measure of channel migration since 1954 to 2019.

หมายเลขบ่อ PW12697

ข้อมูลทั่วไป: ชั้นดินและหิน, ระดับน้ำ, ภาพประกอบ, ข้อมูลจากการสำรวจ

คำบรรยายชั้นดินและหิน (Lithology ...)

ลึกจาก	ลึกถึง	ชั้นดิน/ชั้นหิน	คำบรรยาย
.00	1.00	top soil	Top Soil, brown.
1.00	5.00	clay	Clay, brown, pebble, non plastic.
5.00	11.00	clay	Clay, yellowish brown, compacted.
11.00	19.00	gravel	Granules, brown, very angular, poorly sorted, composed of quartz, shale, sand...

คำบรรยายชั้นดินและหิน (Driller's L...)

จาก	ถึง	ชั้นดิน/ชั้นหิน

หน่วย: เมตร, ระยะของท่อกรอง: (S)12.17-18.25

ความลึก: 19.00, เจาะ: 18.25

Logged By: _____ Checked By: _____

Figure 62 The lithological data from well near ERT survey line at location 1 (Department of Groundwater Resources).

หมายเลขบ่อ MR652

ข้อมูลทั่วไป: ชั้นดินและหิน, ระดับน้ำ, ภาพประกอบ, ข้อมูลจากการสำรวจ

คำบรรยายชั้นดินและหิน (Lithology ...)

ลึกจาก	ลึกถึง	ชั้นดิน/ชั้นหิน	คำบรรยาย
.00	6.00	[clay] ดินเหนียวสีน้ำตาล	
6.00	9.00	[sand] ทรายหยาบ	
9.00	12.00	[gravel/sand] กรวดและทรายละเอียด	
12.00	42.00	[clay] ดินเหนียวสีน้ำตาล	
42.00	44.00	[sand] ทรายละเอียด	
44.00	60.00	[clay] ดินเหนียว	

คำบรรยายชั้นดินและหิน (Driller's L...)

จาก	ถึง	ชั้นดิน/ชั้นหิน

หน่วย: เมตร, ระยะของท่อกรอง: (P)8.00-12.00,(P)40.00-44.00

ความลึก: 60.00, เจาะ: 44.00

Logged By: _____ Checked By: _____

Figure 63 The lithological data from well near ERT survey line at location 2 (Department of Groundwater Resources).

หมายเลขบ่อ	MR368			
ข้อมูลทั่วไป	ชั้นดินและหิน	ระดับน้ำ	ภาพประกอบ	ข้อมูลจากการสำรวจ

ลึกจาก	ลึกถึง	ชั้นดิน/ชั้นหิน	คำบรรยาย
.00	6.00	clay	borwn clay
6.00	7.50	clay	brown clay
7.50	10.50	clay	black clay
10.50	12.00	sand	sand
12.00	15.00	clay	yellow clay
15.00	36.00	clay	yellow clay
36.00	39.00	sand	sandy
39.00	54.00	clay	clay
54.00	55.50	sand/clay	sand + red clay
55.50	60.00	clay	clay
60.00	107.00	clay	red clay

จาก	ถึง	ชั้นดิน/ชั้นหิน

หน่วย ระยะของท่อกรอง

เมตร (S)39.00-39.00,(S)51.00-60.00

ชั้นหินแข็ง

ความลึก

107.00

เจาะ

พัฒนา

60.00

Logged By

Checked By

Figure 64 The lithological data from well near ERT survey line at location 3 (Department of Groundwater Resources).

หมายเลขบ่อ	MR54			
ข้อมูลทั่วไป	ชั้นดินและหิน	ระดับน้ำ	ภาพประกอบ	ข้อมูลจากการสำรวจ

ลึกจาก	ลึกถึง	ชั้นดิน/ชั้นหิน	คำบรรยาย
.00	25.00	clay	grayish brown, plastic.
25.00	110.00	cravel	various colors, coarse gravel, subrounded to rounded, well sorted, composed ...

จาก	ถึง	ชั้นดิน/ชั้นหิน

หน่วย ระยะของท่อกรอง

ฟุต (P)24.00-30.00

ชั้นหินแข็ง

ความลึก

33.00

เจาะ

พัฒนา

33.00

Logged By

Sayan Hanchang

Checked By

Thassanee Nettasana

Figure 65 The lithological data from well near ERT survey line at location 5 (Department of Groundwater Resources).

หมายเลขบ่อ MR457

ข้อมูลทั่วไป ชั้นดินและหิน ระดับน้ำ ภาพประกอบ ข้อมูลจากการสำรวจ

คำบรรยายชั้นดินและหิน (Lithology ...)

ลึกจาก	ลึกถึง	ชั้นดิน/ชั้นหิน	คำบรรยาย
.00	7.50	clay	brown clay
7.50	9.00	sand	sand
9.00	36.00	gravel	gravel

คำบรรยายชั้นดินและหิน (Driller's L...)

จาก	ถึง	ชั้นดิน/ชั้นหิน

หน่วย ระยะของท่อกรอง

เมตร (S)28.00-36.00

ชั้นหินแข็ง เจาะ พัฒนา

ความลึก 36.00 36.00

Logged By Checked By

Figure 66 The lithological data from well near ERT survey line at location 6 (Department of Groundwater Resources).





จุฬาลงกรณ์มหาวิทยาลัย
CHULALONGKORN UNIVERSITY

REFERENCES

- Alabyan, A. M., & Chalov, R. S. (1998). Types of river channel patterns and their natural controls. *Earth Surface Processes and Landforms: The Journal of the British Geomorphological Group*, 23(5), 467-474.
- Alho, P., & Mäkinen, J. (2010). Hydraulic parameter estimations of a 2D model validated with sedimentological findings in the point bar environment. *Hydrological Processes*, 24(18), 2578-2593.
- Bag, R., Mondal, I., & Bandyopadhyay, J. (2019). Assessing the oscillation of channel geometry and meander migration cardinality of Bhagirathi River, West Bengal, India. *Journal of Geographical Sciences*, 29(4), 613-634.
<https://doi.org/10.1007/s11442-019-1618-z>
- Baines, D. (2002). *Migration in a mature economy: emigration and internal migration in England and Wales 1861-1900*. Cambridge University Press.
- Bayliss-Brown, G. (2012). *Adding value to monitoring: The impact of offshore wind farm developments on benthic organisms and sediments in the Eastern Irish Sea*
- Beechie, T. J., Liermann, M., Pollock, M. M., Baker, S., & Davies, J. (2006). Channel pattern and river-floodplain dynamics in forested mountain river systems. *Geomorphology*, 78(1-2), 124-141.
- Bersezio, R., Giudici, M., & Mele, M. (2007). Combining sedimentological and geophysical data for high-resolution 3-D mapping of fluvial architectural elements in the Quaternary Po plain (Italy). *Sedimentary Geology*, 202(1-2), 230-248.
- Binley, A. (2015). DC electrical methods.
- Brice, J. C. (1974). Evolution of meander loops. *Geological Society of America Bulletin*, 85(4), 581-586.
- Bridge, J. S. (1993). The interaction between channel geometry, water flow, sediment transport and deposition in braided rivers. *Geological Society, London, Special Publications*, 75(1), 13-71.
- Buffington, J., & Montgomery, D. (2013). 9.36 Geomorphic classification of rivers.

- Cassidy, N. J., & Jol, H. (2009). Ground penetrating radar data processing, modelling and analysis. *Ground penetrating radar: theory and applications*, 141-176.
- Chant, R. J. (2002). Secondary circulation in a region of flow curvature: Relationship with tidal forcing and river discharge. *Journal of Geophysical Research: Oceans*, 107(C9), 14-11-14-11.
- Chattopadhyay, S., & Edwards, D. R. (2016). Long-term trend analysis of precipitation and air temperature for Kentucky, United States. *Climate*, 4(1), 10.
- Choowong, M. (2011). Basic Geomorphology *Tienwattana Printing Co., LTD*, 202 p.
- Clifford, J., & Binley, A. (2010). Geophysical characterization of riverbed hydrostratigraphy using electrical resistance tomography. *Near Surface Geophysics*, 8(6), 493-501.
- Crosato, A. (2008). *Analysis and modelling of river meandering*. IOS press.
- Daily, W., & Ramirez, A. L. (2000). Electrical imaging of engineered hydraulic barriers. *Geophysics*, 65(1), 83-94.
- David Knighton, A., & Nanson, G. C. (1993). Anastomosis and the continuum of channel pattern. *Earth Surface Processes and Landforms*, 18(7), 613-625.
- Desloges, J. R., & Church, M. A. (1989). Wandering gravel-bed rivers. *Canadian Geographer/Le Géographe canadien*, 33(4), 360-364.
- Downs, P. W., & Piégay, H. (2019). Catchment-scale cumulative impact of human activities on river channels in the late Anthropocene: implications, limitations, prospect. *Geomorphology*, 338, 88-104.
<https://doi.org/https://doi.org/10.1016/j.geomorph.2019.03.021>
- Folk, R. L. (1954). The distinction between grain size and mineral composition in sedimentary-rock nomenclature. *The Journal of Geology*, 62(4), 344-359.
- Friedkin, J. F. (1945). *A laboratory study of the meandering of alluvial rivers*. United States Waterways Experiment Station.
- García-Martínez, B., & Rinaldi, M. (2022). Changes in meander geometry over the last 250 years along the lower Guadalquivir River (southern Spain) in response to hydrological and human factors. *Geomorphology*, 410.

<https://doi.org/10.1016/j.geomorph.2022.108284>

- Glover, B., & Johnson, P. (1974). Variations in the natural chemical concentration of river water during flood flows, and the lag effect. *Journal of Hydrology*, 22(3-4), 303-316.
- Heteren, S. V., Fitzgerald, D. M., Mckinlay, P. A., & Buynevich, I. V. (1998). Radar facies of paraglacial barrier systems: coastal New England, USA. *Sedimentology*, 45(1), 181-200.
- Hickin, E. J. (1974). The development of meanders in natural river-channels. *American journal of science*, 274(4), 414-442.
- Hooke, J., & REDMOND, C. E. (1989). River-channel changes in England and Wales. *Water and Environment Journal*, 3(4), 328-335.
- Hooke, J. M. (2007a). Complexity, self-organisation and variation in behaviour in meandering rivers. *Geomorphology*, 91(3-4), 236-258.
<https://doi.org/10.1016/j.geomorph.2007.04.021>
- Hooke, J. M. (2007b). Spatial variability, mechanisms and propagation of change in an active meandering river. *Geomorphology*, 84(3-4), 277-296.
<https://doi.org/10.1016/j.geomorph.2006.06.005>
- Hooke, R., Martin Duque, J., & de Pedraza, J. (2012). Land transformation by humans: A review. *GSA Today*, 22, 4-10. <https://doi.org/10.1130/GSAT151A.1>
- Hutchinson, G. E. (1957). A treatise on limnology. *Geography, physics and chemistry*, 1015.
- Jackson, R. G. (1976). Depositional model of point bars in the lower Wabash River. *Journal of Sedimentary Research*, 46(3), 579-594.
- Jol, H. M., & Bristow, C. S. (2003). GPR in sediments: advice on data collection, basic processing and interpretation, a good practice guide. *Geological Society, London, Special Publications*, 211(1), 9-27.
- Kiss, T., & Blanka, V. (2012). River channel response to climate-and human-induced hydrological changes: Case study on the meandering Hernád River, Hungary. *Geomorphology*, 175, 115-125.

- Kiss, T., Fiala, K., & Sipos, G. (2008). Alterations of channel parameters in response to river regulation works since 1840 on the Lower Tisza River (Hungary). *Geomorphology*, 98(1-2), 96-110.
- Kleinhans, M. G., & van den Berg, J. H. (2011). River channel and bar patterns explained and predicted by an empirical and a physics-based method. *Earth Surface Processes and Landforms*, 36(6), 721-738.
- Kondolf, G. M. (1994). Geomorphic and environmental effects of instream gravel mining. *Landscape and Urban planning*, 28(2-3), 225-243.
- Kunkel, K. E., Easterling, D. R., Redmond, K., & Hubbard, K. (2003). Temporal variations of extreme precipitation events in the United States: 1895–2000. *Geophysical research letters*, 30(17).
- Lane, E. W. (1957). *Study of the shape of channels formed by natural streams flowing in erodible material*, A Colorado State University. Libraries].
- Leopold, L. B. (1960). *Flow resistance in sinuous or irregular channels*. US Government Printing Office.
- Leopold, L. B., & Wolman, M. G. (1957). *River channel patterns: braided, meandering, and straight*. US Government Printing Office.
- Lotsari, E., Vaaja, M., Flener, C., Kaartinen, H., Kukko, A., Kasvi, E., Hyypä, H., Hyypä, J., & Alho, P. (2014). Annual bank and point bar morphodynamics of a meandering river determined by high-accuracy multitemporal laser scanning and flow data. *Water Resources Research*, 50(7), 5532-5559.
- Magdaleno, F., & Fernández-Yuste, J. A. (2011). Meander dynamics in a changing river corridor. *Geomorphology*, 130(3-4), 197-207.
- Makaske, B., & Nap, R. (1995). A transition from a braided to a meandering channel facies, showing inclined heterolithic stratification(Late Weichselian, central Netherlands). *Geologie en Mijnbouw*, 74(1), 13-20.
- Mama, R., Jung, K., Bidorn, B., Namsai, M., & Feng, M. (2018). The Local Observed Trends and Variability in Rainfall Indices Over the Past Century of the Yom River Basin, Thailand. *Journal of the Korean Society of Hazard Mitigation*, 18(4), 41-55.

<https://doi.org/10.9798/kosham.2018.18.4.41>

- Miall, A. D. (2013). *The geology of fluvial deposits: sedimentary facies, basin analysis, and petroleum geology*. Springer.
- Montgomery, D. R. (1999). Process domains and the river continuum 1. *JAWRA Journal of the American Water Resources Association*, 35(2), 397-410.
- Namsai, M., Bidorn, B., Chanyotha, S., Mama, R., & Phanomphongphaisarn, N. (2020). Sediment dynamics and temporal variation of runoff in the Yom River, Thailand. *International Journal of Sediment Research*, 35(4), 365-376.
<https://doi.org/10.1016/j.ijsrc.2020.03.002>
- Nanson, G. C., & Hickin, E. J. (1983). Channel migration and incision on the Beatton River. *Journal of Hydraulic Engineering*, 109(3), 327-337.
- Neal, A. (2004). Ground-penetrating radar and its use in sedimentology: principles, problems and progress. *Earth-Science Reviews*, 66(3-4), 261-330.
<https://doi.org/10.1016/j.earscirev.2004.01.004>
- Neuendorf, K. K. E., Mehl, J. P. J., & Jackson, J. A. (2011). *Glossary of Geology*. Springer Berlin Heidelberg. <https://books.google.co.th/books?id=LL43MAEACAAJ>
- Nimnate, P., Choowong, M., Thitimakorn, T., & Hisada, K. (2017). Geomorphic criteria for distinguishing and locating abandoned channels from upstream part of Mun River, Khorat Plateau, northeastern Thailand. *Environmental Earth Sciences*, 76(9).
<https://doi.org/10.1007/s12665-017-6657-y>
- Nimnate, P., Thitimakorn, T., Choowong, M., & Hisada, K. (2017). Imaging and locating paleo-channels using geophysical data from meandering system of the Mun River, Khorat Plateau, Northeastern Thailand. *Open Geosciences*, 9(1).
<https://doi.org/10.1515/geo-2017-0051>
- Okazaki, H., Kwak, Y., & Tamura, T. (2015). Depositional and erosional architectures of gravelly braid bar formed by a flood in the Abe River, central Japan, inferred from a three-dimensional ground-penetrating radar analysis. *Sedimentary Geology*, 324, 32-46.
- Ollero, A. (2010). Channel changes and floodplain management in the meandering middle

- Ebro River, Spain. *Geomorphology*, 117(3-4), 247-260.
- Parker, G., Shimizu, Y., Wilkerson, G., Eke, E. C., Abad, J. D., Lauer, J., Paola, C., Dietrich, W. E., & Voller, V. (2011). A new framework for modeling the migration of meandering rivers. *Earth Surface Processes and Landforms*, 36(1), 70-86.
- Pizzuto, J. E. (1987). Sediment diffusion during overbank flows. *Sedimentology*, 34(2), 301-317.
- Pizzuto, J. E. (1994). Channel adjustments to changing discharges, Powder River, Montana. *Geological Society of America Bulletin*, 106(11), 1494-1501.
- Reineck, H.-E., & Singh, I. B. (2012). *Depositional sedimentary environments: with reference to terrigenous clastics*. Springer Science & Business Media.
- Reynolds, J. M. (2011). *An introduction to applied and environmental geophysics*. John Wiley & Sons.
- Rust, B. R. (1977). A classification of alluvial channel systems.
- Scheidegger, A. E. (1982). *Principles of Geodynamics*. Springer Berlin, Heidelberg.
<https://doi.org/https://doi.org/10.1007/978-3-642-68457-9>
- Schmudde, T. H. (1997). FLOODPLAIN Flood plain. In *Geomorphology* (pp. 359-362). Springer Berlin Heidelberg. https://doi.org/10.1007/3-540-31060-6_131
- Schumm, S. A. (1963). *A tentative classification of alluvial river channels: an examination of similarities and differences among some Great Plains rivers* (Vol. 477). US Department of the Interior, Geological Survey.
- Schumm, S. A. (1977). The fluvial system.
- Schumm, S. A. (1981). Evolution and response of the fluvial system, sedimentologic implications.
- Schumm, S. A. (1985). Patterns of alluvial rivers. *Annual Review of Earth and Planetary Sciences*, 13(1), 5-27.
- Shukla, S., Patidar, A., & Bhatt, N. (2008). Application of GPR in the study of shallow subsurface sedimentary architecture of Modwa spit, Gulf of Kachchh. *Journal of earth system science*, 117, 33-40.
- Skelly, R. L., Bristow, C. S., & Ethridge, F. G. (2003). Architecture of channel-belt deposits

- in an aggrading shallow sandbed braided river: the lower Niobrara River, northeast Nebraska. *Sedimentary Geology*, 158(3-4), 249-270.
- Srisunthon, P., & Choowong, M. (2019). Quaternary meandering evolution and architecture of a point bar in the Mun River on the sandstone-dominated Khorat Plateau from northeastern Thailand. *Quaternary International*, 525, 25-35.
<https://doi.org/10.1016/j.quaint.2019.09.005>
- Srisuwan. (2000). <2000_CHARACTER OF CHANNEL PLANFORM CHANGE AND MEANDER.pdf>.
- Suizu, T. M., & Nanson, G. C. (2018). Temporal and spatial adjustments of channel migration and planform geometry: responses to ENSO driven climate anomalies on the tropical freely-meandering Aguapeí River, São Paulo, Brazil. *Earth Surface Processes and Landforms*, 43(8), 1636-1647.
- Theimer, B. D., Nobes, D. C., & Warner, B. G. (1994). A study of the geoelectrical properties of peatlands and their influence on ground-penetrating radar surveying1. *Geophysical prospecting*, 42(3), 179-209.
- Thornbury, W. D. (1954). *Principles of geomorphology* (Vol. 78). LWW.
- Toonen, W. H., Kleinhans, M. G., & Cohen, K. M. (2012). Sedimentary architecture of abandoned channel fills. *Earth Surface Processes and Landforms*, 37(4), 459-472.
- Van Dijk, W., Van de Lageweg, W., & Kleinhans, M. (2012). Experimental meandering river with chute cutoffs. *Journal of Geophysical Research: Earth Surface*, 117(F3).
- Van Overmeeren, R. (1998). Radar facies of unconsolidated sediments in The Netherlands: A radar stratigraphy interpretation method for hydrogeology. *Journal of Applied Geophysics*, 40(1-3), 1-18.
- Wahid, H., Othman, M. H., & Rahim, R. A. (2015). TWO-DIMENSIONAL DC RESISTIVITY MAPPING FOR SUBSURFACE INVESTIGATION USING SOFT COMPUTING APPROACHES. *Jurnal Teknologi*, 77(17).
- Williams, G. P. (1984). Paleohydrologic equations for rivers. *Developments and applications of geomorphology*, 343-367.
- Williams, G. P. (1986). River meanders and channel size. *Journal of Hydrology*, 88(1-2),

147-164.

Woolfe, K. J., & Purdon, R. G. (1996). Deposits of a rapidly eroding meandering river: terrace cut and fill in the Taupo Volcanic Zone. *New Zealand Journal of Geology and Geophysics*, 39(2), 243-249.

Yousefi, S., Pourghasemi, H. R., Hooke, J., Navratil, O., & Kidová, A. (2016). Changes in morphometric meander parameters identified on the Karoon River, Iran, using remote sensing data. *Geomorphology*, 271, 55-64.

<https://doi.org/10.1016/j.geomorph.2016.07.034>

Zăvoianu, I. (1985). Stream and Drainage Densities. *Developments in Water Science*, 20, 135-153.





จุฬาลงกรณ์มหาวิทยาลัย
CHULALONGKORN UNIVERSITY

VITA

NAME Kakkhanang Na Nan

DATE OF BIRTH 25 November 1995

PLACE OF BIRTH Chiangrai

INSTITUTIONS ATTENDED Princess Chulabhorn Science High School Chiang Rai, High school
Chiang Mai University, Bachelor's degrees

HOME ADDRESS 106 Village No.19, Wieng Sub-district, Thoeng District,
Chiangrai Province





จุฬาลงกรณ์มหาวิทยาลัย
CHULALONGKORN UNIVERSITY